Thermal and Hydrological Response of Rock Glaciers to Climate Change: A Scenario Based Simulation Study

by

Jotham Apaloo

A thesis
presented to the University of Waterloo
in fulfillment of the
thesis requirement for the degree of
Master of Science
in
Geography

Waterloo, Ontario, Canada, 2013

Declaration

I hereby declare that I am the sole author of this thesis. This is a true copy of the thesis, including any required final revisions, as accepted by my examiners.

I understand that my thesis may be made electronically available to the public.

Abstract

Snow and glaciers are considered the most important sources of the estimated 32-60% of global water resources which are provided by mountains. Consequently, snow and glaciers have regularly been the focus of climate change studies in mountain regions. Rock glaciers are a type of ice-debris landform characterized by creeping ice-rich permafrost. Recognition of the hydrological significance of rock glaciers is increasing and is of particular relevance to the Arid Andes, where rock glaciers cover greater area than glaciers by an order of magnitude. Little research exists on the hydrological significance of rock glaciers beyond potential water storage capacities and their runoff pathways. Additional knowledge and research approaches pertaining to the seasonal hydrological contributions and climatic sensitivities of rock glaciers are necessary for improved water resource planning in many regions around the world.

This work explored the feasibility of utilizing the energy and water balance model GEOtop to quantify the thermal and hydrological dynamics of rock glaciers under several climate scenarios. Weather data was generated with the intermediate–stochastic weather generator AWE–GEN for a site in the Southeast Swiss Alps, which marked a novel approach in studies of rock glaciers. Weather data for a reference (REF) scenario was generated which approximates conditions during the observation period (1985 to 2012). AWE–GEN produced time series of weather data for the REF scenario with statistical properties of precipitation in close agreement with observations. Air temperature had substantial inaccuracies with mean annual air temperature (MAAT) cooler by 1.82°C due to negative temperature biases in summer months which are attributed to difficulties in estimating parameters of the weather generator model caused by local climatic factors. The influence of climate change was also examined. Data for 8 climate change scenarios were generated by specifying change factors for mean monthly air temperature. MAAT in the climate change scenarios was within +/-0.12°C of the specified change factor from MAAT in the REF scenario.

The thermal and hydrological evolution of rock glacier soils were simulated for 50 years under the climatic forcing of the REF scenario followed by 50 years under each climate change scenario. Mean annual ground surface temperature (MAGST), active layer depth (D_{al}), permafrost total ice content (IWE_{tot}), and the potential summer runoff contribution ($MELT_{sum}$) were quantified and compared before and after the onset of the climate change conditions. Air temperature increases in the climate change scenarios were amplified in MAGST. Stable rock glacier points were resistant to changes in D_{al} and IWE_{tot} under any annual, summer, and winter mean air temperature increase of 1°C, and summer and winter

mean air temperature increases of 3°C despite notable changes in MAGST and MELT_{sum}. Under warming scenarios, the greatest increase in MELT_{sum} occurred for high elevation rock glacier points with the mean possible runoff contribution increasing 88% under 3°C of warming, which corroborates with increased runoff from high elevation permafrost in the Colorado Rockies in recent decades.

Acknowledgements

I would like to thank my supervisor Alex Brenning for years of supervision during many undergraduate research assistantships, introductions to numerous powerful softwares, and provision of incredible opportunities for participating in the mountain permafrost research process and community in addition to ongoing and prompt feedback on this thesis and other works.

My gratitude also goes to Stephan Gruber for the introduction to numerical permafrost modeling, guidance on the usage of GEOtop for the purposes herein, and facilitating the usage of the grid computing for the GEOtop simulations.

Thanks to the GEOtop development and user community in Zürich and Bolzano for enhancing my experience during my stay in Zürich, specifically Stefano Endrizzi who answered many specific questions pertaining to GEOtop.

The prompt assistance of Simone Fatichi in tweaking AWE-GEN to get it operational on the Piz–Corvatsch data was much appreciated. Also regarding weather generators in general, I would like to thank Christopher Fletcher for co-supervising a reading course on that topic.

My thanks goes again to Dr. Gruber and Dr. Fletcher, and also to Claude Duguay, for serving on my defense committee.

My Masters experience would of course not have been possible without the Department of Geography & Environmental Management at the University of Waterloo, of whom Ian McKenzie, Richard Kelly, and Peter Deadman deserve special mention for facilitating my transfer to the department as an undergrad, providing excellent course-based learning experiences and general academic guidance, and providing excellent teaching assistantships respectively. Susie Castela was also enormously helpful throughout. Thanks to you all.

I am also very grateful to Natural Sciences and Engineering Research Council (NSERC) of Canada for the award of the Alexander Graham Bell Canada Graduate Scholarship.

This work was supported by the AAA/SWITCH funded Swiss Multi Science Computing Grid project (www.smscg.ch) with computational infrastructure and support. Customized libraries (ggeotop and GC3Pie) and user support were kindly provided by GC3: Grid Computing Competence Center (www.gc3.uzh.ch).

Dedication

This thesis is lovingly dedicated to:

My parents, Joe and Sherry, for the nature you lend me and the nurture you share. For supporting my university studies and encouraging me to engage other activities during this time.

My wonderful girlfriend, Kirstin. I dedicate this to our future. The quality of this work and my health is owed in much to your support.

Kirstin's family, Dave, Debbie, and Robyn for freeing me of some responsibilities by sharing your home with me during the summer while I wrote much of this document.

And my friends in Waterloo, especially Rob and Deon, for all the good times. And the blokes and birds in the PAC weightroom. Thanks for the positive breaks.

Much love.

Table of Contents

List of Tables

List of Figures

List of Equations

List of Acronyms

AWE-GEN Advanced WEather GENerator

D$_{AL}$ Active layer depth

IWE$_{tot}$ Soil column ice water equivalent

MAAT mean annual air temperature

MAAT$_{obs}$ observed mean annual air temperature

MAGST mean annual ground surface temperature

MELT$_{sum}$ The difference between September 1 and June 1 Soil column ice water equivalent (IWE$_{tot}$)

MSAT$_{obs}$ observed mean summer air temperature

MSDmaxAT$_{obs}$ observed mean summer daily maximum air temperature

MSDminAT$_{obs}$ observed mean summer daily minimum air temperature

MWAT$_{obs}$ observed mean winter air temperature

MWDmaxAT$_{obs}$ observed mean winter daily maximum air temperature

MWDminAT$_{obs}$ observed mean winter daily minimum air temperature

N$_{Cl}$ cloud fraction

NAO North–Atlantic Oscillation

NSRP Neyman-Scott Rectangular Pulse

$\mathbf{P}_{atm}$ atmospheric pressure

Pr precipitation

$\mathbf{PrAnn}_{obs}$ observed total annual precipitation

$\mathbf{PrSum}_{obs}$ observed total summer precipitation

$\mathbf{PrWin}_{obs}$ observed total winter precipitation

RH relative humidity

SWR global shortwave solar radiation

TA air temperature

TA_{max} maximum TA

TA_{min} minimum TA

WS wind speed

Chapter 1

Introduction

Mountains are known as the Global Water Towers (Viviroli & Weingartner, 2004). They comprise approximately 25% of the earth's land surface and are the headwaters of rivers on which half the global population depends for water resources (Beniston, 2006; Messerli et al., 2004). Most of the annual discharge of these rivers is stored for less than a year as snow which has a rapid response to interannual climatic variation. Discharge from glaciers regulates the variability of total basin discharge at the decadal scale as they respond to more persistent trends within climatic variability. Overall, their role in global hydrology is poorly understood considering the implications for the global population (Viviroli et al., 2003).

Permafrost (perennially frozen ground) is another significant storage mode for long term water resources in high mountains (Caine, 2010), particularly in rock glaciers which are a type of ice-debris landforms that contain ice-rich permafrost; rock glaciers span the seasonal to millennial temporal scales of water storage, and cover a much greater area than glaciers in some regions (Azócar & Brenning, 2010). Nonetheless, glacierized catchments have only recently been taken into consideration in hydrological models (Jansson et al., 2003) while the presence of rock glaciers is not yet considered. The hydrological characteristics of rock glaciers are presently not sufficiently understood to enable their immediate inclusion (Gascoin et al., 2011a; Azócar & Brenning, 2010; Croce & Milana, 2002; Gardaz, 1998).

Permafrost models can be categorized into empirical–statistical and process–oriented types, of which the latter apply analytical or numerical solutions to the heat equation (Riseborough et al., 2008). All of these model types can be used to investigate some

aspects of permafrost dynamics (e.g. presence, active layer depth), but numerical models are favored for the capability to capture transient changes in the ground thermal regime and also for the utilization of high frequency upper boundary (i.e. meteorological) conditions. Numerical models are the favored type for modeling local scale permafrost dynamics in high mountains (Harris et al., 2009), but few operate at the level of detail necessary to model rock glacier thermal and hydrological dynamics in an explicit manner. Recent implementations of the GEOtop model (Endrizzi & Gruber, forthcoming) may be suitable for this, as it solves both the energy and water balance of variably saturated permafrost soils and treats snow cover and the surface energy balances in physically explicit manners.

Mountain weather and climate are extremely complex due to the influence of topography across spatial scales (Barry, 2008). An important consideration in the investigation of the thermal and hydrological characteristics of rock glaciers is the influence of climatic variability and climate change, and how the roles of permafrost and seasonally frozen ground may differ in future high mountain hydrological regimes (Caine, 2010). Stochastic weather generators are useful tools for the investigation of such questions for local scale impact studies (Dubrovskỳ et al., 2004; Semenov & Barrow, 1997), perhaps moreso in high mountains due to the limitations of dynamic meteorological and regional or global climate models. However, they are rarely applied in such areas (Uhlmann et al., 2012) and possibly susceptible to limitations which do not affect lowland areas.

1.1 Research overview

This work investigates the thermal and hydrological evolution of rock glacier soils using a numerical model with water and energy budgets (GEOtop). In this paper, the term soil is used to describe the mixture of ice and sediment in a rock glacier; as no other individual term (e.g. substrate, colluvium, permafrost, sediment) conveniently and accurately describes the materials that comprise a rock glacier. Numerous cases of soil type topographic situations are evaluated under the present climate and in response to several alternate climatic scenarios. Meteorological data for each climate scenario is generated with an intermediate-stochastic weather generator which is fitted to observations from a site in the Swiss Alps in close proximity to a rock glacier. The study is not intended to represent any specific location but aims to explore the methodology, which can later be validated for particular rock glaciers or watersheds and other climatic contexts.

The present work is expected to contribute to the greater knowledge pertaining to the hydrology of high mountains. It is considered especially significant to dry high mountains,

such as the arid Andes where rock glaciers are the primary long-term water storage mode (Azócar & Brenning, 2010), but also contributes to high mountains in general. Additionally, the methods and outcomes are, with some minor adaptations, transferable to debris-covered glaciers, which are of particular importance in the Himalaya, where alternatives to intensive in-situ monitoring are required to accurately evaluate regional glacier mass balance trends (Hewitt, 2005). This work will also serve as a test of weather generator performance in high mountains, which will benefit the development of the tools towards superior performance in these climatically complex areas.

1.2 Research objectives

The primary objectives of this research are to examine the thermal and hydrological dynamics of rock glaciers and their response to climate change in a scenario based simulation framework. This is achieved through the following intermediate objectives:

- Generate weather data for several climatic scenarios using a weather generator.
- Perform a quality assessment of the generated meteorological data.
- Conceptualize rock glaciers as points for input to GEOtop based on known rock glacier properties and their thermal and hydrological properties.
- Simulate the evolution of the rock glacier points under the reference climate before subjecting them to the climate change scenarios.
- Quantify the hydrological and thermal dynamics of the rock glacier points in the reference and climate change scenarios.

1.3 Document structure

A context for the motivations, tools, and knowledge relevant to this study is presented in Chapter 2. This includes an overview of macro to local scale topographic drivers of high mountain weather and climate and their influence on the ground thermal regime of mountain permafrost, and the knowledge, or lack thereof, in high mountain hydrology.

The climatic and geomorphic controls on rock glacier presence, and knowledge of their physical characteristics are reviewed. Aspects of climate change observations and forecasts, especially in high mountains, and the theory weather generators are presented in brief. The types of permafrost models, their limitations, and the general process and theory behind process oriented permafrost modeling are also described. Chapter 3 details the regional climatic context and climatic data used for the climate scenarios, the weather generator applied thereon and the methods for assessing the quality of its output; this is followed by a description of the modeling approach of GEOtop and the target variables, parameters and experimental approach utilized herein. The results of the weather generation and GEOtop simulations are provided in Chapter 4. Chapter 5 discusses and contextualizes the results and considers the limitations of the weather generation and permafrost modeling methods; it also presents practical extensions of the methodology. Chapter 4 and Chapter 5 are summarized and conclusions stated in Chapter 6

Chapter 2

Research Context

2.1 High mountain weather and climate

There is no exact definition of mountains or high mountains (Viviroli & Weingartner, 2004). As useful definition herein is land above 1000 m above sea level (a.s.l.) elevation of moderate to high relief (i.e. not plateaus). The condition of the land being above the lower limit of periglacial processes (after Barry, 2008, p. 2) is also relevant. Combining the two narrows the area of consideration to high elevation land of moderate relief in mid to low latitudes, where rock glaciers are most likely to be of considerable hydrological significance to human populations (see Section 2.4.1 and Section 2.3).

Geographical characteristics such as latitude, continentality, seasonality, and topography exert influence on high mountain weather and climate. The relations are based in fundamental physics which can be expressed in various mathematical forms using the laws of motion, ideal gases, radiant emissions and so forth (e.g. Marshall & Plumb, 2008). Familiar meteorological variables are nested between the geographical characteristics and physical laws; this includes air pressure and density, vapour pressure, radiant and turbulent energy fluxes, cloud cover, precipitation, temperature, wind speed and direction etc. The geographical realizations of these variables and their scale dependent relationships characterize local high mountain climates around the world. This section reviews these elements of high mountain weather and climate which may inform extrapolations of this work to other regions. The information in this section is basic and descriptive, but lends to the understanding of the performance and shortcomings of stochastic weather generators in high

mountains and the variables represented in the upper boundary layer of process-oriented permafrost models.

2.1.1 Air temperature

Air temperature decreases with increasing elevation due to adiabatic expansion of air in the free atmosphere and mechanical lifting of air forced up by orographic barriers (e.g. Marshall & Plumb, 2008; Barry, 2008). The lapse rate depends primarily on the vapour pressure of the air (Barry, 2008, p. 260). Greater vapour pressure yields lower lapse rates, as the condensation of water vapour releases latent heat as the air rises. The tendency for air temperature to decrease with elevation only persists on long time scales (Barry, 2008, p. 260). Short term relationships between elevation and air temperature can be weak or inverted, and may show a greater dependence of air temperature on the conditions of the previous day than on elevation.

Daily maximum air temperatures show direct correspondence with solar radiation whereas minima are closely related to site specific air drainage (Barry, 2008, p. 261). When solar input is low during nights or cloudy days the vertical pressure gradient force weakens as the air near the ground is no longer heated. Cool dense air then subsides and flows downslope into depressions or valley bottoms. During night this can cause inversions of the lapse rate as warm air is displaced upward by the cool descending air, resulting in warmer temperatures along valley sides than at valley bottoms (Barry, 2008, p. 264). High level winds, pressure gradient, and topography govern the local and regional outcome of these inversions and cold air drainage.

Near–surface temperature lapse rates are often assumed to take the value 6.5°C km^{-1}, but vary from 1°C km^{-1} to 9 °C km^{-1} spatially, at sub–daily and greater time scales, with broader atmospheric conditions, with surface proximity, and with wind exposure (Minder et al., 2010; Blandford et al., 2008; Rolland, 2003). Lapse rates are generally higher in summer than winter, and for daily maximum compared to daily minimum or daily mean temperatures (Blandford et al., 2008; Rolland, 2003).

2.1.2 Precipitation

Precipitation is frequent in high mountains due to the orographic effect, i.e. lifting and cooling of air as it passes a topographic obstacle, yielding cloud and precipitation. The

interactions between the processes driving precipitation are highly complex and span local to regional scales. The factors governing snow cover properties are of foremost interest with respect to rock glaciers because of the influence of snow on the thermal regime of the ground (Section 2.2) through the surface energy balance (Section 2.1.3). In this section, some general remarks on precipitation in high mountains are made, followed by some elaboration on snowfall tendencies.

Cyclonic systems are the main driver of precipitation during the winter in mid–latitude high mountains, onto which topography forces some elevation–dependent patterns of precipitation quantities (Barry, 2008, p. 274). Precipitation generally increases with elevation under unstable (i.e. cyclonic) atmospheric conditions on the windward side of mountain ranges due to an increase of precipitation intensity with elevation. Lee sides of mid-latitude mountain ranges tend to be drier than windward sides (Barry, 2008, p. 285). Hydrothermal characteristics of the source air masses govern some of the regional outcomes of high mountain precipitation. In the easterlies through which equatorial high mountains pass and in mid-latitudes during the summer convective precipitation dominates and the elevational increase can be less pronounced due to relative reduction of orographic lifting effects and weak altitudinal wind speed gradients (Barry, 2008, p. 274). These complexities result in precipitation being effectively predicted by interaction terms between elevation, aspect, and slope angle at the meso-scale (Barry, 2008, p. 287).

The preceding remarks about precipitation apply to snow, but some additional remarks on snow occurrence and elevational trends are now included. Suffice for now to state that snow cover depth, duration, and snowpack properties at local scales are extremely variable due to topography and local winds. Elaboration on these trends and their influence on the thermal conditions of the ground are offered in Section 2.2.

Snow is by far the dominant mode of precipitation in high mountains. The fraction of precipitation which falls as snowfall increases with elevation due to the air temperature lapse rate (Barry, 2008, p. 293). The threshold temperature (i.e. the temperature at which there are equal probabilities of snow and rain occurrence) which discriminates rain and snow may also increase with elevation.

Snow redistribution is an important process imposed on precipitation in high mountains (Barry, 2008, p. 323). Falling snow is carried by wind to locations other than immediately below its source. Loose snow can be relocated by winds as small as 15 km h^{-1} while more packed snow may require winds of 90 km h^{-1} or more. Moisture content is directly proportional to the coherence of snow. Where turbulent air movement is small, snow particles may roll and bounce along the surface; these mechanisms are known as creep and

saltation respectively (Figure 2.1). Suspension involves the lifting of snow in turbulent eddies to heights of 1–100 m, from which it can be carried great distances by strong winds. Deposition occurs where winds decelerate such as in lee of ridges or large hollows (Barry, 2008, p. 325). The local wind field, topography, and the interactions between these two variables are of primary importance to snow distribution patterns.

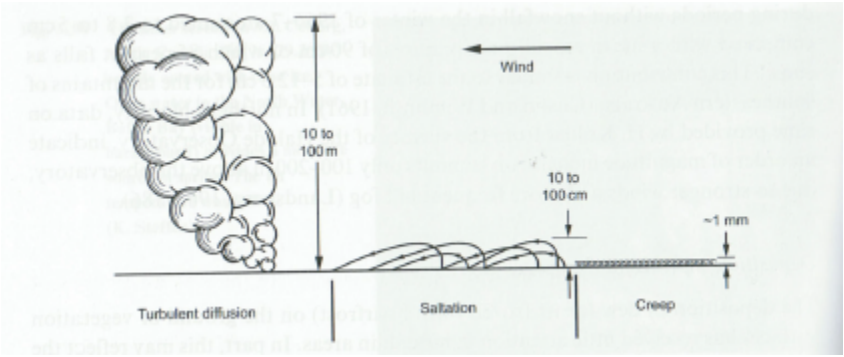

Figure 2.1: Modes of snow redistribution by wind (Barry, 2008, p. 324)

It should be noted that precipitation is difficult to measure accurately in high mountains due to complex wind fields, especially in large valleys which tend to differ more from regional precipitation due to strong valley winds, (Barry, 2008, p. 287). Errors can reach 15% and 50% for rain and snow respectively (Barry, 2008, p. 306).

2.1.3 Radiant and turbulent energy fluxes

Net radiation is the energy available to do work (e.g. evaporate, heat) and many of its controlling factors are influenced in a predictable way by characteristics of high mountain weather and climate. For a surface, net radiation can be approximated by

$$Q^* = K\downarrow(1-\alpha) + L_{in} + L_{out} \tag{2.1}$$

where Q^* is net radiation, $K\downarrow$ is incoming shortwave radiation, L_{in} and L_{out} are longwave radiation, and α is the surface albedo (Oke, 1987, p. 22–23). Albedo is the amount of incoming shortwave radiation which is reflected and is expressed as a unitless

value from 0 to 1. The radiant terms are energy flux densities with units W m^{-2}. Energy fluxes toward the surface have a positive sign whereas those directed away from the surface have a negative sign.

Solar radiation amounts are inversely related to vapour pressure through its effect on atmospheric transmissivity. The decrease in atmospheric water vapour with elevation creates conditions of high solar radiation intensity, with a relatively greater increase at lower elevations (Barry, 2008, p. 251). This relationship will follow the regional relationship between altitude and vapour pressure. High elevation clouds also tend to have high transmissivity, further lending to the increase of solar radiation with elevation (Barry, 2008, p. 252).

Equation 2.1 demonstrates the importance of albedo in controlling net radiation energy at the surface. In high mountains the spatial variation of albedo is low due to generally homogeneous rock cover (albedo 0.12 to 0.15 Muneer, 2004) and sparse or absent vegetation. Snow on the other hand can have albedo values from 0.40 (old snow, lower limit) to 0.95 (new snow, upper limit) (Muneer, 2004) and is a major controlling factor in net radiation. Observed consequences of these factors and relevant properties of snow are described in Section 2.2.

L_{out} is related to surface temperature and can be estimated with the Stefan–Boltzmann equation. It will generally follow the elevation–surface temperature trends during the snow-free period. In snow covered conditions, L_{out} is determined by snow surface temperature and emissivity, which is higher than that of rock.

At the soil surface, net radiation is dynamically partitioned into energy fluxes with the ground, atmosphere or surface cover, and evaporation or other latent heat transfer processes. This can be expressed as

$$Q^* = H + LE + G + \frac{\partial Q}{\partial t} \tag{2.2}$$

where $\frac{\partial Q}{\partial t}$ is a term that represents the change in energy (mass, latent, temperature) storage and H, LE, and G are the sensible, latent, and ground heat fluxes respectively (Oke, 1987, p. 34). Units and sign convention follow Equation 2.1. The sensible heat flux is energy transfer between the soil and overlying atmosphere and the latent heat flux is the energy used in phase changes of water. The sensible and latent heat fluxes depend on gradients in their respective variables between the surface and overlying atmosphere and both

are enhanced with wind speed and surface roughness, which promote mixing and restoration of gradients in the boundary layer. G is the ground heat flux or the exchange of energy between the active surface and ground below. Conduction is the primary mechanism for this energy exchange; it is governed by the temperature gradient and thermal conductivity of the soil. However, advective energy transfer can play a role in frozen soils (Kane et al., 2001). In the infinitesimal surface approximation the change in energy storage approaches 0 and net radiation is then equivalent to the H, LE, and G. However, the storage term is important to this work where energy exchanges in a volume (i.e. rock glaciers) are of primary concern.

Spatial variation in the heat flux terms is very high in mountain regions due to topographic and wind effects. Snow–melt is a major component of the high mountain radiation budget as a latent heat sink (Barry, 2008, p. 253). Elevational gradients in the heat fluxes are largely determined by snow cover differences (Barry, 2008, p. 259). In the snow covered period the elevational trends in these variables tend to disappear (Barry, 2008, fig 4.4).

2.1.4 Cloud cover

Thermal and mechanical forces cause cloud formation in high mountains. In stable and unstable atmospheric conditions orographic lift will cause stratus and cumulus cloud formation at the lifting condensation level and level of free condensation respectively (Barry, 2008, p. 267). Air flowing around an obstacle may cause lift and yield clouds in lee of the obstacle where convergence occurs. Heating of sunward slopes also encourages convective lift, often enhanced by resultant anabatic winds (see Section 2.1.5), and cloud formation at the level of free condensation.

There are differences in cloud cover related to atmospheric circulation and moisture sources that differentiate cloud regimes between regions and entire mountain systems. In high mountains at low latitudes, and during the summer in the mid–latitudes, most cloud formation is due to convective lift (Barry, 2008, p.266). Cyclonic systems dominate cloud formation in the mid–latitude winters. During autumn in the mid–latitudes, or elsewhere under stable atmospheres, stratus cloud types dominate and have comparably high transmissivity.

Regarding elevational trends in high mountains, cloud cover frequency loosely follows precipitation amount trends, i.e. a general increase with elevation, but the relationship may not be as strong since high precipitation amounts are associated with high precipitation

intensities, not greater frequencies (Barry, 2008, p. 283). Cloud cover is generally abundant but also very complex in high mountains due to the different mechanisms available to lift air and cause cloud formation. Another element of complexity is that the locations which clouds affect are subsequently determined by the wind field, an extremely variable element of high mountain environments.

2.1.5 Wind

Wind speed typically increases with elevation, with some notable exceptions. The elevational increase can be due to an altitudinal increase of wind speed in the free atmosphere due to reduced friction at the altitude of high mountains and due to compressional or Bernoulli effects on air as it passes over mountain tops (Barry, 2008, p. 70, 71). These are only notable where the greater atmospheric trend is for increased wind speed with altitude (i.e. mountains in the path of mid–latitude westerlies), the opposite can be observed in the Tropics.

Mountain topography modifies wind patterns at local to planetary scales. Winds associated with the effects of mountain topography can be categorized as mechanical or thermal winds. Mechanical winds are the result of direct interactions between the atmosphere and topography. Modification and generation of mechanical winds at greater spatial scales include phenomena such as lee cyclogenesis (and enhancement), modification of synoptic systems, cross range and barrier jets etc (Barry, 2008, p. 125). Among mechanical winds are the Föhn winds of the Alps, which are the result of adiabatic heating and/or vapour pressure increases of air descending the lee side of mountain ranges (Barry, 2008, p. 171). Potential temperature differences in lee due to moisture exhaustion on the windward side has been proposed as a mechanism but not observed as necessary, although warming on the lee side is proportional to atmospheric instability in some cases (Barry, 2008, p. 172). Similar phenomena occur in other high mountains areas: e.g. Chinooks in the Rockies and Santa Ana winds of the Sierra Nevada.

Thermal winds are very important to near surface weather and climate in high mountains. They are frequent under conditions of weak regional pressure gradient when surface heating and cooling can take over local air motions (Barry, 2008, p. 186). These local scale thermal winds, or slope winds, occur due to radiative heating and cooling at different elevations which creates potential temperature differences orthogonal to gravitational forces (Figure 2.2). During radiative input (loss), i.e. daytime (nighttime), the pressure gradient is toward (away from) the slope, resulting in an upslope (downslope) air flow termed

anabatic (katabatic) wind. Both wind types are strongest under stable atmospheric and clear sky conditions. Anabatic tend to be faster than katabatic flows due to the larger radiative forcing and both may have constant or periodically changing velocity (Barry, 2008, p. 195). For the same reason, sunward slopes also generally have higher anabatic wind speeds. Other variables include slope length, slope angle, slope curvature, ambient temperature, lapse rate, and sensible heat flux etc. which can be used to estimate thermal wind speeds (Barry, 2008, p. 190–192).

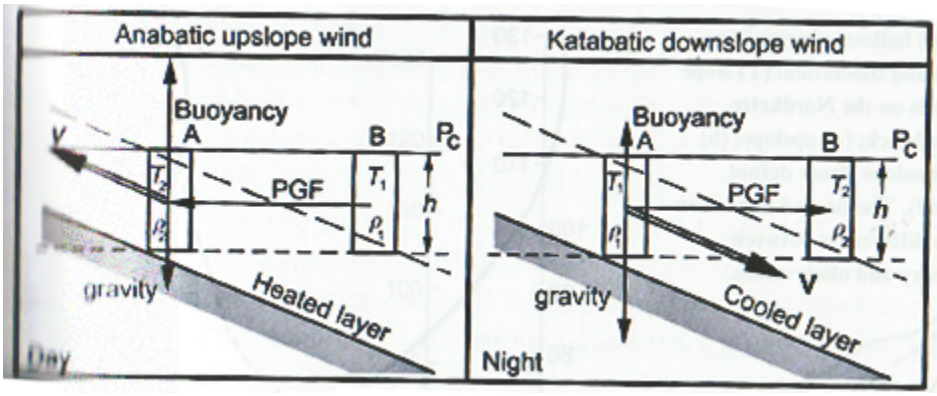

Figure 2.2: Diagrams of the forces in anabatic and katabatic winds (Barry, 2008, p. 187). PGF–pressure gradient force, ρ–air density, T–air temperature, V–resultant wind vector.

Anabatic winds are typical during summer whereas katabatic winds are more common in the winter. Katabatic winds are also faster and more persistent in the winter when longwave emissions are high due to the presence of snow, or in glacierized valleys (Barry, 2008, p. 189). The winds extend from the slope surface to heights on the order of tens of metres. Katabatic winds may decouple from air near the surface; in this situation turbulence in the near–surface air is enhanced, increasing the sensible heat flux (Barry, 2008, p. 194).

In large valleys rather than on slopes similar air movements occur due to radiative differences between mountain topography and forelands (Barry, 2008, p. 198). These upward (towards the mountain) and downward (towards the foreland) flows are known as mountain and valley winds respectively. Return (anti) flows exist above valley and mountain flows, and may warm the upper reaches of valley sides in the valley wind case (Barry, 2008, p. 264). Mountain and valley flows may combine with anabatic and katabatic flows on the valley sides to make for extremely complex diurnally periodic conditions in which the near surface winds may occur in all directions throughout the day at any

given point (Barry, 2008, p. 205). The gradient wind complicates the wind field due to interactions with slope, anti–mountain, and anti–valley flows. The combination of these factors yields unique valley wind fields and near–surface climates.

2.2 High mountain topoclimate and ground thermal regime

The microclimates of high mountains form a mosaic which demonstrates the controlling influence of topography; the result is termed topoclimates (Barry, 2008, p. 96). Topoclimates concern the variation of near surface climatic measures on spatial scales of 10^1 to 10^4 m. Topoclimates are important to rock glaciers for their affect on the ground thermal regime, which broadly refers to the distribution and variation of temperature and heat flow in the ground. The principal factors in determining the ground thermal regime at some location are the geothermal gradient, near–surface climate, surface cover, and soil properties. Mean annual ground surface temperature (MAGST) is often used as a bulk description of the ground thermal regime (examples below) whereas the basal temperature of winter snowpack can be used to identify locations with permafrost based on empirically determined thresholds (Hoelzle et al., 1993). Here, numerous topoclimatic variables present in high mountains are described with reference to examples of their effects on elements of the ground thermal regime.

Slope angle, aspect, and horizon are the primary variables behind topoclimatic forcing (Barry, 2008, p. 102). The means by which these variables influence topoclimate include controls on: solar radiation input, near surface winds, and snow cover characteristics. Solar radiation incident on any given point consists of direct, diffuse, and reflected components which are sourced from the sun, atmospheric scattering, and nearby surfaces respectively (Kumar et al., 1997). Global (the sum of direct, diffuse, and reflected) solar radiation is proportional to direct solar radiation (Kumar et al., 1997). Direct solar radiation is primarily a function of slope angle, aspect, latitude, and sky view factor (Barry, 2008, p. 90–91) although atmospheric properties can play a role (e.g. Section 2.1.3). Sky view factor is a function of the surrounding topography and is defined as the fraction of hemispherical view which is unobstructed (Corripio, 2003). As a general rule, unobstructed sunward surfaces receive the highest solar radiation. In the northern (southern) hemisphere surfaces with southerly (northerly) aspects receive the most solar radiation. Equatorward of 40° latitude, the situation can reverse (Barry, 2008, p. 87). In mid and high latitudes the

aspect effects are enhanced on steep and gentle slopes during winter and summer months respectively (Barry, 2008, p. 87).

Measurement of solar radiation is challenging in mountain topography due to the variability imposed by topography. Potential incoming solar radiation as estimated in geographic information systems applications (Corripio, 2003; Kumar et al., 1997, e.g.) has been used in many studies to represent the topoclimatic effects of solar radiation on elements of the ground thermal regime. In general, strong correlations (Etzelmüller et al., 2006; Julián & Chueca, 2007) and significant regression coefficients (Lewkowicz & Ednie, 2004; Bonnaventure & Lewkowicz, 2011) have been found between potential incoming solar radiation and basal temperature of winter snowpack at mid to high latitudes; in one case in the Swiss Alps for example it was found to be warmer by 1.3°C on south compared to north facing slopes based on a regression model (Brenning et al., 2005). The variance of MAGST may also be higher on sun–exposed slopes due to the large influence of solar radiation compared to shaded slopes (Salzmann et al., 2007). At lower latitudes the effects of topographic forcing on the ground thermal regime through potential incoming solar radiation have been observed as comparably weaker (Apaloo et al., 2012).

Slope angle and aspect also affect wind and sensible heat transfer as described in Section 2.1.5, but this impact is presumably much less than that of shortwave radiation inputs due to the relative contribution of solar radiation to the radiation balance. Efforts at explicitly including wind exposure indices in the MAGST component of the ground thermal regime suggest wind exposed slopes are cooler, but the effects are not statistically significant (Apaloo et al., 2012). Then tendency for reversals of local wind patterns in the diurnal cycle is a possible mediating factor, but the effect of wind exposure may be reflected in snow properties, and sophisticated efforts at modeling the wind field in high mountains have shown good correspondence with observed and simulated snow thicknesses (e.g. Dadic et al., 2010).

Near surface ground properties and surface cover are relevant to topoclimates in that they affect the terms in Equation 2.2. Vegetation is such a surface cover but is sparse in high mountains. Coarse blocks are common in high mountain environments and are frequently found on rock glaciers (Apaloo et al., 2012), talus slopes (Delaloye et al., 2003), and block fields (Juliussen & Humlum, 2008). Their topoclimatic effect is cooling of surface temperatures, reductions of MAGST in bouldery topography from 7°C to 0.6°C (when possible confounding variables are considered) have been observed (Apaloo et al., 2012; Juliussen & Humlum, 2008; Harris & Pedersen, 1998). Mechanisms such as density settling of cold air, enhanced turbulent heat fluxes, and inhibited geothermal heating of the surface under

snow cover due to the low thermal conductivity of the blocky layer have been proposed (Harris & Pedersen, 1998; Gruber & Hoelzle, 2008) and probably operate collectively.

Snow is another important topoclimatic variable; it affects net radiation as per Section 2.1.3 and net radiation partitioning by impedance of the sensible heat and provision of a large latent heat sink above the surface (Ge & Gong, 2010). The controls on local snow cover are also topoclimatic variables. Snow tends to be transported from wind exposed to wind sheltered areas where winds accelerate and decelerate respectively (p. 101 Barry, 2008; Mott et al., 2010). Slope morphology also affects snow redistribution. Steep slopes (30°–50°) favour gravitational redistribution of snow resulting in thicker snow cover at slope bases (Lehning et al., 2008). In high mountains, spatial autocorrelation in snow thickness persists on distances of a few tens of metres, depending on topography (Pigeon & Jiskoot, 2008; Hiemstra et al., 2006). Snow thickness variability (semivariance) varies interannually due to regional scale meteorological factors (Erickson et al., 2005), but a rule of thumb of 25% of mean snow thickness may be of use (Pigeon & Jiskoot, 2008). Snow thickness and redistribution can be modeled accurately based on wind field processes but at a high computational cost (Mott et al., 2010). Statistical approaches may offer computational advantages but require intensive field study for use in specific spatial domains (Erickson et al., 2005).

Snow thickness and disappearance date are the properties which determine the topoclimatic influence of snow on the ground thermal regime. A thick snow cover increases the lag time and decreases the amplitude of ground surface temperature changes in response to air temperature changes (Gadek & Leszkiewicz, 2010). This effect is also proportional to the thermal conductivity (i.e. density) of the snow cover (Rixen et al., 2004). The entire snow–soil system warms with increasing snow depth due to greater storage soil heat, but the ground and sensible heat flux decrease and increase respectively due to steeper temperature gradients imposed by the cold snow–atmosphere interface (Ge & Gong, 2010). Snow depths of 50 cm or more are considered effective depths for insulating the ground from the cold atmosphere (Ge & Gong, 2010; Hanson & Hoelzle, 2004) and 80 cm is considered safe for ensuring quality basal temperature of winter snowpack measurements (Hoelzle et al., 2003). The tendency for thick snow packs to have relatively high density due to self compaction adds a complication to the general rule of the increase of the insulative property of snow with thickness (Morin et al., 2010).

The effects of snow onset date on soil temperature and MAGST are small perhaps due to limited spatial variability compared with disappearance date or due to small gradients between air and ground temperature compared to snow melt periods (Apaloo et al., 2012; Ge & Gong, 2010). A thin snow cover in autumn may promote enhanced cooling of the

ground due a steep temperature gradient, the change in albedo, and high emissivity that increases longwave emissions (Keller & Tamás, 2003). Snow disappearance date on the other hand exerts a strong influence on the ground thermal regime, with a later snow disappearance having a cooling effect on MAGST (Apaloo et al., 2012; Ge & Gong, 2010).

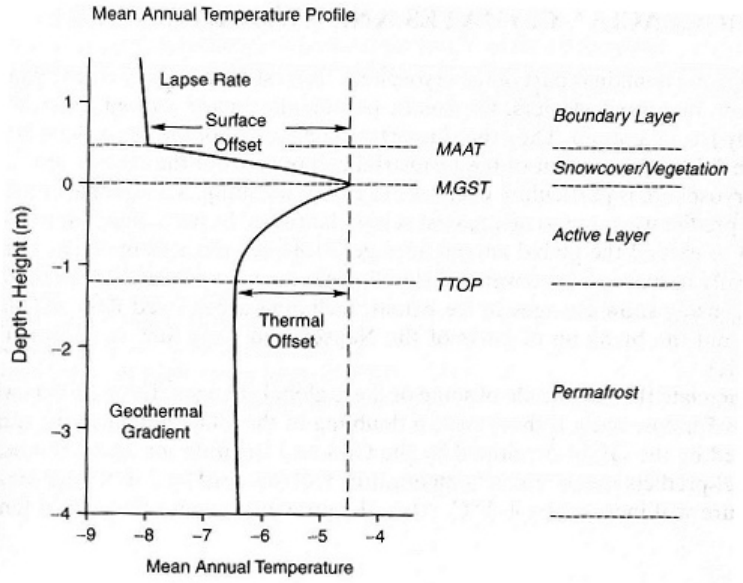

Figure 2.3: An illustration of the ground thermal regime of permafrost soils. MGST–Mean Ground Surface Temperature, MAAT–Mean Annual Air Temperature, TTOP–Temperature at Top of Permafrost (French, 2007; Smith & Riseborough, 1996)

2.3 State of knowledge in high mountain hydrology

Mountains are the cornerstone of global hydrological resources, providing 32-60% of total global discharge and as much as 95% in arid regions (Figure 2.4). As per Section 2.1, the amount of precipitation increases with elevation; high mountains can therefore be considered a critical sub-component in this relationship. In arid regions, more than half of mean annual discharge is estimated as originating in mountains. Major rivers to which mountains contribute 90% or more of mean annual discharge include Rio Negro, Nile, Amu Darya, Orange, Euphrates, and Colorado while the 75% of mean annual discharge in the Tigris, Indus, and São Francisco originates in mountains (Viviroli & Weingartner, 2004);

these regions are at latitudes within 15°of the atmospheric high pressure zones underneath the descending portion of global Hadley cells and may have relatively dry high mountain climates with the exception of the Indus basin, which is affected by the Indian monsoon (Figure 2.4).

Hydrological processes in high mountains take place above the ground to an extent greater than that in low elevation periglacial regions (Gardaz, 1998). Following this, the roles, processes, economic significance, climatic sensitivities, and pertinent analytical tools of mountain snow and glacier hydrology are intensively researched (e.g. Kasurak et al., 2011; Stewart, 2009; Barnett et al., 2005; Aizen et al., 1997). Snow and glaciers are generally considered the primary hydrological resources of high mountains. Their hydrological role is in the governance of temporal fluctuations of runoff by preventing direct precipitation–to–runoff, generally releasing stored water in spring and summer months (Jansson et al., 2003). The specifics of this are related to the local climatic conditions. Temporal scales relevant to these hydrological resources range from seasons to centuries (Figure 2.5).

The contributions of snow and glaciers to late spring – early summer discharge from mountains varies regionally. In the Austrian Alps the glacial contribution is estimated between 0% and 10% (Koboltschnig & Schöner, 2010) whereas glaciers contribute 50–70% in the Himalaya (Barnett et al., 2005); snowmelt from the Rockies is estimated to account for 50-80% of late spring – early summer streamflow in the Western United States (Stewart, 2009). Spatial variability within regions is notable (Verbunt et al., 2003).

Nival hydrological regimes dominate runoff in mountain regions, but much passes through the ground or high mountain sediments, some of which is stored and released throughout the year, but as much as half may reach streams during spring thaw through infiltration (McClymont et al., 2010). The present understanding of the processes controlling ground water storage and flow in high mountain environments is limited (Langston et al., 2011) but understanding of ground water systems in high mountain watersheds is increasing (e.g. McClymont et al., 2012; Hood et al., 2006). Furthermore, the timing of snowmelt runoff will shift to earlier parts of the year due to climate change with estimates on the order of 30 days (Barnett et al., 2005; Stewart, 2009), increasing the relative contribution of groundwater to lowland river discharge during summer months.

Hydrological modeling in high mountain environments is subject to many sources of uncertainty including spatial variability and measurement of calibration data, transferability of processes over scales, process parameterizations, sub-grid variability etc (Garambois et al., 2013; Verbunt et al., 2003; Klok et al., 2001; Bergström & Graham, 1998).

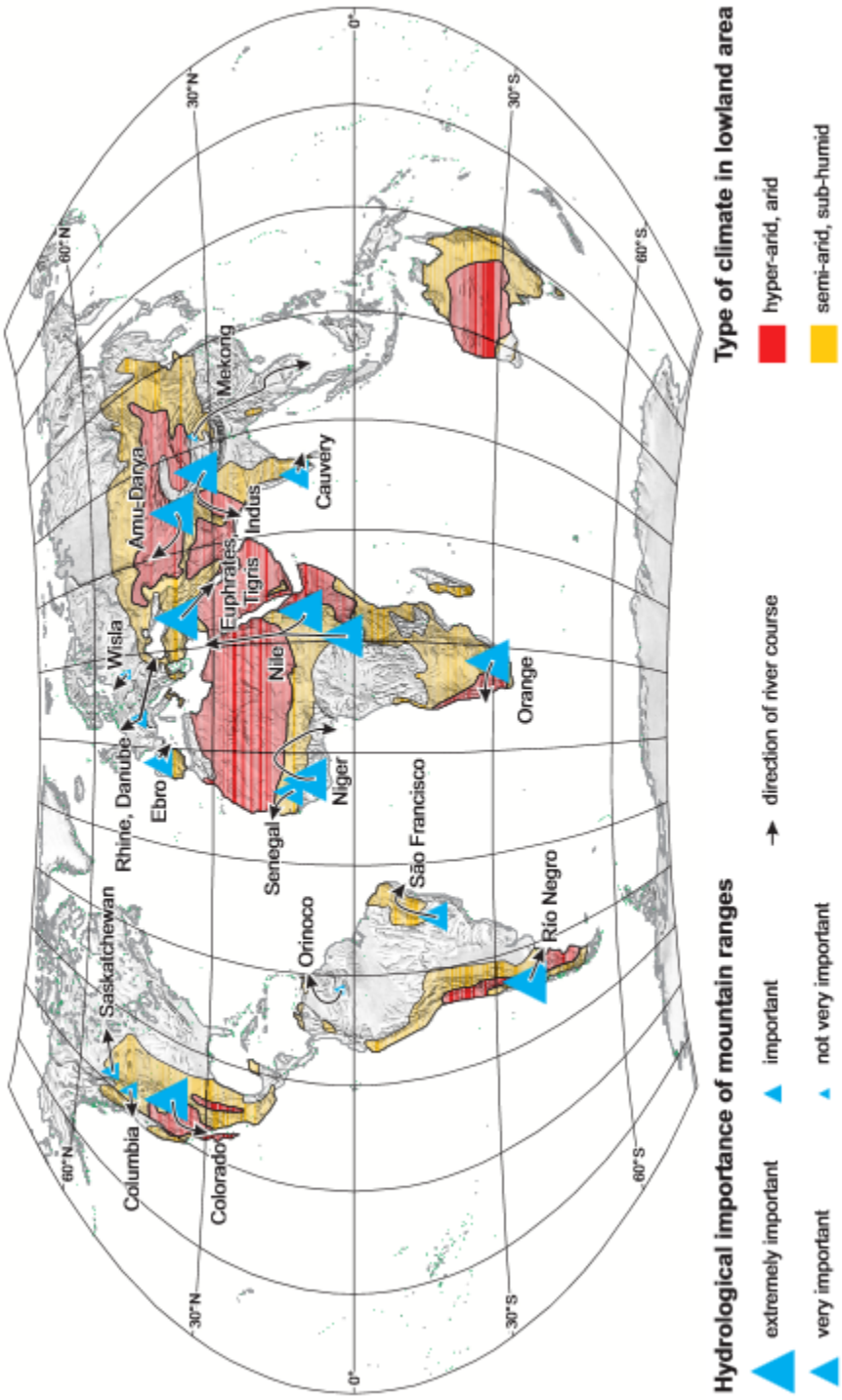

Figure 2.4: An illustration of the relative importance of mountain runoff to total river discharge for several important river basins across the world (Viviroli & Weingartner, 2004).

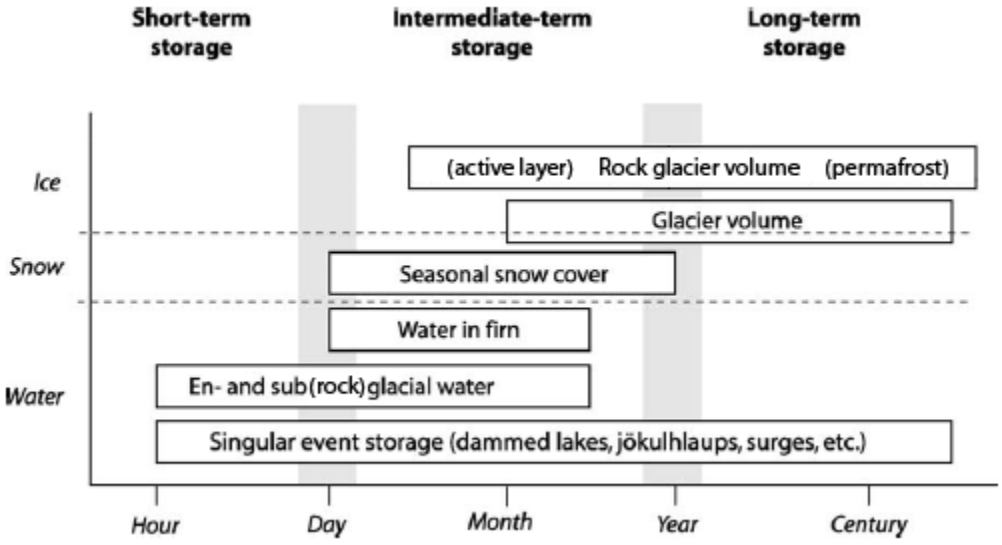

Figure 2.5: An illustration of the temporal scales of high mountain water storage in glaciers and snow cover modified after Jansson et al. (2003) to include rock glaciers.

Only recently have hydrological models differentiated the processes in glacierized and non-glacierized catchments (Jansson et al., 2003). With present day computing resources, it is unnecessary that such models omit the storage and transport of water in ice–debris landforms typical in high mountains. Ground ice is an especially important consideration in arid regions such as the Sierra Nevada and Arid Andes, where the contribution of glaciers is relatively small.

Observations support the case for hydrological significance of non–glacier ice in high mountains. The contribution of permafrost to autumn discharge in the Colorado Rockies has increased in past decades under atmospheric warming (Caine, 2010). In the Agua Negra Basin of Argentina ice in rock glaciers amounts to 70% of the ice found in glaciers, and rock glaciers and permafrost account for 30% of summer baseflow (Schrott, 1996). Across the border in the Agua Negra Basin of Chile, rock glaciers are estimated as accounting for 13% of annual streamflow (Croce & Milana, 2002). However, rock glaciers and high mountain permafrost have received little scientific investigation with regard to contributions to the hydrological system (Gardaz, 1998). The field is certainly growing (e.g. Krainer & Mostler, 2002; Favier et al., 2009; Azócar & Brenning, 2010, and Section 2.4.3), but additional work is required to bring the knowledge of these elements of the high mountain cyrosphere to that of snow and glaciers to inform future resource management efforts.

2.4 Rock Glaciers

Rock glaciers are found in high mountains and lowland periglacial areas around the world. Even in marginal high mountains, such the Appalachians of Maine, relict rock glaciers exist (Putnam & Putnam, 2009). The definition of a rock glacier has been disputed for the last few decades based on genetic and morphological criteria which were aligned with the perspectives (i.e. glacial and permafrost) of different researchers (Trombotto et al., 2008; Haeberli et al., 2006; Whalley & Palmer, 1998; Clark et al., 1998; Martin & Whalley, 1987). Along with debris–covered glaciers and ice–cored moraines, rock glaciers can be considered as an emergent property of ice-debris landforms (Berthling, 2011). Thus, adapting the definition of an emergent property (O'Connor, 1994), a rock glacier is a self-describing entity in that comes to existence by, and operates on, more fundamental processes or laws by which a rock glacier cannot [yet] be wholly characterized.

For the consideration of the hydrological significance of rock glaciers, a definition which has no semantic exclusions based on their ice origins, debris source, shape, etc, but effectively distinguishes rock glaciers from other ice-debris landforms is desired. Thus, a rock glacier is defined as the visible expression of long term creep of ice–rock mixtures under permafrost conditions (Berthling, 2011). Debris covered glaciers do not meet these criteria and are outside the scope of this discussion but they deserve similar consideration in hydrological models and bear some similarity to rock glaciers. The terms of the definition warrant some elaboration.

Permafrost is any ground which remains at or below 0°C for at least two consecutive years (French, 2007; Harris et al., 1988) – a necessary condition to support the existence of ice in rock glaciers. Thus rock glaciers have often been used as indicators of the presence of mountain permafrost in general (Bodin et al., 2010; Barsch, 1996). The variety of thermal conditions and soil (ice–rock matrix) types present in rock glaciers around the world is reviewed in Section 2.4.2.

The result of the permafrost and creep conditions yield the familiar rock glacier form (Figure 2.6). Relevant kinematic and deformational aspects of rock glaciers are reviewed in Section 2.4.4. Using creep velocity estimates, climate reconstructions, radiocarbon dating and other methods rock glaciers are commonly aged to the order of 10^3 years to 10^4 years old (Azócar & Brenning, 2010; Frauenfelder & Kääb, 2000; Haeberli et al., 1999; Palmentola et al., 1995). Rock glaciers also play a role in sediment storage and transport and are appreciable (∼20%) components of sediment budgets in high mountains (Otto et al., 2009; Brenning, 2005).

Rock glacier surfaces are characterized by ridges and furrows and unconsolidated debris of varying sizes. Fronts mark the lower limit of rock glaciers and can often be used to discriminate active and inactive rock glaciers, the distinction being that inactive rock glaciers are not undergoing creep due to topographic or debris supply changes (Figure 2.6 B; Barsch, 1996). Thus stable fronts of inactive rock glaciers may present lichens and slightly smaller slope angles than those of active rock glaciers (Burger et al., 1999). The activity status of rock glaciers can be inferred from remotely sensing and aerial imagery (Angillieri & Yanina, 2009). Amalgams of active and inactive rock glaciers are possible (e.g. Trombotto & Borzotta, 2009) and may be the result of climatic variability between conditions that support and inhibit rock glacier development (Wahrhaftig & Cox, 1959). Other complex rock glaciers may result from the convergence of individual rock glaciers (Bodin et al., 2010).

Relict rock glaciers are ice–free due to climatic change and as a result the physical properties of relict rock glaciers are appreciably different (e.g. gentle frontal slopes, abundant vegetation). They are useful indicators of paleoclimatic conditions (Aoyama, 2005) and may have some hydrological significance in terms of water pathways and aquifers, but are not widely considered an immediate water resource and further commentary on their characteristics is omitted.

2.4.1 Climatic and geomorphic controls

The presence of rock glaciers is governed by geomorphic and climatic factors. Geomorphic factors include local topography and nearby debris supplies. Talus slopes and glacial deposits alone or in combination provide debris (Kaufmann & Ladstädter, 2009; Kellerer-Pirklbauer et al., 2008; Chueca & Julián, 2005; Clark et al., 1998). Talus slopes are fed by weathering rock walls which are estimated to retreat at rates on the order of 10^{-1} mm a^{-1} to 10^{0} mm a^{-1} (Farbrot et al., 2007; Humlum, 2000), with retreat rates generally higher in relatively humid climates or along geological faults (Burger et al., 1999; André, 1994). Rock wall weathering rates also show some dependence on aspect and rock glaciers may prefer slopes under rock walls which receive higher solar radiation inputs due to higher weathering rates (Humlum, 2000). Rock glaciers form from debris of pebble to boulder particle sizes with large variation in particle size within any given rock glacier (Serrano et al., 2010, Table 1); source rock types include igneous, sedimentary, and metamorphic without discrimination (Ikeda & Matsuoka, 2006; Damm & Langer, 2006a; Burger et al., 1999).

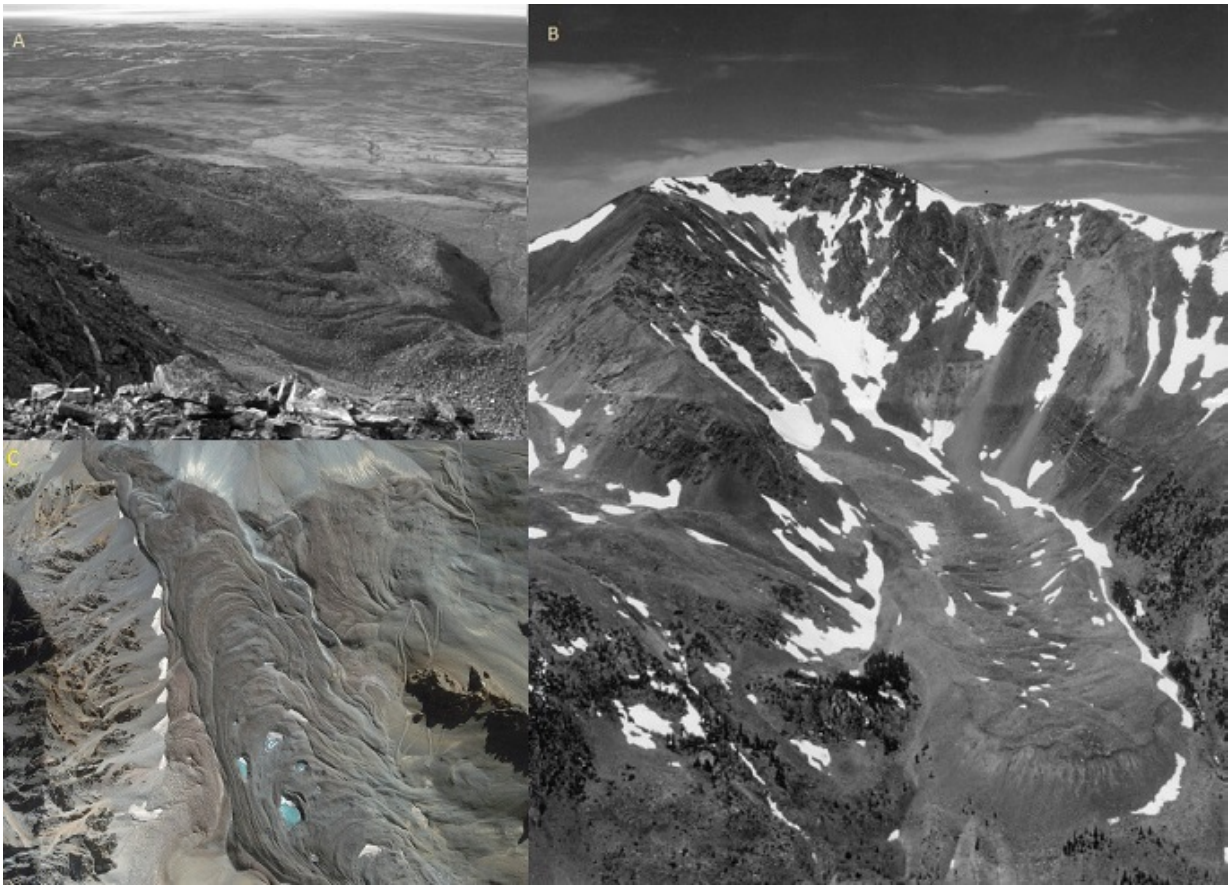

Figure 2.6: Examples of rock glaciers from A) Svalbard (Farbrot et al., 2005), B) California (Burger et al., 1999), and C) Chile (photo credit: Alex Brenning, Ikonos Imagery. C shows the characteristic ridges and furrows of rock glacier surfaces. The steep and well defined front of the rock glacier in B indicates its active status.

Relevant topographic variables include slope angle, curvature, aspect, elevation, size of the contributing area and interactions between the variables (Azócar & Brenning, 2010; Janke & Frauenfelder, 2008; Brenning & Trombotto, 2006). A sloped surface is necessary for the creep process. Rock glaciers are found on surfaces of many slope angles, and changes in slope angle along the length of a rock glacier also affect morphology due to debris convergence and divergence.

Regarding climatic factors, elevation is important as a proxy for mean annual air temperature (MAAT), which, in combination with local topoclimatic factors, must support

permafrost existence for the presence of rock glaciers. Rock glacier termini are commonly found at elevations with MAAT near or above 0°C (Baroni et al., 2004; Azócar & Brenning, 2010) where permafrost may not be expected. Gravitational transport of permafrost in rock glaciers into areas of relatively high MAAT and/or increased temperatures due to climatic variability or change are in part responsible for the azonal presence of permafrost. Cooler conditions are presumably required for rock glacier formation. Rock glacier presence may not be very sensitive to radiation as rock glaciers are found in areas with some of the highest solar radiation inputs in the world. Active layer thickness depends in part on solar radiation and snow cover characteristics (Croce & Milana, 2002).

Snow from perennial accumulations, avalanche deposits, firn, and/or glacial ice are incorporated into rock glaciers (see e.g. Serrano et al., 2010; Degenhardt, 2009, for evolution of rock glacier permafrost). Precipitation, or snow accumulation more precisely, must locally be less than that required for glaciation but otherwise is highly variable in rock glacier areas. In New Zealand annual precipitation totals near rock glaciers ranges from 800 to over 6000 mm, for example (Brazier et al., 1998). Regionally, temperature is the primary control on rock glacier presence, with the altitude of the 0 to 1 °C MAAT providing a good discriminator of rock glacier presence while the abundance of rock glaciers in higher elevations is inversely related to precipitation amounts (Payne, 1998; Azócar & Brenning, 2010). Thus in relatively arid regions, rock glaciers dominate the high mountain cryosphere and play a decreasing role as precipitation increases, but do not disappear entirely(Figure 2.7).

2.4.2 Physical properties

Rock glaciers come in a wide range of geometries which reduce to lobate, tongue shaped (i.e. length to width ratios), and complex forms, the last of which are typically amalgams of several basic rock glaciers (Johnson, 1998; Martin & Whalley, 1987; Wahrhaftig & Cox, 1959). Thickness is an additional important geometric aspect of rock glaciers and is critical for estimating rock glacier volumes (Azócar & Brenning, 2010). Geometries of several rock glaciers are summarized in Burger et al. (1999, Table 2); lengths range from 10 to 3500m, widths from 40 to 3000m, and thicknesses or frontal heights from 10 to 125 m. Mean slope angles along rock glacier profiles range from 5° to ∼50° (e.g. Janke & Frauenfelder, 2008; Giardino, 1979).

MAGST on rock glaciers is highly variable, even on individual rock glaciers. MAGST on a complex rock glacier in the Andes of Santiago ranged from +7.6 to -1.1 °C, for example (Apaloo et al., 2012). The thermal status of rock glacier depths is assessed using

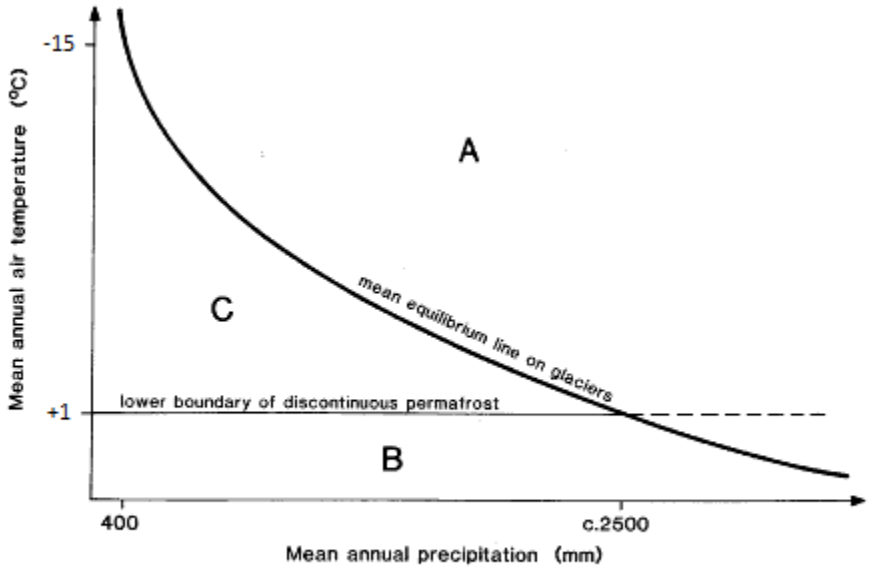

Figure 2.7: A) Glacier dominated, B) dry colluvium dominated, and C) rock glacier dominated climatic zones after (Brazier et al., 1998)

boreholes. The temperature profile through rock glacier permafrost may be near or well below 0 °C and depends on the temperature beneath the permafrost (near 0°C when liquid water is present, see below) and at the top of permafrost (Mühll et al., 2003). Zero–curtain temperatures are indicative of permafrost degradation (Monnier & Kinnard, 2013) as are increases of active layer depth or trends of increasing temperature in the rock glacier permafrost volume (Trombotto & Borzotta, 2009).

Physical properties of rock glacier interiors are often assessed with geophysical methods that rely on measurements of the acoustic, seismic, or electromagnetic properties of the rock glacier soil. Substantial differences in material properties enable the identification of permafrost, bedrock, and the active layer and some discrimination of the properties (i.e. ice, air, water, debris content) within each layer (Leopold et al., 2011; Maurer & Hauck, 2007; Ikeda, 2006). Boreholes may also be utilized to these ends. Application of such methods in complex high mountain terrain is a logistical and technical challenge and ensemble methods are recommended (Hausmann et al., 2012; Vonder Muhll et al., 2000).

Rock glacier soil profiles (Figure 2.8) show similar characteristics in rock glaciers around

the world. A four layer structure is typical with: 1) an active layer comprised of boulders or debris vertically sorted by size, 2) the permafrost layer with numerous varieties of ice types and ice volumetric fractions, and 3) a bottom layer which consists of either water at the melting point or ice–poor permafrost followed by 4) bedrock in the permafrost state (Leopold et al., 2011; Trombotto & Borzotta, 2009; Arenson et al., 2002; Elconin & Lachapelle, 1997; Zhu et al., 1996).

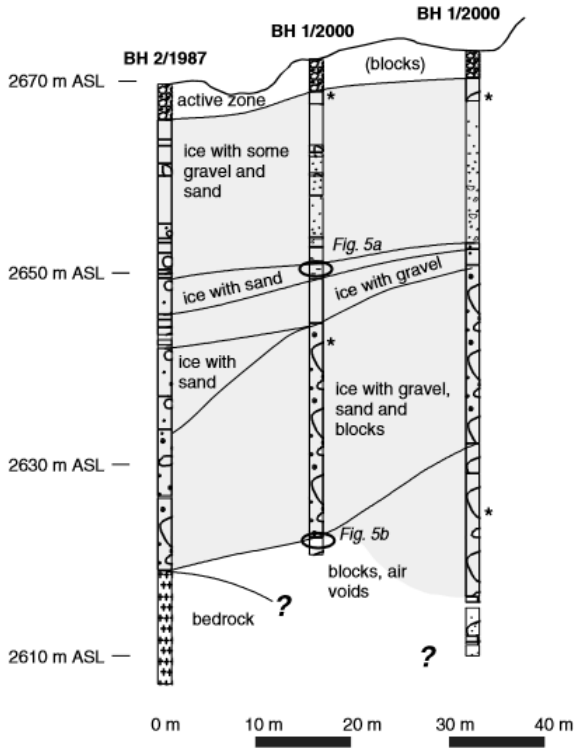

Figure 2.8: Borehole derived stratigraphy of Murtèl rock glacier showing the active layer, and layers of ice mixed with sand or gravel (Arenson et al., 2002)

The properties of the permafrost layer in rock glaciers are highly variable and substantial uncertainty is present; volumetric ice content may vary from 0% to 100% throughout the vertical profile (Figure 2.9) and median lower and upper total volumetric ice content estimates are 47% and 70% respectively (Brenning, 2010; Haeberli et al., 2006). Ice may be present in a massive form (glacier remnants), interstitially or melanged with debris, in alternating debris-ice layers (avalanche and debris inputs), and superimposed from active layer melt (Humlum et al., 2007; Hanson & Hoelzle, 2004; Ishikawa et al., 2001). Glacier ice

incorporated into rock glaciers need not remain in a massive form (Evin et al., 1997), and combinations of ice sources are typical in individual rock glaciers (Ribolini et al., 2010). The source rock may govern the soil profile to some degree, for example a pebbly rock glacier may tend to be more ice-cemented and slightly supersaturated with small ice lenses (Ikeda & Matsuoka, 2006). Along the rock glacier length, relatively low ice contents are typical in the rooting zone and at the front, and may be highest where the bedrock profile leads to convergence of water and debris (Hausmann et al., 2012; Burger et al., 1999). Liquid water may be present within the permafrost body while the volume of air bubbles is considered negligible (Barsch & Jakob, 1998).

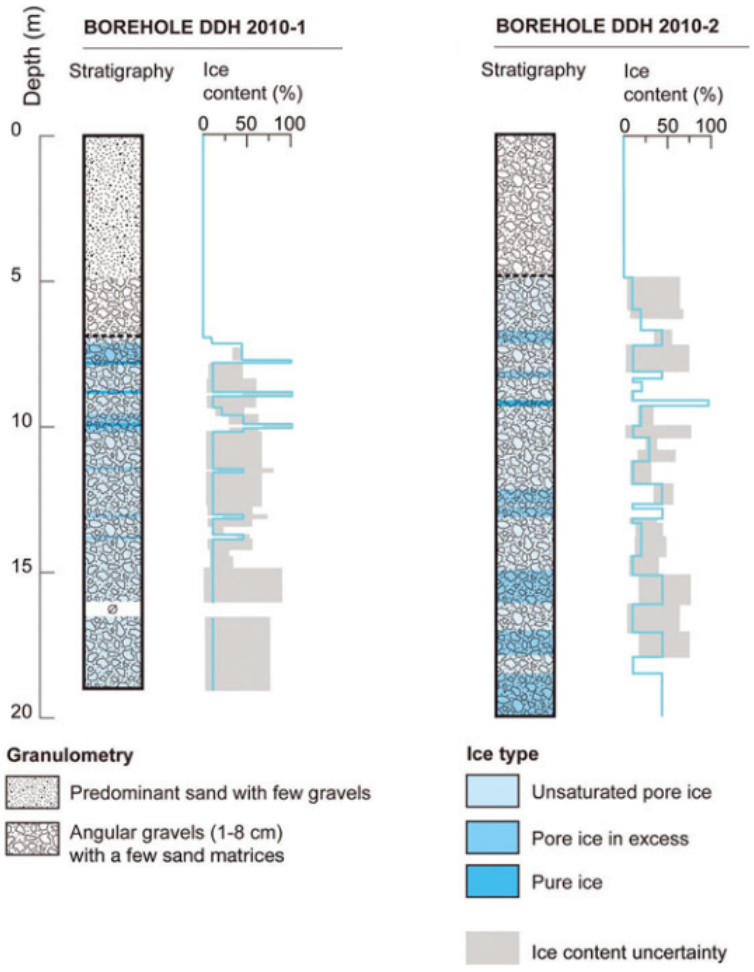

Figure 2.9: Borehole and GPR derived stratigraphy of Andean rock glacier after Monnier & Kinnard (2013)

2.4.3 Hydrological characteristics

At the scale of individual rock glaciers, inputs to the water balance include: direct precipitation, runoff, snow of various sources, massive ice, and ground water (Figure 2.11). Output modes include surface runoff, subsurface discharge, ice degradation, subsurface seepage, sublimation, evaporation (Figure 2.11).

The sources (e.g. direct and throughflow from snowmelt, ground or subpermafrost water) of discharge can be inferred with geochemical analysis (Williams et al., 2006). Discharge from rock glaciers may have diurnal variation due to weather conditions (Gardaz, 1998; Krainer & Mostler, 2002). The lag time of snowmelt and rainfall inputs are typically a few hours (Krainer & Mostler, 2002). The seasonal variation of rock glacier discharge and its primary sources are as follows (Williams et al., 2006; Krainer & Mostler, 2002; Burger et al., 1999):

- Autumn to late winter: active layer is frozen, discharge comes from groundwater beneath rock glacier
- Late spring to early summer: direct and throughflow from snowmelt
- Mid-summer: progression of active layer melt, groundwater beneath rock glacier, throughflow from summer rainfall
- Late summer to early autumn: minimal amounts from groundwater beneath rock glacier

The physical structure of rock glaciers relating to these discharge sources is shown in Figure 2.11. Prospects for future research include the development of continuous geophysical imaging which could help assess the temporal variability of rock glacier discharge and its sources (Leopold et al., 2011), and additional applications of geochemical signature analysis for the identification of flow sources and pathways in rock glaciers (Williams et al., 2006).

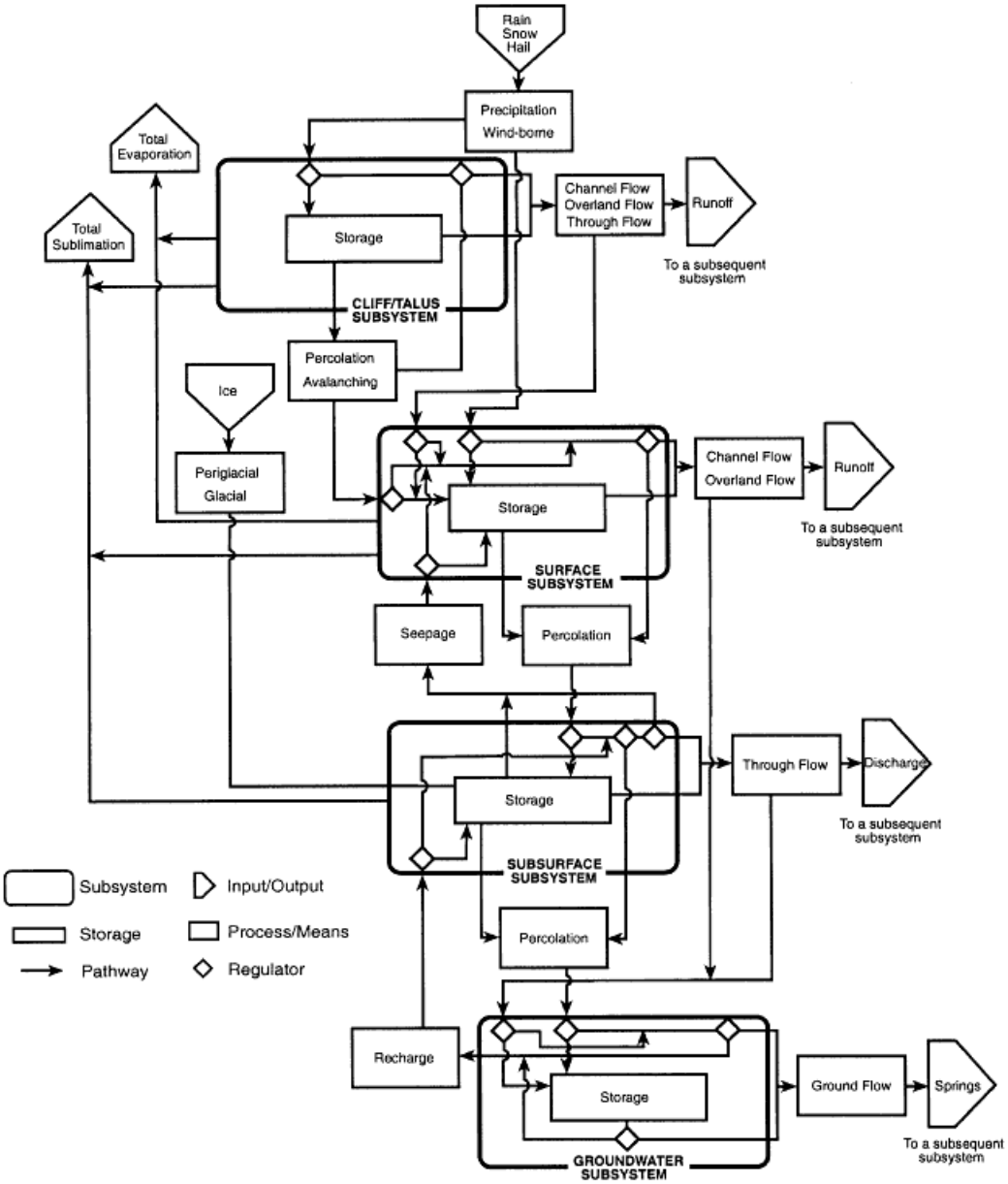

Figure 2.10: The complex cascading hydrological system of rock glacier from Burger et al. (1999).

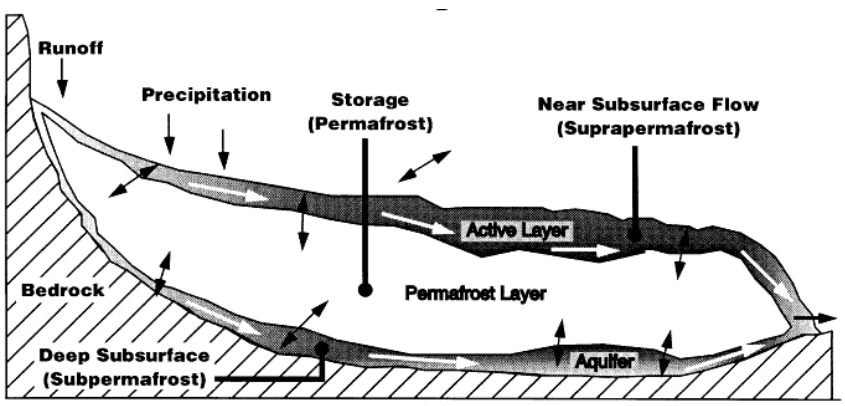

Figure 2.11: This figure visualizes the sources of rock glacier discharge (Burger et al., 1999). However, not all rock glaciers present an aquifer between the permafrost and bedrock (Zhu et al., 1996), perhaps due to climatic, topographic (i.e. bedrock curvature), or bedrock drainage characteristics

2.4.4 Kinematics

Rock glacier kinematics include vertical and horizontal surface movements, internal deformations, debris transfer between the active layer and permafrost body, and downslope movement of the entire rock glacier body (e.g. Serrano et al., 2010). The processes by which rock glacier movement occurs include massive and internal ice or debris–ice matrix creep and basal slippage (Burger et al., 1999). Basal slippage may be minimal on rock glaciers with dry bases (see previous two sections). Kinematic properties also relate to the state and dynamics of rock glacier permafrost, and importantly can be indicative of its degradation or aggradation (Roer et al., 2008; Ikeda et al., 2003). Catastrophic rock glacier collapses rarely occur but present a potent hazard due to debris volumes and may increase under a warming climate with more extreme weather events (Krysiecki et al., 2008).

Rock glacier creep rates vary from place to place and within individual forms. Long term creep can be assessed with in–situ or remotely sensed surveying methods while short term creep requires precise tools such as real-time kinematic GPS (Lambiel & Delaloye, 2004; Kääb et al., 1997; Wahrhaftig & Cox, 1959). Surface creep rates of a few centimetres to several tens of centimetres per year have been observed (Serrano et al., 2006; Koning & Smith, 1999). Vertical surface displacements are related to horizontal changes and are sensitive to the same factors. The creep rates of rock glaciers can change at millennial to seasonal time scales due to development of the rock glacier body and shifts in the climatic or geomorphic regime; creep rate changes on sub–seasonal time scales are not considered relevant to the long term evolution of rock glaciers (Kääb et al., 2007). Across a rock glacier surface, creep rate variability is on the same order as interannual variation of creep rates for individual points (Bodin et al., 2010; Avian et al., 2005).

Creep rates are controlled by lithology, topography, climate, and composition (Haeberli et al., 2006; Ikeda & Matsuoka, 2006). Within individual rock glaciers there is a tendency for increased surface creep rates slightly above slope angle increases of the underlying topography and at rock glacier fronts (Delaloye et al., 2008; Koning & Smith, 1999). Climate may exert a very regionalized control. For example, several rock glaciers in the Alps all display the same interannual variation of mean surface creep rates which are strongly correlated to MAGST with the lag of a few months, which also indicates that the observed creep fluctuations are related to changes in the conditions of the upper permafrost (Delaloye et al., 2008). Regarding the composition and thermal state of rock glaciers, creep rates are proportional to permafrost temperature and ice content, and rock glaciers close to 0°C are more sensitive to climate forcing due to the immediate contribution of energy inputs to latent heat (Kääb et al., 2007). Higher velocities have also been attributed to

thicker winter snow which can advect heat into, and effectively warms, the core of the permafrost body (Delaloye et al., 2008; Ikeda et al., 2008).

2.5 Climate change

The earth is undergoing unprecedented rates of climate change due to anthropogenic activities, principally the emission of carbon dioxide and other greenhouse gases into the atmosphere (Forster et al., 2007; Jones et al., 2007). Because of the high sensitivity of rock glaciers to climate, and to inform part of this work, it is pertinent to review some aspects of observed and forecasted climate change with emphasis on high mountains.

During the 20th century, the earth's mean surface temperature increased by 0.74°C, with the rate of warming in the latter half of the century double that of the first half (Jones et al., 2007). The frequency and severity of heat waves have increased as have daily minimum temperatures (faster than daily maximum temperatures), extreme and persistent cold conditions are on the decline. In the first decade of the 21st century, record heat has been observed around the world, and the decade is by far the hottest on record (Jones et al., 2007). No appreciable change in mean global precipitation occurred, but an increase in the frequency of heavy precipitation events has been recorded (Forster et al., 2007). The expectation is that these trends will continue and accelerate throughout this century (Meehl et al., 2007).

There are many uncertainties associated with regional deviations from these global predictions. The spatial scale of global climate models used in climate change forecasts is insufficient for resolving the effects of climate change within mountains, and the representation of topography (typically as the mean elevation within cells) may also not be effective in describing the effects of mountains on large-scale atmospheric processes (Beniston, 2006; Randall et al., 2007; Beniston et al., 1997). Regional climate models can use global climate model output as boundary conditions, but still suffer from inadequate resolution (Salzmann et al., 2007) while those which resolve greater spatial details are only applied in small areas due to the intense computational requirements (e.g. Lapp et al., 2005). Furthermore, there is an observational bias towards lowland areas and few mountain ranges are climatologically monitored with enough intensity to make use of statistical downscaling methods. Finally, the paucity of observation also makes validation of regional climate modeling efforts in mountain regions very difficult. Thus, mountains do not correspond well to the scientific forecasts on global climate change.

The Alps are an exception to the trend of limited observation in high mountains. Widespread systematic meteorological observation has been ongoing for decades, and records from a few sites include over 100 years of data (Beniston, 2006). Temperature anomalies in the Alps correspond to global anomalies since the 1950's and have been around 3 times the global anomaly since the 1980's. This may represent an elevational amplification of global warming in mountain regions as has been thought to occur with altitude in the troposphere (Santer et al., 2005). The persistence of the positive North Atlantic Oscillation state played a role in the observed warming (Beniston, 2006). Nonetheless, projections for the Alpine region predict warm humid winters, dry summers, increased frequency of heavy precipitation events, fewer cloudy days, and snow durations reduced by months by 2071-2100 (Beniston, 2006).

To extend the discussion it is necessary to consider environmental proxies (Beniston et al., 1997) for climatic conditions. Since the mid 19th century, mountain glaciers are losing volume and their negative mass balance trend accelerating in all mountains except the Himalaya (Scherler et al., 2011), indicating widespread warming at high elevations concurrent with global atmospheric conditions (Vuille et al., 2008; Haeberli et al., 2007; Hoelzle et al., 2007; Oerlemans, 2005; Rignot et al., 2003; Arendt et al., 2002; Dyurgerov & Meier, 2000). The regional and interannual variability of estimated mass balance among glaciers are high due to their sensitivity to precipitation and temperature conditions.

Permafrost on the other hand is slightly less sensitive to precipitation, or at least has indirect sensitivities through the effect of snow cover on the ground thermal regime. The response of permafrost to atmospheric warming includes active layer thickening, permafrost temperature increase, and basal melting (Haeberli, 1993). Fewer records of mountain permafrost than glaciers exist, but they indicate warming climate in the mountains of Europe and Scandinavia through increased active layer thickness and permafrost temperatures (Harris et al., 2009). However, one rock glacier borehole does not quite follow the trend of ice–poor permafrost boreholes, perhaps due to the massive latent heat demands and decoupling of the atmosphere from ground by the presence of coarse debris above the permafrost body (Figure 2.12). Rock glacier surface velocity accelerations have also been attributed to climatic warming (Bodin et al., 2009; Kääb et al., 2007) while catastophic rock glacier collapse has been observed and linked to climate change in at least one case at the lower limit of their presence in high mountains (Krysiecki et al., 2008). Destabilizations also have some correspondence with exceptionally warm years (Damm & Langer, 2006b).

The main considerations from this section is that warming is accelerating, and high mountains appear to be warming faster than global averages. Persistent heat waves and

increased daily minimum temperatures relative to climatic normals are expected. Precipitation is highly variable but more extreme events are expected. The elevation at which snow dominates will increase with warming temperatures. Longwave inputs from the atmosphere will increase due to higher greenhouse gas concentrations, and shortwave inputs may increase due to fewer cloudy days (Meehl et al., 2007). The Fifth Assessment Report of the Intergovernmental Panel on Climate Change is scheduled for release later this year (IPCC, 2013) and may shed new light on the present scientific consensus on climate change in high mountains.

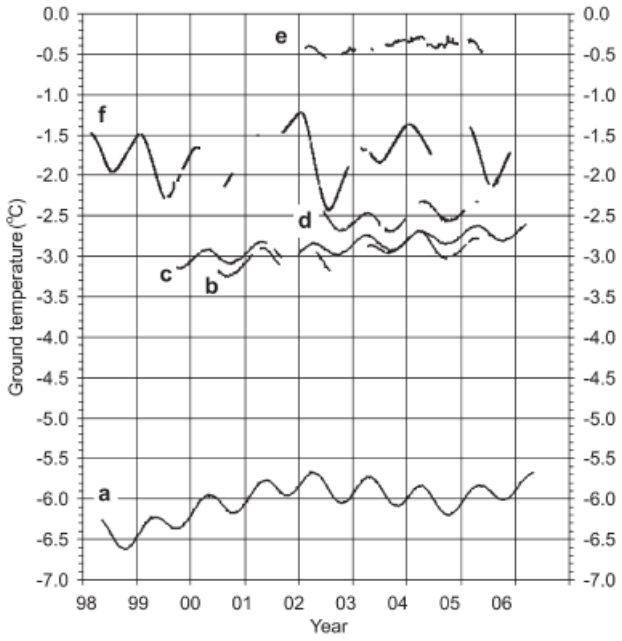

Figure 2.12: Ground temperature observations at the depth of 0.5°C annual amplutide at several permafrost boreholes in Europe, (f) is Murtèl-Corvatsch is the only rock glacier and is the only site not to show a temperature increase trend (from Harris et al., 2009)

2.6 Weather generators

Accurate meteorological data are required for numerous applications in environmental sciences and management. Observational data often suffer issues of inadequate spatial and temporal coverage, scope limitations, and completeness. Stochastic weather generators, or

weather generators, are tools which have been developed to address these issues. Weather generators have been applied in studies of crop management (Anwar et al., 2006), acid mine drainage (Annandale et al., 1999), and lake thermal properties (Uhlmann et al., 2012), among others, and have been proposed and developed as tools for downscaling of global climate model output (Fatichi et al., 2013; Charles et al., 1999; Semenov & Barrow, 1997). Weather generators also serve a pressing need in environmental sciences and management which is the provision of indefinitely long time series of plausible meteorological data under climate change scenarios (Wilks & Wilby, 1999).

Weather generators are a class of models which produce time-series of meteorological variables that strive to retain the observed statistical properties of an input/reference climate. Weather generators are stochastic (the term is inferred) models – they treat meteorological observations as the outcome of random variables, and weather as a random process. Dynamic meteorological models, which are used for weather forecasting rather than data generation, also produce meteorological variables but use explicit process descriptions and generally require more parameters and computing power (Srikanthan & McMahon, 2001). Intermediate–stochastic weather generators also treat meteorological observations as random variables, but the meteorological variables are linked in mimicry of the relevant process dependencies, rather than arbitrarily in terms of physical dependence as with simple weather generators.

Simple weather generators (e.g. CLIMGEN McKague et al., 2005) can be broken down into sub-models of precipitation occurrence, precipitation amounts, and additional variables. Precipitation occurrence is typically modeled as a Markov Process for which at least two parameters (transition probabilities) must be estimated or specified: the probability of precipitation on a day conditional on the previous day having precipitation and the probability of precipitation on a day conditional on the previous day having no precipitation (Wilks & Wilby, 1999). Another approach is explicit modeling of the run-lengths of wet or dry states in an alternating renewal process (Srikanthan & McMahon, 2001).

The Markovian approach to precipitation occurrence offers some useful extensions. Precipitation on a day can be conditioned on more than precipitation on the previous day. Higher order lags (i.e. precipitation occurrence two days previous) and synoptic scale atmospheric variables may be useful conditioning variables and improve the agreement between the observed and simulated variances, provided training data are sufficient (Katz & Parlange, 1998; Bardossy & Plate, 1991). Conditioning on atmospheric states is a particularly useful method as it can implicitly preserve some spatial dependence in multi-site weather generation and link weather generators to global climate model output (Srikanthan & McMahon, 2001).

Models of precipitation amounts on wet days utilize the exponential or two–parameter gamma distribution; the latter is generally favored for offering better representation of observations (Wilks & Wilby, 1999). Precipitation amounts on any given wet day are typically considered independent and identically distributed and attempts at efforts which explicitly incorporate persistence have yielded little improvement in the agreement between generated and observed data (Srikanthan & McMahon, 2001).

Additional meteorological variables such as daily extreme temperatures and solar radiation are also frequently required of weather generators. In simple weather generators, the standardized distributions of such non-precipitation variables are conditioned on precipitation occurrence and modeled as a multivariate linear autoregression of the first order (Srikanthan & McMahon, 2001), i.e. the variables are considered dependent on the previous day's values. A deviation term in the autoregression permits the generation of unique sequences and the relationships between meteorological variables are represented implicitly using coefficient matrices for the deviate and autoregressive terms (Wilks & Wilby, 1999). In the data generation, standard scores for these variables are converted to meteorological values using means and standard deviations that are allowed to vary seasonally through periodic functions or splines. The same approach is used for incorporation of seasonal variation of precipitation occurrence and amount. The autoregressive component does not consider seasonal variation in the interrelationships and deviances from mean conditions (Wilks & Wilby, 1999) which may be present (Guenni et al., 1990).

Further details and descriptions of variants on this classical approach to weather generation approach are available in Wilks & Wilby (1999); Richardson (1981). Resampling based weather generators are an additional option, but require more data than the 30 years recommended for parametric weather generators (Srikanthan & McMahon, 2001). The intermediate–stochastic approach differs appreciably (Section 3.2.1).

The quality assessment of weather generator output should extend beyond reproduction of variable means – comparisons of properties such as variance, skews, and run lengths or state survival curves are of additional importance (Wilks & Wilby, 1999). Typical weather generator shortcomings include underrepresented interannual variation of precipitation and over(under)-representation of short(long) run lengths of precipitation occurrence. Factors in these deficiencies include the possibility of non–stationary monthly climate (Chen et al., 2010) parameters and models which cannot describe the range of high or low frequency precipitation processes (Katz & Parlange, 1998). The conditioning of parameters on synoptic scale climatological factors addresses these assumptions and model limitations and can improve weather generator performance (Wilks & Wilby, 1999; Katz & Parlange, 1998).

Furthermore, no readily available weather generators consider the statistical significance of estimated parameters which may be of no consequence to most users primary concern in weather generator applications, i.e. the ability of the tools to replicate statistical moments and other properties of observed weather (Katz & Parlange, 1998), but parameter significance would inform model selection and specification. For example, seasonal parameters may be preferred over monthly parameters from a model parsimony standpoint, and could be justified with significance values or other assessments of parameter significance. Additionally, the number of parameters in many weather generator models practically ensures some are statistically insignificant per multiple testing (e.g. Benjamini & Hochberg, 1995) – a cause for concern. A generalized linear model approach to weather generation offers some solutions in this regard (Furrer & Katz, 2007) but other approaches are extendible (Charles et al., 1999).

Simple weather generators can be used to create daily, monthly, and annual frequency data. Hourly data on the other hand is not practical, but it also not required as input (Srikanthan & McMahon, 2001). Daily data can be disaggregated into hourly values (Safeeq & Fares, 2011) but performance suffers and disaggregation adds another stage to the modeling hierarchy at which uncertainty is generated. The intermediate–stochastic approach has some practical and philosophical advantages, including finer temporal resolution output and explicit representation of dependence structures in meteorological variables.

Weather generators can better serve local scale information needs than global or regional climate models which are suited to the simulation of meso to macro scale climatic processes but may have insufficient detail for, e.g. watershed impact studies (Srikanthan & McMahon, 2001; Semenov & Barrow, 1997; Wilks, 1992). They are therefore used to produce meteorological data under climate change scenarios simply by manipulating parameters arbitrarily or based on readily available scenarios from global or regional climate model output (Figure 2.13). An advantage of weather generators in this regard is the ability to manipulate climatic variability in addition to means, which are often available at the monthly level from global climate model outputs and suitable for direct usage in weather generator models (Wilks, 1992). A caveat of this procedure is the possibility of unintended changes in climatic statistics in unmanipulated variables (Katz, 1996).

An alternative to direct manipulation of weather generator model parameters is the conditioning of the model parameters on synoptic atmospheric states in non-homogeneous hidden Markov models (Bellone et al., 2000, e.g.). Such a method requires the classification of atmospheric states and additional data, but the results may perform slightly better in representation of actual weather under reference and changed climates since extreme events

and higher order climate statistics can be better characterized with the use of such weather-state models (Bellone et al., 2000; Charles et al., 1999). For climate scenarios, the climatic shift of the data is provided by using global climate model output as atmospheric states, but the quality of the global climate model output is critical, and time series of arbitrary length cannot be simulated.

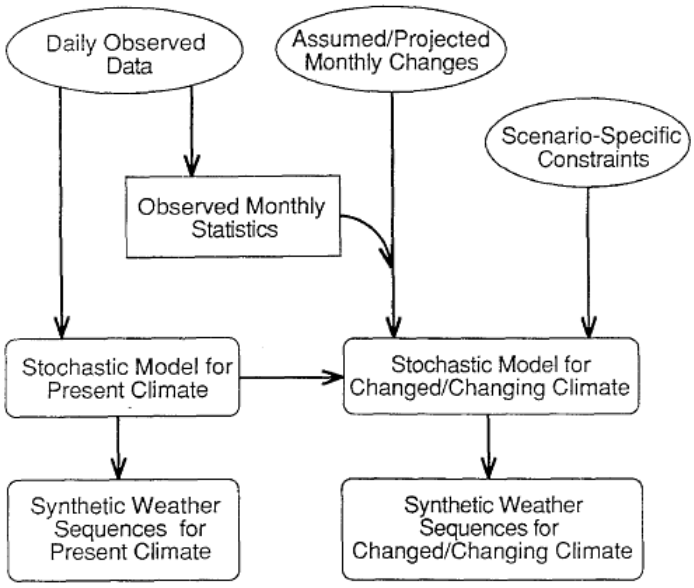

Figure 2.13: Schematic of the use of weather generators to simulate meteorological data under observed and alternative climates (Wilks, 1992).

2.7 Permafrost models

A model is essentially a representation of a phenomenon which serves as a tool for reasoning, evaluation, and hypothesis testing (Riseborough et al., 2008). The value of a model depends on its purpose–specific utility, an important factor in model selection in addition to available computational resources and the availability and requirements of data. Permafrost models describe thermal characteristics of the ground and can be categorized into process–oriented, empirical–stochastic, and multi–criteria types.

Multi criteria methods refer to overlays in geographic information systems software (Riseborough et al., 2008); such models produce qualitative indices of permafrost favorabil-

ity and reasonable representations of permafrost distribution at the local or broader scales, but suffer from the subjectivity of the index definition and the drawbacks of empirical–stochastic models described below (e.g. Etzelmüller et al., 2006).

Empirical–stochastic models relate (directly, or by a proxy) permafrost presence or absence to topoclimatic factors using statistical models which optimize the representation of a permafrost property response variable based on some defined explanatory variable (e.g. elevation, slope angle). The response variable may be permafrost probability (or logits, more precisely) in logistic-regression models, or basal temperature of winter snowpack, or MAGST in linear regression models which can be used as permafrost indicators (Boeckli et al., 2012; Apaloo et al., 2012; Li et al., 2009; Julián & Chueca, 2007; Lewkowicz & Ednie, 2004; Gruber & Hoelzle, 2001). Machine learning techniques can also be used for permafrost modeling based on such explanatory variables but are not widely applied (Hjort & Marmion, 2009; Leverington & Duguay, 1997).

Data requirements for empirical–stochastic models are low: a training data set of the response variable and a digital elevation model are sufficient (Etzelmüller et al., 2001b). Another advantage of such models is the treatment of uncertainty in permafrost proxy or permafrost occurrence within well known statistical frameworks. Thus they are particularly useful for spatial modeling of permafrost occurrence in high mountains where topoclimatic factors exert a strong control on permafrost occurrence across catchment to regional spatial scales. Intelligent sampling, or more sophisticated modeling techniques are required in order to avoid sampling pitfalls (Brenning et al., 2005). The major limitations of such models are the assumption of equilibrium between climate and permafrost, the omission of permafrost conditions at depth, inapplicability of fitted models outside of the reference domain, and the practical limitation of one response variable (Harris et al., 2009).

Process–oriented models can overcome the limitations of empirical–stochastic models at the expense of computational and input data requirements through use of the physical laws which govern the ground thermal regime. The basis for such models is the second law of heat conduction, a partial differential equation given in one dimension for isotropic material by

$$C\frac{\partial T}{\partial t} = K\frac{\partial^2 T}{\partial z^2} \tag{2.3}$$

where C is the volumetric heat capacity [J m^{-3} K^{-1}], K thermal conductivity [W m^{-1} k^{-1}], T is temperature [K], and t [s] and z [m] are time and depth respectively. Freezing

and thawing in permafrost soils require the consideration of latent heat, modifying the heat capacity term in Equation 2.3 (Riseborough et al., 2008). The interest is in solving the heat equation at some time and point in the material; for this there are two approaches. The first is analytical solutions, which require simplifications of real world variables such as the atmospheric temperature to a defined function (e.g. sinusoidal) and the assumption of uniform soil materials (Riseborough et al., 2008). The Kudryavtsev model uses such a solution and provides the annual depth of thaw and the mean annual temperature at the bottom of the active layer (Riseborough et al., 2008); the temperature at the top of permafrost model extends the Kudryavstev model to estimate temperature at the top of permafrost – an important indicator of the permafrost state under the assumption of primarily conductive heat transfer within the permafrost (Smith & Riseborough, 1996).

Although agreement has been observed between the temperature at the top of permafrost model and more sophisticated methods (described below), models based on analytical solutions to the heat equation provide limited characteristics of the ground thermal regime, rely on the assumption of a steady-state periodic thermal regime in the ground, and drastically simplify atmospheric and soil properties such that their use is limited to mapping purposes and tenuous inferences regarding real-world permafrost dynamics (Wright et al., 2003; Smith & Riseborough, 2002; Henry & Smith, 2001). Furthermore, they are of limited utility in high mountain scenarios where interannual and spatial variability of the boundary condition limits the representativeness of N-factors or other boundary layer simplifications (Juliussen & Humlum, 2007). However, the formulation and outputs of analytical solutions are exact (although their inputs are not) and data requirements are on par with empirical–stochastic models while having an explicit basis in physical processes. Data requirements are also relatively low compared to the second approach to solving the heat equation – i.e. numerical approximations, which offer full transient permafrost dynamics.

The research approaches in mountain permafrost modeling are shifting from an empirical–stochastic one to a numerical one (Harris et al., 2009) in favor of their full characterization of the ground properties, boundary conditions, and ultimately the transient thermal regime largely thanks to the present ubiquity of high power distributed computing resources. After Riseborough et al. (2008), the standard approach for numerical permafrost modeling is as follows

1. Define the modeled space: an initiation and end time, and upper and lower boundaries.

2. Set discretizations of time (time step) and space (soil column).

3. Specify the thermal properties of the soil materials for each point in the soil column.
4. Specify the boundary conditions for each time step.
5. Specify an initial temperature for every point in the soil column.
6. Calculate the temperature profile for each time step based on the combination of thermal properties, antecedent, and boundary conditions.

Depth and time dicretizations of 0.02 metres and 1 hour or less are recommended for accuracy with the Goodrich numerical model, especially with increasing rates of active layer thawing (Romanovsky et al., 1997). An exponential relationship for the soil discretization allows for increasing layer thickness with depth, which is useful due to the thermal signal attenuation with depth and allows effective use of computational resources (e.g. Gubler et al., 2013). The total soil depth should exceed the depth at which thermal signals are attenuated for the modeled time scale according to the following relationship (Alexeev et al., 2007)

$$h \approx \sqrt{d_0 n} \tag{2.4}$$

where d_0 is a diffusion coefficient (ratio of the conductivity to heat capacity) which varies from 1 to 20 for most soils and n is the number of years. This has not been tested for ice-rich permafrost, i.e. rock glacier soils.

Some numerical permafrost modeling applications simplify the atmospheric boundary and snow conditions, which can be useful for sensitivity analyses (Goodrich, 1982) but overlooks possible real world complexities. An explicit description of the boundary layer energy exchanges and processes (e.g. snow accumulation, surface energy balance) is most characteristic of real world conditions but necessitates high quality meteorological data. The same applies to the thermal and, where considered, hydraulic properties of the soil column. The boundary condition for the bottom of the soil column may be the geothermal or zero heat flux (Goodrich, 1982; Lawrence et al., 2008), the latter of which does not reduce simulation accuracy (Zhang et al., 2008).

Calculation of temperature profile based on Equation 2.3 is achieved with finite element (e.g. Zhang et al., 2005) or difference (e.g. DallAmico et al., 2011) methods. For simplicity,

some numerical models only consider conductive heat transfer (e.g. Zhang et al., 2005), but the non-conductive heat transfer (e.g. water infiltration) may play an important role in rock glaciers. Such heat transfer mechanisms have been included in recent numerical permafrost modeling applications (Ling & Zhang, 2004; Scherler et al., 2010; DallAmico et al., 2011; Jiang et al., 2012).

Numerical models can transcend spatial scale, being applicable at micro and thus across broader scales when distributed (Etzelmüller et al., 2001a, Figure 2), but spatial applications are limited due to computational complexity and the need for local meteorological and soil information. Computational complexity can be addressed with a subgrid methodology (Fiddes & Gruber, 2012) but accurate soil information and meteorological inputs are still required. Others use them at large resolution 25-60 km with gridded climate data (Marchenko et al., 2008), but this approach is limited in high mountain context due to spatial variation of the boundary condition associated with topoclimatic forcing. Another limitation of local scale numerical permafrost modeling in high mountains is the practical computational limitation to one-dimensional, as lateral heat fluxes may affect permafrost dynamics in complex terrain (e.g. Noetzli & Gruber, 2009).

Uncertainty is an important aspect of process–oriented permafrost models (Harris et al., 2009), but unlike in empirical–statistical models its formulations are not inherent. For process–oriented models it can be assessed through a model's sensitivity to its own parameters which can be treated within the model (Gubler et al., 2013). A statistical formulation which explicitly includes parameter uncertainty of a process-oriented permafrost model is available in Blanchet & Davison (2012). Numerical models can be validated against borehole data (Scherler et al., 2010) and compared with analytical solutions for simplified cases (DallAmico et al., 2011; Romanovsky et al., 1997).

2.8 Summary

Mountains provide approximately half of the world's fresh water resources through nival and glacial dominated hydrological regimes. These aspects of high mountain hydrology are well studied but research gaps exist in the role of groundwater, particularly with respect to water in ice-debris landforms, which have longer lags than glaciers to climate change and play an important hydrological role in summer months.

Mountains are characterized by highly variable climates due to elevational gradients, interactions with synoptic scale atmospheric motions, and topographic variability. The

knowledge on climate change in high mountains is very limited and subject to much uncertainty. Based on a small host of observations, glacier mass balances, and permafrost dynamics, it is reasonable to believe nonetheless that high mountain climates are warming in correspondence with global trends, with an elevational amplification dependent on regional and local factors. Additionally regardless of the degree to which regional to synoptic scale forcings of climatic variability are responsible for observed climatic changes in high mountains, an improved understanding and capacity to make high mountain climate projections benefits watershed management efforts.

Rock glaciers are particularly interesting ice-debris landforms for their abundance and omission from hydrological models. Rock glaciers are highly complex and spatially variable landforms with the primary controls being geomorphic and climatic processes. Rock glaciers are more sensitive to climatic conditions, due to the relatively higher variability of climatic over geomorphic processes, with the main controls on rock glacier distribution being the elevation of 0°C mean annual air temperature. The hydrological component of interest in rock glaciers is ice-rich permafrost, the sensitivities of which to climatic conditions are poorly known. Greater understanding of the hydrological processes and sensitives, which are directly related to thermal states through the necessity of permafrost conditions, could benefit the parameterization of rock glaciers in distributed hydrological models.

Numerical permafrost models may be useful tools for assessing the thermo–hydrological sensitivities of rock glaciers to climatic and topographic factors, provided realistic boundary conditions can be described. Such models are seeing increasing application in mountain regions. Weather generators can be used to produce meteorological data for input to process-based environmental models if sufficient and quality reference data is available; they have immediate and practical extensions to use for climate change scenarios. However, few applications of weather generators exist in high mountain environments.

Chapter 3

Methods

3.1 Overview

This work examines the seasonal and interannual water balance and thermal regime of rock glaciers, and their potential response to climate change, using the numerical water and energy balance model GEOtop (Endrizzi & Gruber, forthcoming; Rigon et al., 2006). Given the infancy of numerical permafrost modeling in high mountains, lack of applications to rock glaciers, shortage of observation of rock glacier hydraulic and thermal properties, and paucity of weather observations in rock glacier environments, the research is of an exploratory nature.

Rock glacier soils are simplified at this stage in order to demonstrate the feasibility of the methods for future application to real world rock glaciers. Pseudo–random time series of weather variables are generated with the intermediate–stochastic weather generator Advanced WEather GENerator (AWE-GEN) under present day and several alternative climatic scenarios and are used as the boundary condition of the rock glacier simulations. The weather generator model is fit to observations from Piz Corvatsch in the Upper Engadin Valley of Eastern Switzerland, just a kilometre from the intensively researched Murtèl–Corvatsch rock glacier. Some context for the Alpine climate is presented to serve the quality assessment and discussion of the generated weather data. An overview of the methods is provided in Figure 3.1.

This simulation study is based in the geographic context of the Murtèl-Corvatsch rock glacier near Piz Corvatsch in the Upper Engadin Valley of Eastern Switzerland. This

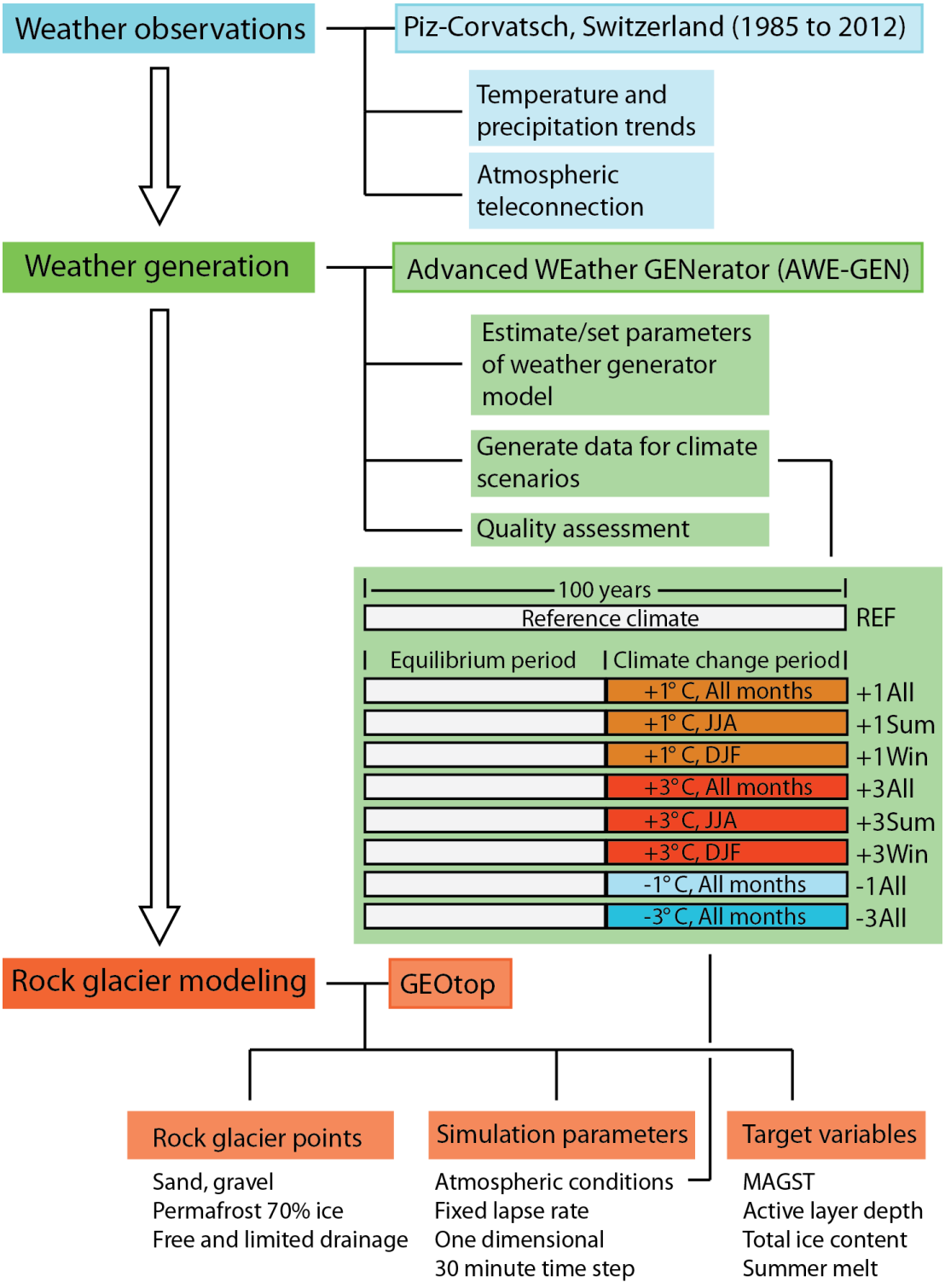

Figure 3.1: Flow chart of the methods and tools utilized in this work

site boasts extensive geomorpholgical (Wagner, 1992), ground-thermal (Hoelzle & Gruber, 2008; Hoelzle et al., 2003, 1999), geophysical (Salzmann et al., 2007; Vonder Mühll & Klingelé, 1994), and additional observations (e.g. Haeberli et al., 1999). It is the most thoroughly investigated rock glacier in the world (Arenson et al., 2010) and has decades of climatological observations recorded by the Swiss Federal Office of Meteorology and Climatology (MeteoSwiss), thus Murtèl-Corvatsch offers an excellent basis for this study.

3.1.1 Regional climatic context

The climate of Switzerland varies from temperate to continental in both the lowland and high Alpine areas; this is due to the physical influence of the Alps combined with interacting continental, polar, and Mediterranean air masses (Beniston, 2006; Sturman & Wanner, 2001; Beniston et al., 1994). South central Switzerland lies at the convergence of bands of high mean annual precipitation which run east to west on the north and south flanks of the Alpine divide (Barry, 2008, p. 388). Mean annual precipitation ranged from approximately 500 mm w.e. in continental lowlands and continental high alpine areas to 2300 mm w.e. in humid high Alpine areas during the period 1971 to 1990 (Beniston et al., 1994; Barry, 2008, p. 392). The seasonality of precipitation amounts also varies within the country with a summer maximum present in the continental zones of the southeastern part of the Alps and in the inner Alpine valleys whereas the central Swiss Alps have relatively consistent precipitation through the seasons while a double (spring and autumn) maximum occurs to the south (Beniston, 2006; Barry, 2008, p. 387). The seasonality of air temperature is fairly uniform across the country and local values are primarily dependent on elevation with night time and short term deviations due to the effects of inversions in many valleys below 1000 m a.s.l. (Beniston, 2006).

In the observational record (1864-present), the climate of Switzerland was fairly stable prior to 1970, with the exception of a notable warm period during the 1940's and relatively high variance of temperature in the summer half of the year (Bader & Bantle, 2004). Since 1970, climate in Switzerland has undergone marked changes (Beniston, 2006); mean temperatures during the summer and winter periods have increased, daily minimum (nocturnal) temperatures are especially affected, and total winter precipitation and the frequency of summer-time heavy precipitation events are on the rise (Beniston et al., 1994).

Since 1864, the trends in mean annual temperature have been $+0.0123°C\ a^{-1}$ and $+0.009°C\ a^{-1}$ in North and South Switzerland respectively (MeteoSwiss, 2013). Seasonal

trends are consistent, with slightly greater and smaller trends for the winter (Dec, Jan, Feb) and summer (Jun, Jul, Aug) season respectively. From 1961 to present the trends in mean annual temperature for both the north and south parts of the country were approximately 4 times greater: $+0.040°C\ a^{-1}$ and $+0.039°C\ a^{-1}$in the north and south respectively.

Seasonality in the temperature trends has been more pronounced during the 1961-present time period and is not consistent with the 1864-present trends; spring and summer trends since 1961 were higher than (approximately double) those of fall and winter for both the north and south regions of the country (MeteoSwiss, 2013). All of these temperature trends are highly significant (p–value < 0.001) except for the trend of the winter months in Northern Switzerland (p–value $= 0.022$).

Except for winter precipitation in Northern Switzerland from 1864–present, which had a $+2.4$ mm a^{-1} trend (p–value $= 0.001$), there were no statistically significant (i.e. p–value > 0.1) trends in annual or seasonal precipitation at the regional or national scale since 1864 or 1961 (MeteoSwiss, 2013; Beniston et al., 1994).

A strong link between synoptic and regional climates in Switzerland exists through the North–Atlantic Oscillation (NAO) which yields persistent blocking episodes and high pressure anomalies especially in winter and autumn months (Beniston et al., 1994). It is not present in all years but was especially strong during the 1980's. However, the mountains themselves limit the influence of the NAO southward where Mediterranean air masses exert a strong influence (Beniston et al., 1994).

3.2 Weather generation

This study required weather data which allows for evaluation of hydrological and thermal permafrost dynamics in a numerical permafrost model. The primary requirements the weather generator utilized in this work are the treatment of all GEOtop meteorological variables at the hourly level with the possibility of generation of weather data under climate change scenarios.

AWE-GEN is a recent weather generator, an extension of the weather generator presented in Ivanov et al. (2007), which implements the rarely applied but powerful intermediate–stochastic framework. Such a model includes more explicit descriptions of the physical processes involved in weather outcomes than the basic stochastic weather generator described in Section 2.6. Intermediate–stochastic models also facilitate the finer temporal

resolution unique to AWE-GEN among current daily stochastic weather generators, the rest of which would require disaggregation and do not treat all the weather variables required by GEOtop (e.g. CLIMGEN, LARS-WG, WGEN Semenov et al., 2002; Nelson, 2002; Richardson & Wright, 1984). The approach to weather generation by AWE-GEN is summarized below; full technical details are available in Fatichi et al. (2011a).

The quality of the weather data is assessed as described in Section 3.2.3. The quality assessment is basic and pertains simply to the reproduction of statistical characteristics of the observational data set, the most common requirement of weather generators (Katz & Parlange, 1998). Extended investigation regarding the application of AWE-GEN, with its heavily parameterized approach and the possible implications of statistical significance thereto are outside the scope of this work.

3.2.1 AWE-GEN

Precipitation in AWE-GEN is modeled with the Neyman-Scott Rectangular Pulse (NSRP) Poisson cluster model. Wet and dry days are not modeled explicitly as with a two-state Markov chain, but follow from aggregation of the hourly precipitation. Hourly precipitation is simulated with the NSRP, which creates pulses (representing weather cells) of random number, intensity, and duration (Fatichi et al., 2011a). Storm origins are modeled as a Poisson process and for each storm a number of cells are generated with a geometric distribution. Exponential distributions are used for the delay of the cell from the storm origin and the cell duration, while rainfall intensity in the cell is modeled with a two-parameter Gamma distribution. This method is known to perform well in replicating precipitation characteristics from long time scales to extreme events in temperate mid-latitude climates (Burton et al., 2008).

The NSRP model is coupled to an autoregressive model of the first order which works toward preservation of the annual mean and variability in the generated rainfall. In AWE-GEN, the precipitation is generated one year at a time (Fatichi et al., 2011a). Each year of hourly precipitation from the NSRP model is compared with the total annual precipitation generated by the autoregressive model, and accepted only if it is within a certain fractional tolerance. Otherwise a new year-long series of hourly precipitation is generated with the NSRP, and the process repeated. This process can be very time consuming and routines exist in AWE-GEN to correct the closest NSRP result to the years annual rainfall from the autoregressive model with a correction factor if no satisfactory results are yielded by the NSRP after a specified number of iterations (Fatichi et al., 2011a).

In AWE-GEN air temperature is modeled as the sum of a stochastic and deterministic component (Fatichi et al., 2011a). The latter is related to the air temperature and incoming long-wave radiation which relates back to the cloud cover. The deterministic component also depends on solar radiation which is calculated explicitly based on geographic location and the position of the sun in the sky. The deterministic cycle of air temperature is modified by random perturbations that are generated based on the mean and variance of observed air temperature residuals, which are estimated for each hour of the day for each month (Fatichi et al., 2011a). Air temperature is generated solely by its stochastic component when its correlations with its deterministic components are weak (in this case, parameters for the deterministic component cannot be estimated).

Relative humidity is generated via modeling of vapour pressure deficit in the same fashion as that of temperature, i.e. with deterministic and stochastic components. For vapour pressure, the deterministic component is regression of vapour pressure on a cubic function of the immediate temperature and 1-hour and 2-hour lags of shortwave radiation (Fatichi et al., 2011a). The deterministic component is again rested from observed data to estimate the parameters of the stochastic component. Atmospheric vapour pressure and relative humidity are obtained from the resultant vapour pressure deficit and saturation vapour pressure. The assumptions of the approach rely on a stable atmosphere without the interaction of air masses (Fatichi et al., 2011a). The method has some bias towards extremes (0 and 1 relative humidity) due to the presence of overshoots and subsequent correction to the limits.

Wind speed is modeled through its weak correlation with lagged solar radiation as a proxy for the winds induced through dissipation of sensible heat from the ground surface (Fatichi et al., 2011a). This proxy does not hold in environments with strong advective processes (e.g. exposure to free atmosphere in high mountains). The same approach is used for wind speed as for temperature and relative humidity described above: a deterministic component (i.e. regression coefficients for a linear model using 0 to 3 hour lagged solar radiation) and a stochastic component with parameters represented by an autoregressive model of the first order for the hours of the day with a transformation to preserve the skew typically observed in wind speed data (Fatichi et al., 2011a). Wind speed parameters are estimated on an annual basis so that the only seasonality incorporated corresponds to that of solar radiation (Fatichi et al., 2011a). In the case of small correlations with observed data, the stochastic component dominates the wind speed model.

During storms as generated with the NSRP module, cloud fraction is assumed to be equal to 1 (Fatichi et al., 2011a) whereas cloud fraction is assumed stationary and modeled by its first two statistical moments (mean and variance) during inter-storm periods. In

transition periods between storm and fair–weather conditions, the reduction of cloud fraction is modeled with the exponential function. AWE-GEN uses cloud fraction and some assumptions on atmospheric transmittance properties to calculate solar radiation with a fully deterministic model (Fatichi et al., 2011a). Air pressure uses an autoregressive model of the first order, but with no deterministic linkages and parameters which are estimated on an annual basis (i.e. without seasonality). Generation with AWE-GEN requires 1280 parameters in total, which must be estimated from observations or otherwise specified (Fatichi et al., 2011b).

Regarding the generation of weather data for climate change scenarios, it is possible to link AWE-GEN to global climate models from which numerous factors of change for statistical moments of weather variables can be derived using a Bayesian approach (Fatichi et al., 2011c, 2013). In this work, a simple approach readily available in AWE-GEN is used in which data is generated for climate change scenarios based only on specified mean monthly temperature factors of change (Fatichi et al., 2011a,b).

3.2.2 Weather observations and generated scenarios

Hourly climatological data for Piz Corvatsch (46.4180°N, 9.8214°E; 3315 m a.s.l.) was acquired from the MeteoSwiss online data portal (Figure 3.2 MeteoSwiss, 2012). MeteoSwiss maintains a network of 72 automatic climate stations (ANETZ) which record 10-minute means of continuously monitored air temperature, air humidity, air pressure, solar radiation, precipitation total, wind speed, and wind direction (MeteoSwiss, 2010). The network was first established between 1975 and 1989 and underwent a comprehensive update between 2005 and 2009 (Suter et al., 2006). These data undergo approximately 190 quality control tests that check extreme values (hard and soft limits), variance (minima and maxima), consistency with other parameters, and consistency with nearby stations (Musa et al., 2003). The data are not homogenized and may be subject to small shifts with the introduction of a new sensor, for example. Additional details on the data procedures are available in Perl et al. (2010).

The Piz Corvatsch station is 650 m higher and approximately 1 km distant from Murtèl–Corvatsch rock glacier. The Piz Corvatsch station is fully equipped with high quality sensors and few or no data gaps even under severe weather conditions (Suter et al., 2006). The data covered the period September 1, 1985 to January 1, 2012, were without gaps, and required no processing before input to the weather generator. Piz Corvatsch has a slightly continental high Alpine climate with a summer time precipitation maximum related to

southwesterly Mediterranean air masses (Hoelzle et al., 2003). Mean annual precipitation during full years of the observation period was 890 mm w.e. (sd = 165 mm w.e.), with 324 mm w.e. (sd = 61 mm w.e.) or 36.4% occurring during the months of June, July and August. Mean annual air temperature was -5.110 °C (sd = 0.571°C).

AWE-GEN was obtained from the University of Michigan HYDROWIT site, with modifications to the generation of temperature as described in Section 3.2.1. AWE-GEN is a MATLAB package and was utilized in MATLAB 7.12.0.635. AWE-GEN requires as input, and produces, hourly time series of the following weather variables:

- precipitation (Pr)
- cloud fraction (N_{Cl})
- air temperature (TA)
- global shortwave solar radiation (SWR)
- relative humidity (RH)
- wind speed (WS)
- atmospheric pressure (P_{atm})

Optional inputs include direct and diffuse shortwave solar radiation, annual precipitation, mean monthly temperature change factors for climate change scenarios, and atmospheric transmittance parameters. Except for precipitation, all parameters may be specified instead of estimated from observed data. All of the required input variables were readily available from the Piz Corvatsch data with the exception of N_{Cl}. In this case, existing parameters from another high elevation site in the Swiss Alps were used and the replacement is not anticipated to have any adverse impact on the quality of the generated weather data (Simone Fatichi, personal communication, August 10, 2012). Using the specified cloud parameters and the remaining parameters estimated from the observed data, weather data was generated for the scenarios detailed in Table 3.1. Wind direction is not treated AWE-GEN, for simplicity it was randomly generated on a uniform [0,360) distribution at the hourly level.

Table 3.1: Climate scenarios and generated weather data applied in this work.

TAMonthly Factor of Change	Months Applied	Number of Years Generated	Scenario Name
0	All	100	REF
+1	All	50	+1All
+1	Jun, Jul, Aug	50	+1Sum
+1	Dec, Jan, Feb	50	+1Win
+3	All	50	+3All
+3	Jun, Jul, Aug	50	+3Sum
+3	Dec, Jan, Feb	50	+3Win
-1	All	50	-1All
-3	All	50	-3All

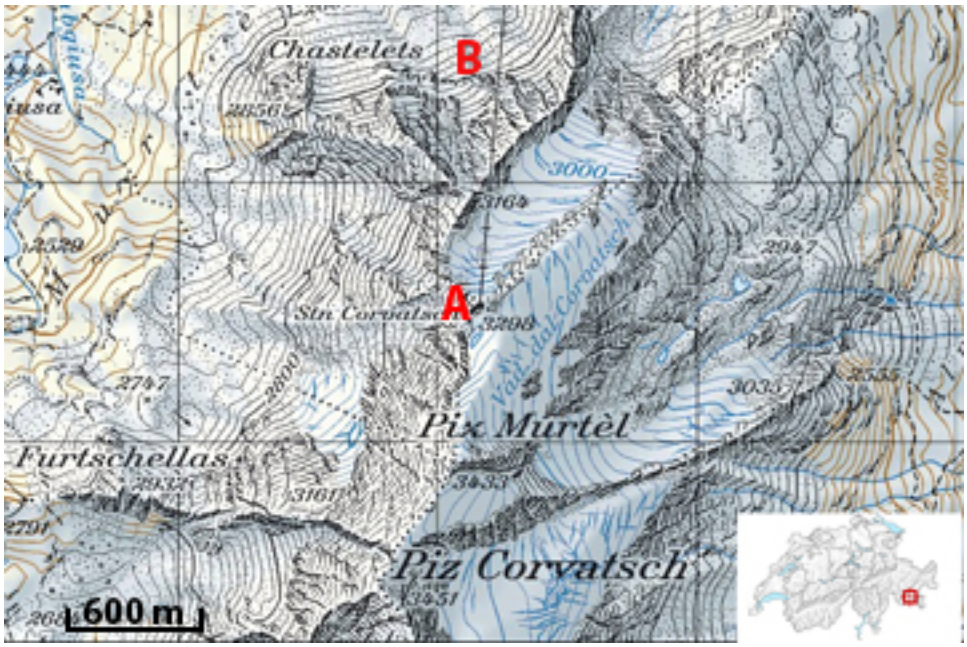

Figure 3.2: Location of A) Piz Corvatsch climate station and proximity to B) Murtèl–Corvatsch rock glacier (map source: http://map.geo.admin.ch/). Inset shows location within Switzerland.

3.2.3 Quality assessment

The first step in the quality assessment is a brief examination of the stationarity of the observational climate; the following variables are assessed for relationships with the mean value of the the corresponding seasonal or annual NAO index (data source: NOAA, 2013) during years of the observation period where full seasons are available (1985-86 winter to 2011 summer):

- observed total annual precipitation (PrAnn_{obs})
- observed total summer precipitation (PrSum_{obs})
- observed total winter precipitation (PrWin_{obs})
- observed mean annual air temperature (MAAT_{obs})
- observed mean summer daily minimum air temperature ($\mathrm{MSDminAT}_{obs}$)
- observed mean summer daily maximum air temperature ($\mathrm{MSDmaxAT}_{obs}$)
- observed mean summer air temperature (MSAT_{obs})
- observed mean winter daily minimum air temperature ($\mathrm{MWDminAT}_{obs}$)
- observed mean winter daily maximum air temperature ($\mathrm{MWDmaxAT}_{obs}$)
- observed mean winter air temperature (MWAT_{obs})

The quality of the generated weather data is assessed with the functionality included in the AWE-GEN package which allows for evaluation of the reproduction of statistical characteristics of the observational data set. This includes the following graphical comparisons between the generated and observational data:

1. Precipitation
    - mean and standard deviation of total monthly Pr
    - monthly one–hour and 24–hour aggregations of Pr:
        - mean and standard deviation

    - lag–1 autocorrelation
    - skew
    - non-precipitation frequency
    - wet-wet transition probability
  - fraction of all hours with Pr larger than 1, 10, and 20 mm
  - relative frequency histograms and the mean and variance of wet and dry spell lengths

2. Global Solar Radiation
   - monthly mean and standard deviation of global shortwave radiation
   - annual hourly global shortwave radiation

3. Air Temperature
   - monthly one–hour and 24–hour aggregations of TA mean and standard deviation
   - monthly 24–hour aggregations maximum TA (TA_{max}) and minimum TA (TA_{min}) mean and standard deviation
   - return period of heat (day has temperature $>90^{th}$ percentile) and cold (day has temperature $<10^{th}$ percentile) waves

4. Relative Humidity
   - monthly mean and standard deviation of relative humidity

5. Wind Speed
   - diurnal wind speed cycle and wind speed histograms

6. Atmospheric Pressure
   - atmospheric pressure histograms

Cloud fraction is not compared due to lack of observational data at Piz Corvatsch. Some ad-hoc analysis is performed where additional detail is relevant. Priority is given to the REF scenario while brief qualitative comparisons are made between the climate change scenarios and regional projections. There are no standards for overarching statements regarding the quality of data created with a weather generator, so the nature of this

quality assessment is qualitative with the main intent being the identification of issues within the generated weather data which affect the degree to which it is representative of climate and weather conditions at Piz Corvatsch and therefore transferability of the results to the Murtèl–Corvatsch rock glacier.

3.3 Rock glacier modeling

GEOtop is a fully distributed hydrological model which numerically solves the water and energy balance in the ground (Endrizzi & Gruber, forthcoming). The water balance can be solved in three dimensions but this requires an extensive map based domain characterization and is extremely computationally demanding, therefore one–dimensional simulations are used here. GEOtop follows the standard approach for numerical permafrost modeling described in Section 2.7. Water flow equations are treated jointly with the heat equation – an advantage in the simulation of the ice–rich permafrost (i.e. rock glacier) hydrological and thermal regimes. Other advantages of GEOtop in this regard include a robust treatment of freezing and thawing processes in variably saturated soils (DallAmico et al., 2011) and topoclimatic controls on the near surface climate including explicit snow accumulation, metamorphism, and ablation processes forced by a full meteorological characterization of the upper boundary condition (Endrizzi, 2007). Additional details are offered in Section 3.3.1, while full details are available in (DallAmico et al., 2011; Endrizzi, 2007; Rigon et al., 2006). The experimental approach, target variables, and relevant GEOtop parameters are provided in Section 3.3.2. Sensitivity and uncertainty analysis are important to simulation studies (Gubler et al., 2012) but are excluded from this work due to time constraints; such is a logical continuation of this work.

It is worth mentioning that a complete model of rock glacier dynamics would, per Haeberli et al. (2006) and Section 2.4, include:

1. Rock weathering, snow redistribution by wind and avalanches, and rockfall with particle size sorting on debris slopes
2. Energy and mass balance with phase change in the rock glacier body
3. The thermohydro–mechanical deformational processes that account for:
   (a) internal debris transport

(b) collective down–slope creep

In this sense, this work corresponds to 2 in the list above; however this is a good approximation for assessing the response of rock glaciers to climate change on the assumption that the the first and third items are significant to rock glacier dynamics at time scales an order of magnitude higher than the decadal time scale of the climate change considered herein. However, they would be important to evaluation of the target variables herein in the context of rock glacier genesis and long term evolution.

3.3.1 GEOtop

This section describes some of the theory behind the GEOtop. Aspects of heat and water transfer in the ground are presented followed by the surface energy balance with brief remarks on the treatment of snow cover. Between the centres of soil layers in the discretized soil column, GEOtop applies the heat equation in the form (Endrizzi et al., 2011b)

$$\frac{\partial(U)T}{\partial t} = \frac{\partial}{\partial z}\left(k\frac{\partial T}{\partial z}\right) \tag{3.1}$$

where t is time [s], z is the displacement normal to the surface [m], T is soil temperature [K], k is the soil thermal conductivity [W m^{-1} s^{-1}], and U is the soil internal energy [J m^{-2}] which accounts for freezing and thawing of variably-saturated soil, given by

$$U = C(T - T_f) + L_f \rho_w \theta_w \tag{3.2}$$

where T_f is the water freezeing temperature [273.15 K], L_f is the latent energy of fusion [3.34 x 10^6 J Kg^{-1}], ρ_w is the liquid water density [1000 kg m^{-3}], and θ_w is the volumetric water fraction [unitless].

θ_w is very nonlinear near the freezing temperature therefore it is defined via freezing-soil characteristic curves which are specified in GEOtop with the Van Genuchten model (DallAmico et al., 2011; Van Genuchten, 1980) which requires 4 parameters for the soil: θ_s

saturated water content, θ_r residual water content, n a measure of soil pore size distribution, and α related to the inverse of air entry suction.

Additive non-linear mixing laws are used for C and k respectively to account for the variation of these properties due to changes in θ_w (Endrizzi et al., 2011b). The treatment of water flow within the soil is analogous to heat flow. The Richards equation describes water flow in porous media and is given in one dimension by (Endrizzi et al., 2011b; Rigon et al., 2006)

$$\frac{\partial \theta_w}{\partial t} = \frac{\partial}{\partial z}\left(K\frac{\partial H}{\partial z}\right) + S \tag{3.3}$$

K is the soil hydraulic conductivity [m s^{-1}], S is a storage term [s^{-1}] , and H is the hydraulic head [m^{-1}]. θ_w and K depend on the hydralic head and given by the Van Genuchten and Mualem model, requiring the addition of soil (vertical and horizontal) conductivity parameters. The heat and Richards equations are discretized in time and space and solved numerically using the Newton method (DallAmico et al., 2011; Endrizzi et al., 2011b).

For brevity, and because the parameters of the surface energy balance and snow cover are not under primary consideration in this work, equations pertaining to these aspects of GEOtop are omitted. Regarding the surface energy balance (recall Equation 2.2), solar radiation is directly supplied by meteorological data and distributed based on topographic shading factors (slope angle and aspect). Turbulent heat fluxes are estimated with gradient methods to which wind speed and surface aerodynamic roughness are of special importance (Endrizzi et al., 2011b). A minimum wind speed (0.5 m s^{-1}) is specified to avoid issues with possible artificial inhibition of turbulent heat fluxes (Gubler et al., 2013). Longwave downward radiation is estimated with the Stefan-Boltzmann equation with cloud conditions incorporated through the estimation of atmospheric transmissivity based on observed and calculated clear-sky shortwave radiation (Gubler et al., 2012). A multilayer snowpack representation is applied, with water and energy balance solved with complete coupling to ground and atmospheric conditions. Snow dynamically accumulates and undergoes metamorphism based on precipitation inputs given by the meteorological data, snow threshold temperature, the snow energy balance, and temperature and vapour gradients within the snowpack (Endrizzi, 2007). This work used GEOtop 1.225-9 with simulations processed on the computational infrastructure of the Swiss Multi–Science Computing Grid (http://www.smscg.ch/).

3.3.2 Experimental design

Numerous parameters pertaining to point characterization and general model settings are required in GEOtop. A flow chart of the specification process is shown in Figure 3.3. Parameters manipulated to describe different rock glacier models or considered of importance herein will be described. A table of fixed parameters considered of secondary importance and their values is provided in Appendix B.

Point characterizations

Points are modeled after rock glaciers through the use of topographic and soil parameters. Topographic parameters varied include point elevation, slope angle, aspect. Points otherwise have planar surfaces with unobstructed horizons. Soil parameters varied include the Van Genuchten parameters and normal and lateral hydraulic conductivity (θ_s, θ_r, n_{VG}, α_{VG}, K_N, and K_L). Different soil discretizations were also tested. GEOtop also allows the specification of an arbitrary parameter, FreeLD, which defines the depth to which free lateral drainage occurs. This is varied herein to try and account for the lack of soil consolidation after permafrost thaw, where low values lock melted ice in the soil thereby increasing the thermal conductivity by retaining water in what would otherwise be artificially large voids. Lastly, the heat capacity and conductivity of soil solids are fixed within the range of values for granitic rock (Table 3.3).

General parameters

General fixed parameters were specified after (Gubler et al., 2013) for accuracy, where possible. Water and energy balance calculations are performed with a time step of 1800 seconds. The elevation of the meteorological station is 3315 m a.s.l. corresponding to Piz Corvatsch. Temperature is distributed elevationally using a constant lapse rate of 6.5 K km^{-1}. The rain and snow threshold temperature is set to 1°C and -3 °C respectively; above and below these temperatures, all precipitation is rain or snow. Fresh snow is assigned albedo values of 0.9 and 0.65 in the visible and near infrared wavelengths respectively. At snow depths below 10 mm, albedo is interpolated between snow and soil values. Snow emissivity is set to 0.99. Soil is given default values for albedo (0.2), emissivity (0.96), and roughness length (10 mm) approximately corresponding to a pebbly rock surface.

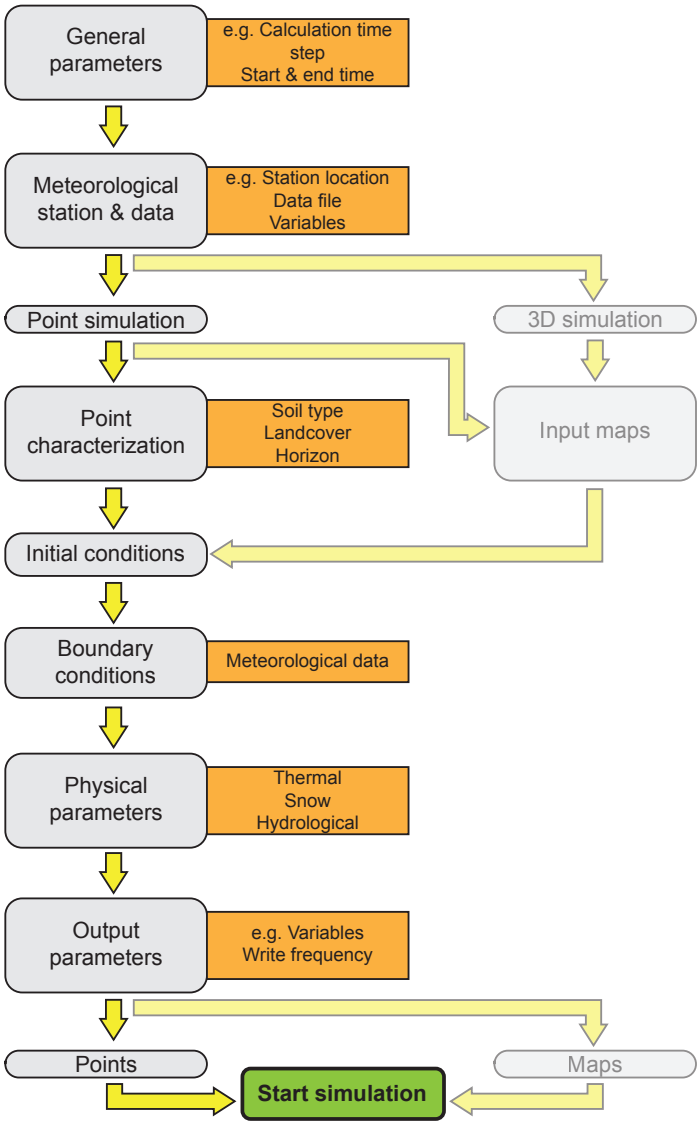

Figure 3.3: The steps in a GEOtop simulation from the user point of view (after Endrizzi et al., 2011a). Steps pertaining to 3D simulations are semi-transparent and do not apply to this study.

Observed model outputs

Simulated temperature, water content, and ice content (volumetric) are recorded daily at 07:00 at depths of 0.1, 0.2, 0.4, 0.8, 1.2, 1.8, 2.6, 3.6, 5.1, 7.5, and 12 m (interpolated from layer nodes) and used for visualization of the temporal evolution of these variables within the soil profile. Soil column depth is limited to 15 m. Additional output includes air temperature, snow depth, surface temperature, soil heat flux, snow water equivalent, snow temperature, incoming shortwave radiation, net shortwave radiation, and incoming longwave radiation.

The target variables of this study are:

- MAGST as a bulk assessor of the ground thermal regime
- Active layer depth (D_{AL}) as a bulk assessor of the ground thermal regime
- IWE_{tot} as a measure of long–term water storage potential
- The difference between September 1 and June 1 IWE_{tot} ($MELT_{sum}$) as a measure of rock glacier contribution to summer hydrological cycle

Pilot study

A pilot study was performed to establish a satisfactory point representation of a rock glacier. Over 800 points with varying topographies and soil columns are simulated under the first 50 years of the REF scenario.

Constant and exponentially increasing soil discretization schemes to which θ_s, θ_r, K_N, and K_L were applied in manners of 1 (uniformly), 2 (separately to active layer and permafrost), and 3 (separately to active layer, permafrost, and supersaturated zone in between) bulk layer rock glacier structures corresponding to the active layer permafrost layers in the generalized rock glacier structure (Section 2.4.2). In this work, a wet or ice–poor bottom layer were not tested. FreeLD values of 1, 1.5, 2, 2.5, 3, 10, and 15 m were also applied over the soil configurations. Regarding topographic scenarios, points with north and south aspects and 0°, 15°, and 30° slope angles at elevations of 2700, 3000, and 3300 m were utilized.

Results are omitted for brevity and relevance but a few remarks included here. The key difference between the pilot study and the main study was the number of soil configurations utilized and the use of the REF scenario only. No appreciable differences were apparent between the soil discretization schemes and the different strategies for applying the soil thermal and hydrological properties in the soil column, perhaps due to the fixed output depths as described below. The outcome was a simple rock glacier point with an ice-rich (∼70%) permafrost layer under seasonally frozen ground, maintained under the REF scenario. The final soil specification is provided in the following section.

Main study

In the main study, 36 points (Table 3.2) are simulated for 100 years using the REF scenario, or the first 50 years of the REF scenario followed by each of the climate change scenarios. When referring to the rock glacier simulations, the 100 year climate scenarios are referred to by the same names used for the standalone scenarios (e.g. the scenario of 50 years under REF climate followed by the +1All climate is called +1All).

The soil thermal and hydraulic parameters are specified after generic values for sand and gravel (Table 3.3). The soil discretization is shown in Figure 3.4. All layers are initialized at -2°C and the water table (i.e. permafrost top) at 2 m depth. The dynamics of the target variables are analyzed graphically and with some descriptive statistics.

Table 3.2: The parameter values which combine to define the 36 rock glacier points simulated in the main study.

Parameter	Values
Elevation [m a.s.l.]	2700, 3000, 3300
Slope Angle [°]	15
Aspect [°]	0, 180
FreeLD [mm]	0, 2000, 15000
Soil	1–sand, 2–gravel

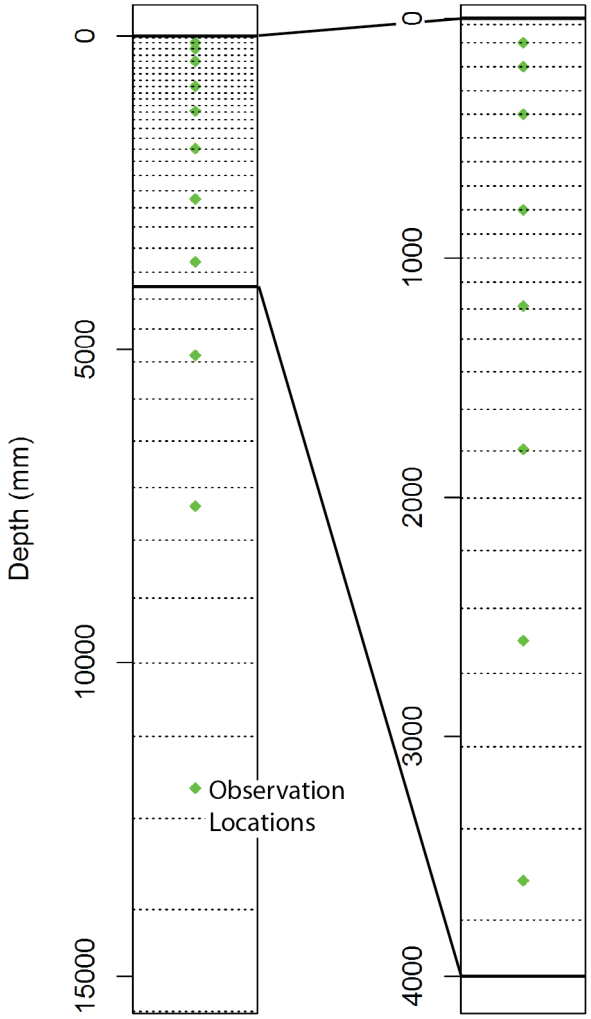

Figure 3.4: The Soil discretization and location of output depths (green). Dotted lines indicate the layer boundaries of the soil discretization.

Table 3.3: The parameters and values used for rock glacier soil columns based on generic values for sand and gravel (Gubler et al., 2013; USDA, 2012), with some modifications for observations on rock glacier ice contents. Values separated by ";" correspond roughly to above and below 2 m depth which approximates an initial active layer

Property	Parameter	Soil 1 (Sand)	Soil 2 (Gravel)
saturated water content	θ_s	0.374; 0.7	0.374; 0.7
residual water content	θ_r	0.055; 0.075	0.055; 0.075
pore size distribution	n_{VG}	3.2	2
air entry suction	α_{VG}	0.003	0.1
vertical hydraulic conductivity	K_N	0.083	10
lateral hydraulic conductivity	K_L	0.083; 0.001	10; 0.5
specific heat capacity	C	2.25×10^6 J m^{-3} K^{-1}	
thermal conductivity	k	2.5 W m^{-1} K^{-1}	

Chapter 4

Results

4.1 Weather generation

Some evidence of an influence of climate change on MAAT at Piz Corvatsch is observed along with teleconnections between the NAO and MAAT at Piz Corvatsch during the 27 year observation period. The weather generation is of good quality with the exception of TA during April, July, August, and September which are remarkably cooler in the generated data on average. However, daily maximum TA during the summer months, an important element of snow melt controls, was unaffected. Conditions in the climate change scenarios correspond closely to the applied factors of change with only TA being affected, as intended. Other than April, July, August and September minimum and mean TA, the generated data is considered representative of climatic conditions at Piz Corvatsch. The influence of these differences on rock glacier modeling is subject to discussion in Chapter 5.

4.1.1 Stationarity of observed climate

Trends and the influence of the NAO on climatic variables at Piz Corvatsch were assessed using generalized least squares regression models with autocorrelated residuals (Equation 4.1) which accounts for the interannual autocorrelation in the climatic data. The models take the form

$$Y = \beta_0 + \beta_1 YEAR + \beta_2 NAO + \sigma \tag{4.1}$$

where β_0 is an intercept term, β_1 is the trend effect, β_2 is the effect of the NAO index, and σ are temporally autocorrelated residuals. The climate at Piz Corvatsch is not perfectly stationary. A trend of 0.027°C a^{-1} in MAAT was present ($\rho = 0.072$; Table 4.1). The NAO index ranged from -1.153 to 0.702 during the observation period and had a significant effect with an increase of 1 in the NAO index corresponding to a 1.013°C increase in MAAT ($\rho = 0.001$). The NAO had a similar effect on mean winter daily maximum temperatures ($\rho = 0.075$; Table 4.1). Relationships of this nature which account for some variability in the observed climate are not accounted for by the weather generator. No statistically significant trends were present in the other analyzed variables, the effect of the NAO in the mean annual precipitation model was very large (Table 4.1).

Table 4.1: Trend and NAO coefficients in regression models of climatic variables used to assess climate stationarity at Piz Corvatsch during the observation period. Annual aggregations include the years 1986 to 2010 (n=25) while winter and summer aggregations include 1985-86 to 2010-11 and 1986 to 2011 respectively (n=26). Precipitation and temperature trends have units mm a^{-1} and °C a^{-1} respectively. p-value:*** <0.01, ** <0.05 , * <0.1

Variable	Trend coefficient	NAO coefficient
$PrAnn_{obs}$	0.552	-142.329
$PrSum_{obs}$	-0.300	-18.224
$PrWin_{obs}$	-0.731	-11.060
$MAAT_{obs}$	0.027*	1.013***
$MSDminAT_{obs}$	0.077	-0.131
$MSDmaxAT_{obs}$	0.004	-0.398
$MSAT_{obs}$	0.030	0.137
$MWDminAT_{obs}$	0.103	0.767
$MWDmaxAT_{obs}$	-0.052	0.916 *
$MWAT_{obs}$	-0.029	0.545

4.1.2 Reference climate scenario

Precipitation amounts and occurrence

The distribution of monthly total Pr amounts in the generated data is very close to that of the observational data (Figure 4.1). The monthly standard deviation of the generated Pr data was equal to or less than that of the observed data in all months except March and July.

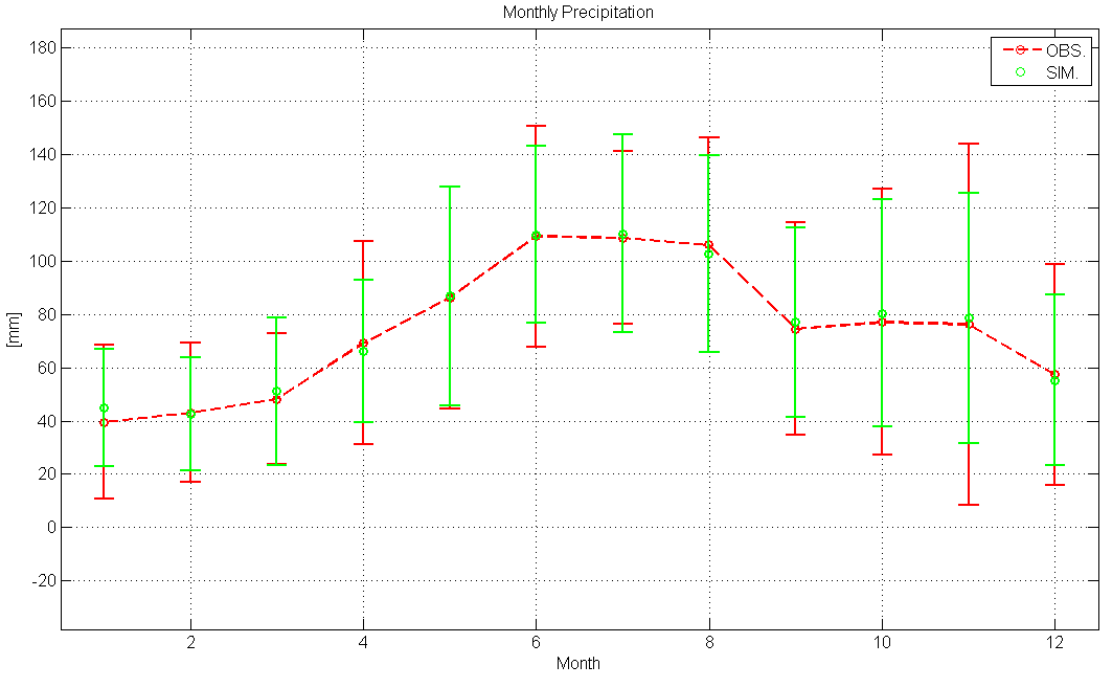

Figure 4.1: Comparison of mean monthly precipitation totals between observations and REF scenario. The bars represent +/− 1 standard deviation. Sim (Simulated) refers to the generated data.

At the hourly aggregation, the mean and variance of observed and generated monthly Pr data are practically identical (Figure 4.2 a, b). The lag-1 autocorrelation of Pr occurrence generated data is higher by approximately 0.1 than that of the observed data in the months of February, May, and September (Figure 4.2 c). Otherwise the values are fairly close. This is also reflected in the wet-wet transition probability (Figure 4.2 f). In other words, the

persistence of the wet state of the days is higher during these months in the generated data. The skewness of monthly precipitation in the generated data is less than that of the observed data in all months with the single exception of November, with a tendency for the difference to be larger in the winter and spring months (Figure 4.2 d) indicating underrepresentation of extreme hourly Pr intensities. The frequency of hours without Pr is higher in the generated data in all months.

At the daily level of aggregation the variance of monthly precipitation is lower than observed in June, July, August, November, and December whereas correspondence between monthly mean daily precipitation remains high (Figure 4.3 a, b). The lag one autocorrelation and wet-wet transition probability are consistently lower in the generated data (Figure 4.3 c, f), in this case showing under-persistence of the wet state of days. With the exceptions of September and December, where the skewness of daily precipitation is lower in the generated data than observational data, the skewness of daily precipitation amounts in the generated data closely matches that of the observed data (Figure 4.3 d). Extreme daily precipitation is therefore well represented. The frequency of days without Pr is similar in the generated and observed data, with approximately half of the months (January, February, March, May, September, October, December) having a higher frequency of non-precipitation days and vice–versa (Figure 4.3 e); in this case the seasonality in daily Pr non-occurrence is amplified. Such a result of -0.1 (+0.1) difference between observed and generated Pr non-occurrence frequency in June, July, and August (February, September, December) is approximately 3 fewer (additional) days of precipitation on average in the respective months over the length of the time series.

The run lengths of wet and dry days show typical weather generator performance, i.e. an under representation of medium and longer run lengths (5 days or more for dry and 3 days or more for wet) in the generated data (Figure 4.4 b, c). Wet spells lengths are slightly better represented in the generated data, being only marginally shorter on average and less variable (difference in: expected value 0.276 and standard deviation 0.208 days), than the observed data compared to dry spells (difference in: expected value 1.077 and standard deviation 1.813 days; Figure 4.4 b, c). Hourly precipitation amounts greater than 20 mm occur less often in the generated data than in the observed data. The opposite is true for 1 mm and 10 mm, which are slightly over represented (Figure 4.4 a). The difference increases with the length of the aggregation period.

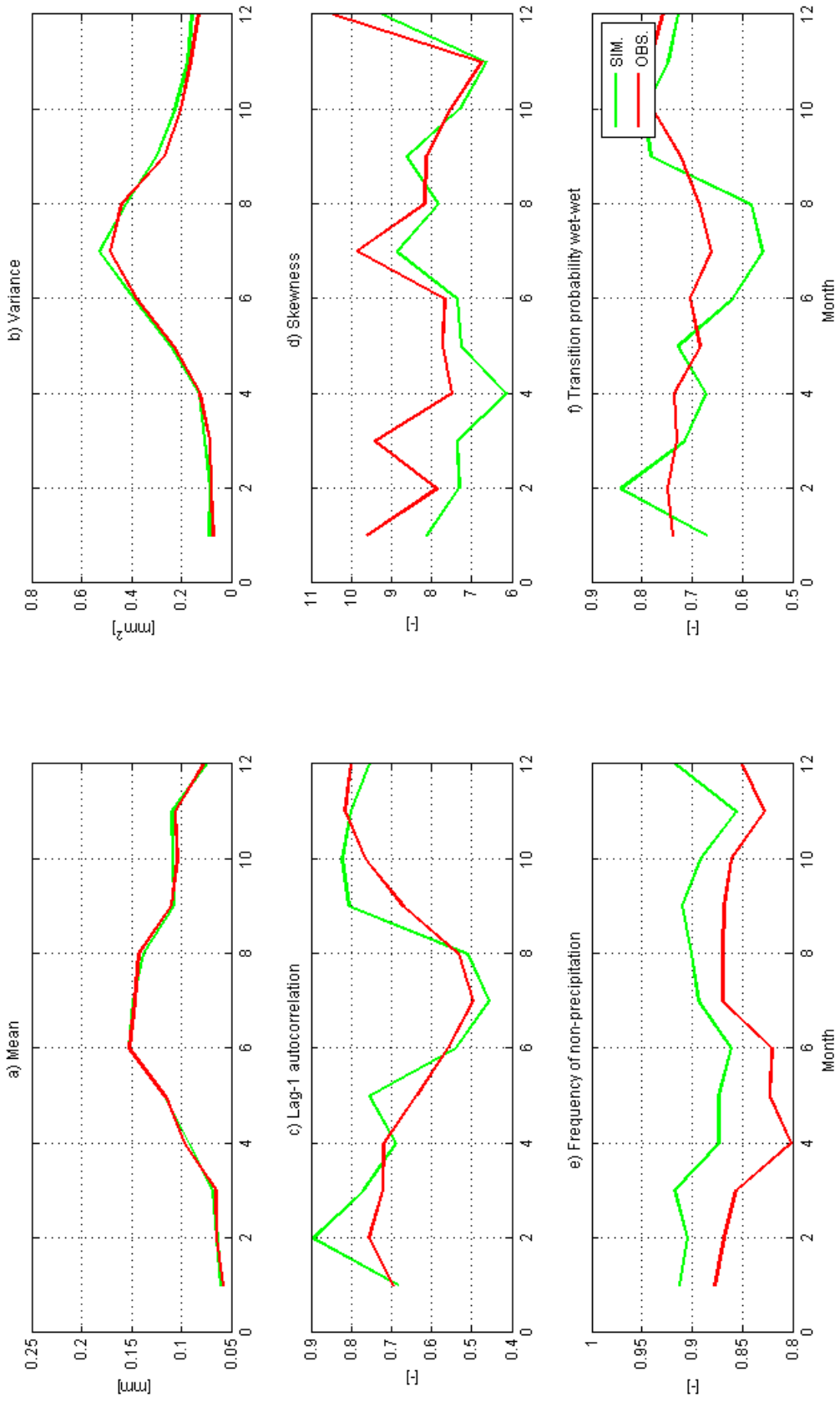

Figure 4.2: Comparison of monthly precipitation statistics between observations and REF scenario at hourly aggregation.

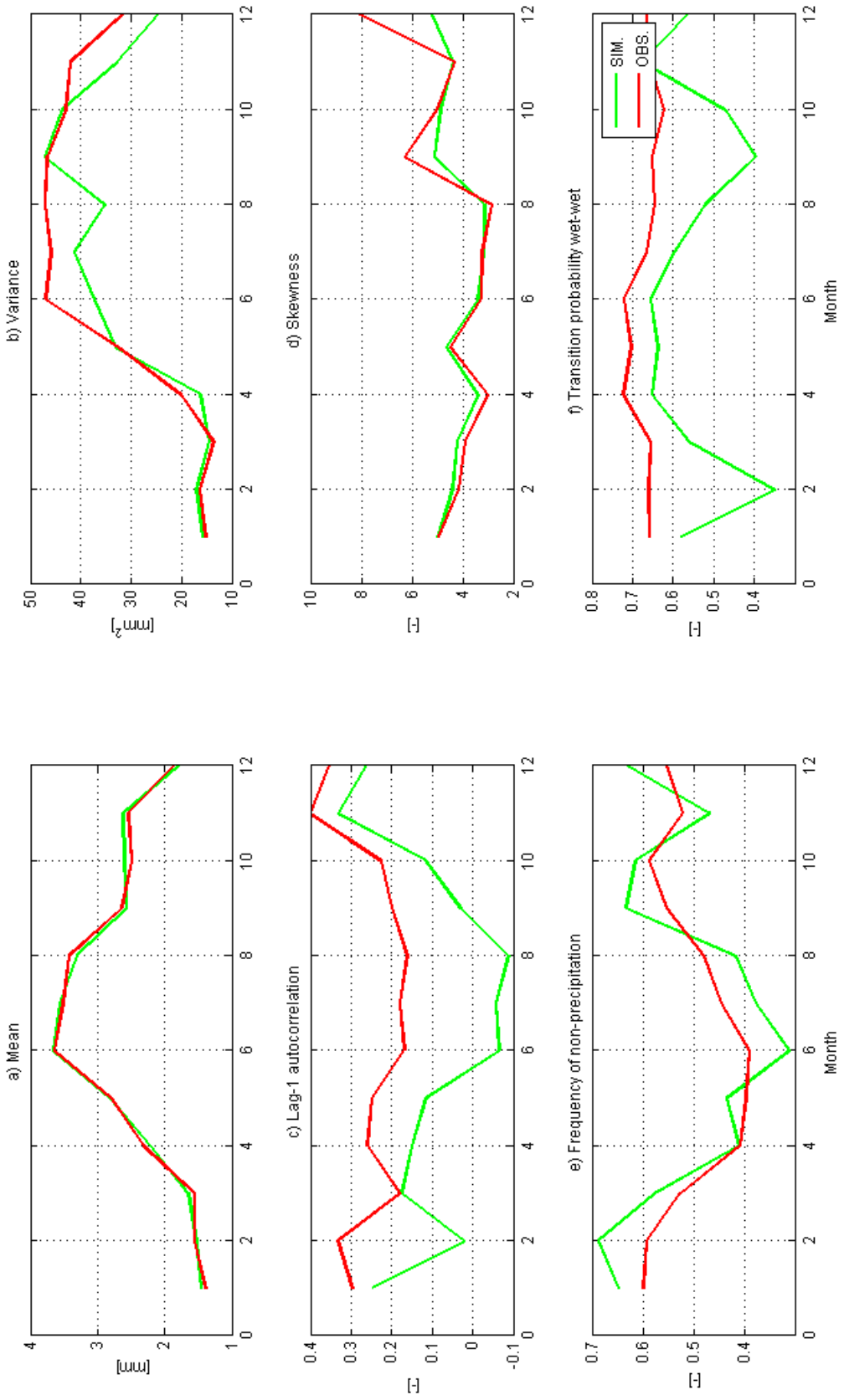

Figure 4.3: Comparison of monthly precipitation statistics between observations and REF scenario at daily aggregation.

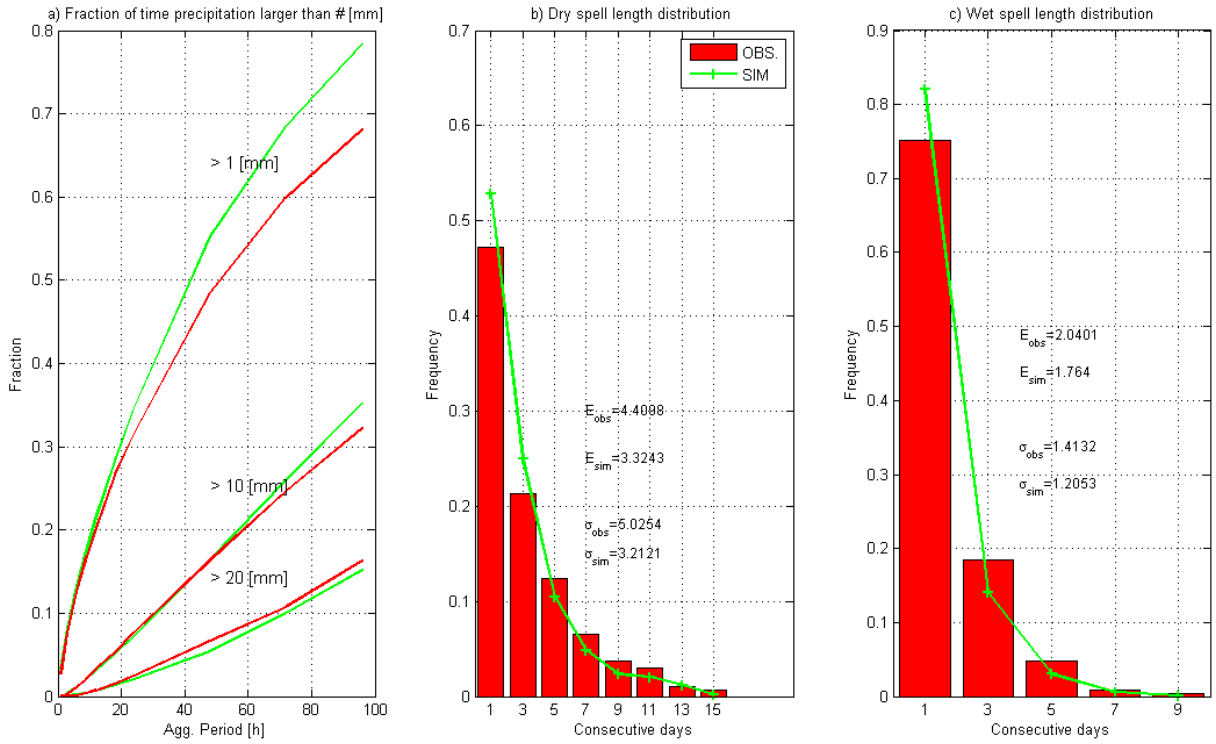

Figure 4.4: Comparison of the relative frequency of select precipitation intensities and the distributions of wet and dry spell lengths.

Temperature

The mean and standard deviation of hourly and daily TA in the generated data is remarkably close to that in the observational data with the notable exceptions of April, July, August, and September; said variables are drastically cooler (by as much as 7°C) and greater respectively in these months (Figure 4.5). July, August, and September are noteworthy as mean daily TA in these months is at or above 0°C in the observational data whereas it remains at or below 0°C in the generated data (Table A.3). However, mean daily maximums are only so affected in April (Table 4.2) whereas mean daily minimums follow the pattern described for daily means and are cooler by as much as 12°C (Figure 4.6, Table A.5). Overall, AWE-GEN produced a time series with a MAAT 1.82°C lower than observations due to these differences in the poorly represented months (Table 4.4).

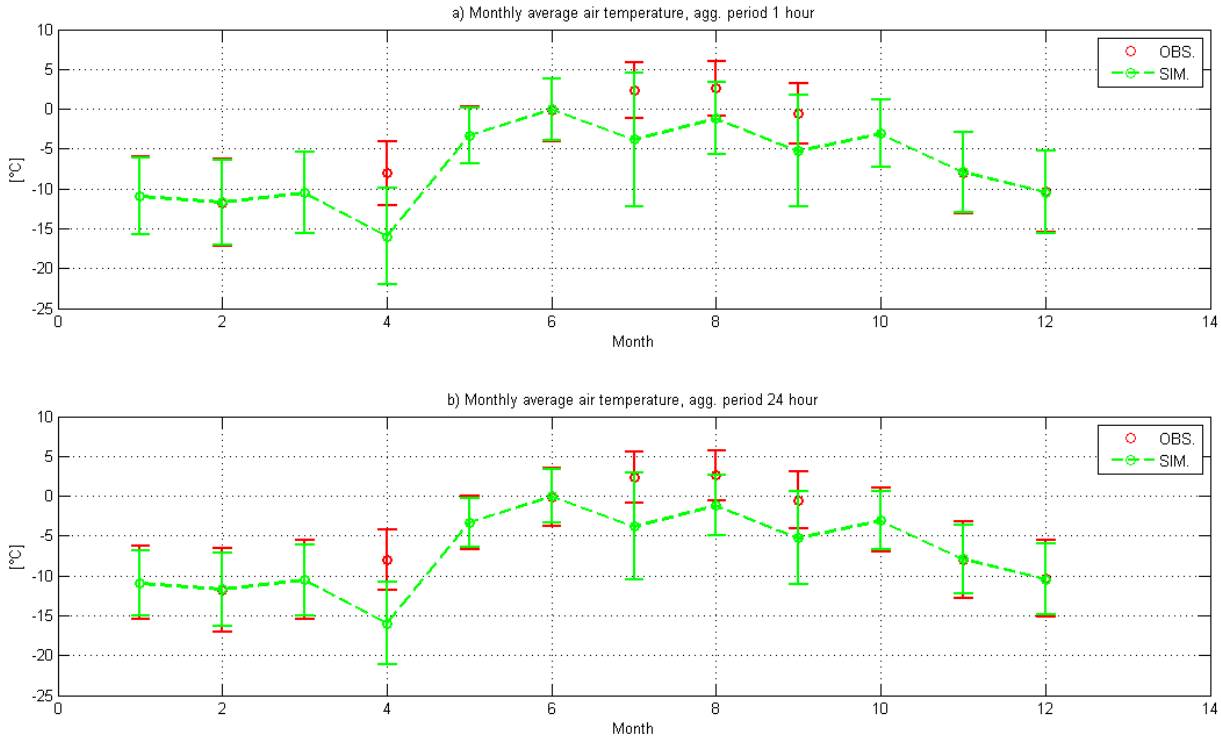

Figure 4.5: Comparison of monthly mean hourly temperature between observations and REF scenario. The bars represent +/− 1 standard deviation

Heat waves and cold waves are under represented. The return periods of cold waves

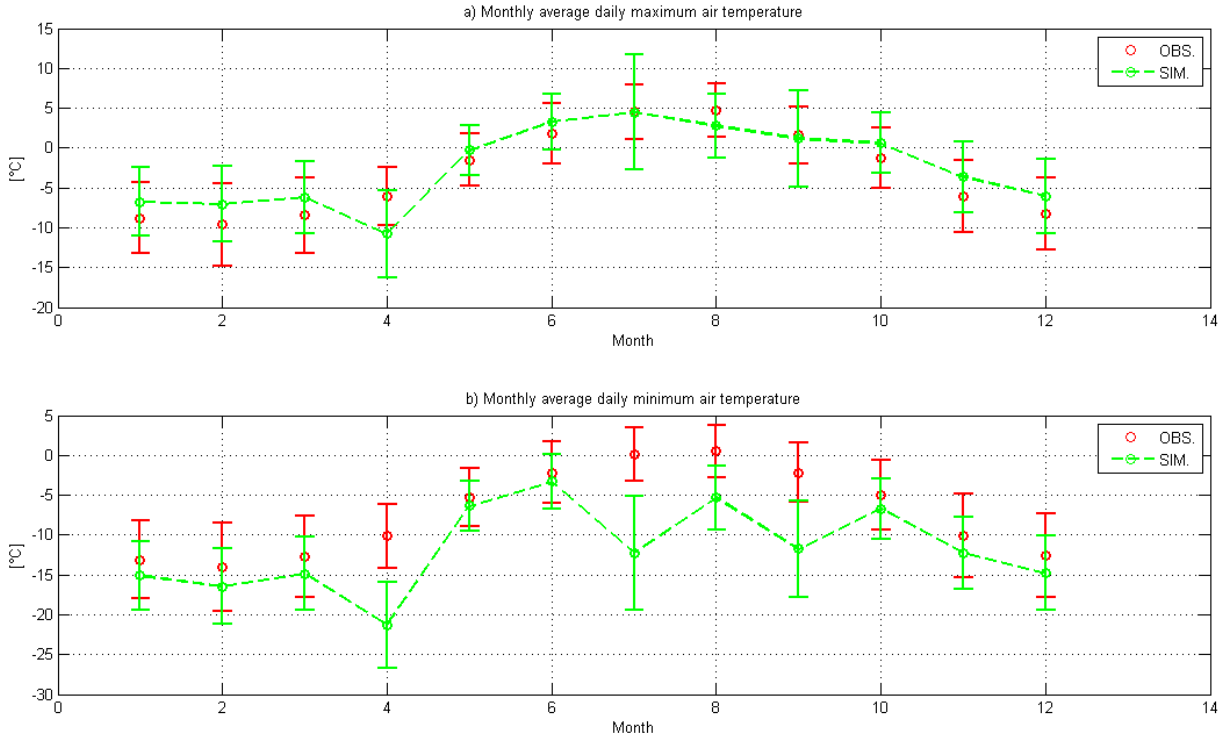

Figure 4.6: Comparison of monthly mean daily temperature between observations and REF scenario. The bars represent +/− 1 standard deviation

begin to diverge appreciably at cold wave lengths of approximately 11 days. The return periods of heat waves are generally much longer, presumably due to the reduced seasonality described above.

Additional variables

Generated SWR matches the observational data very well. Mean monthly total SWR is slightly higher in the generated data through the months of June to September (Figure 4.8) but otherwise corresponds very closely to observations. The diurnal progression of SWR through the year is also well replicated in the generated data with the tendency for the summerward shift of maximum SWR inputs evident in the daylight hours (Figure 4.9).

The mean and standard deviation of relative humidity are very close when comparing

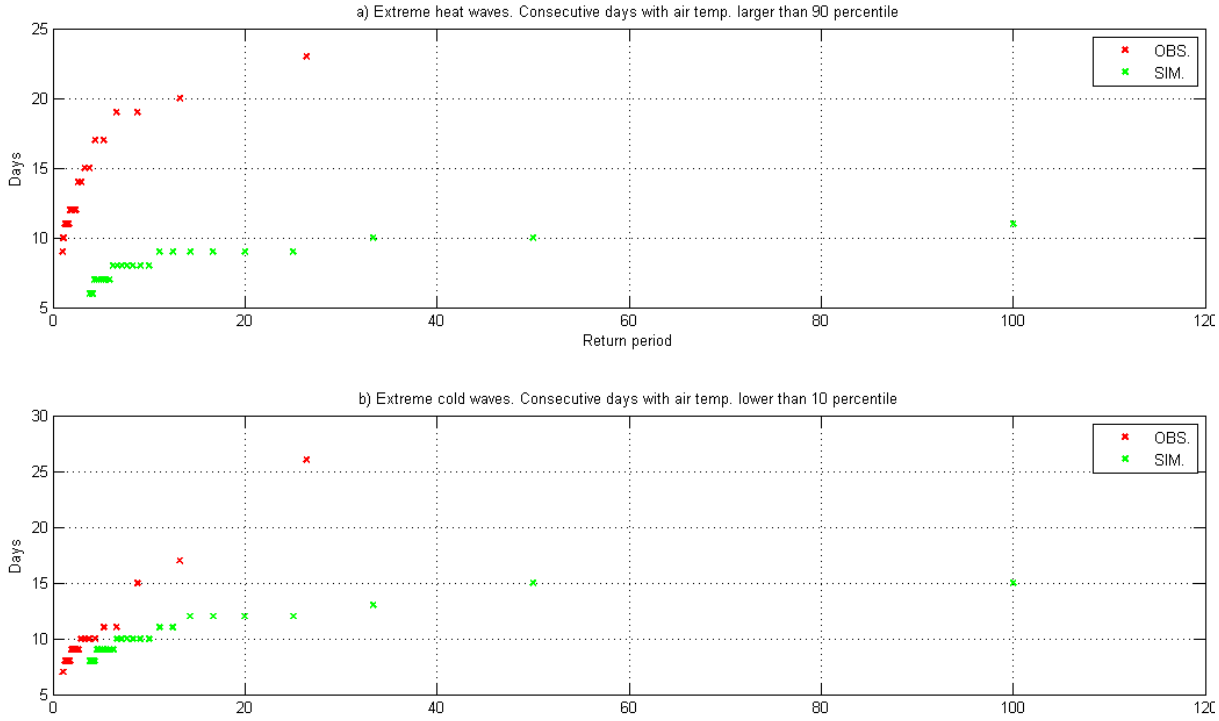

Figure 4.7: Comparison of the return periods (years) of heat and cold waves between observations and REF scenario. The length of a temperature wave is represented by the Y axis while its return period (years) is represented by the X axis.

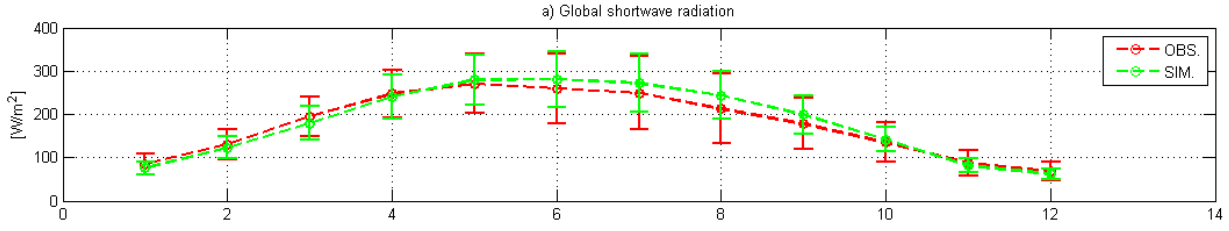

Figure 4.8: Comparison of monthly mean hourly global solar radiation between observations and REF scenario. The bars represent +/− 1 standard deviation

hourly and daily aggregation periods through the months (Figure 4.10). There is a minor difference between the generated and observed air pressure with a slight left skew in ob-

served air pressure absent from the generated data (Figure 4.11). High wind speeds are under represented and low wind-speeds are over represented, lowering the annual mean (Figure 4.12 a, b). The standard deviation of hourly wind speed is also slightly lower than observed. These differences in WS stem from a total omission of the seasonality in the variable (Table A.11, Table A.11), a result of the AWE-GEN approach which excludes seasonal variation in WS parameters.

Table 4.2: Mean daily maximum TA at Piz Corvatsch and for all generated climate scenarios. $1-50$ and $51-100$ indicate the years of the REF scenario used for the statistics, and are separated since each climate change scenario begins with REF_{1-50}.

month	Piz Corvatsch	REF_{1-50}	REF_{51-100}	+1All	+1Win	+1Sum	+3All	+3Win	+3Sum	-1All	-3All
1	-8.818	-6.778	-6.805	-5.830	-5.843	-6.830	-3.830	-3.868	-6.830	-7.830	-9.846
2	-9.633	-7.024	-7.075	-6.165	-7.162	-7.165	-4.165	-7.157	-7.165	-8.165	-10.118
3	-8.451	-5.958	-6.460	-5.088	-6.088	-6.088	-3.088	-6.088	-6.088	-7.088	-8.978
4	-6.115	-10.581	-10.953	-9.611	-10.611	-10.611	-7.611	-10.611	-10.611	-11.611	-13.758
5	-1.486	-0.123	-0.408	0.748	-0.252	-0.239	2.748	-0.252	-0.213	-1.252	-3.231
6	1.741	3.331	3.275	4.427	3.427	4.424	6.427	3.427	6.419	2.427	0.057
7	4.543	4.809	4.169	5.556	4.556	5.556	7.556	4.556	7.556	3.556	1.553
8	4.699	2.750	2.821	3.794	2.794	3.781	5.794	2.794	5.755	1.794	-0.460
9	1.197	1.176	1.125	2.147	1.147	1.150	4.147	1.147	1.155	0.147	-2.019
10	-1.285	0.648	0.544	1.277	0.289	0.277	3.277	0.315	0.277	-0.723	-2.522
11	-6.120	-3.818	-3.399	-2.625	-2.627	-3.625	-0.625	-0.633	-3.625	-4.625	-6.601
12	-8.233	-5.882	-6.236	-5.059	-5.059	-6.059	-3.059	-3.059	-6.059	-7.059	-8.860

Table 4.3: standard deviation of daily maximum TA at Piz Corvatsch and for all generated climate scenarios. $1-50$ and $51-100$ indicate the years of the REF scenario used for the statistics, and are separated since each climate change scenario begins with REF_{1-50}.

month	Piz Corvatsch	REF_{1-50}	REF_{51-100}	+1All	+1Win	+1Sum	+3All	+3Win	+3Sum	-1All	-3All
1	4.486	4.240	4.367	4.387	4.388	4.387	4.387	4.398	4.387	4.387	4.097
2	5.142	4.585	4.945	4.845	4.843	4.845	4.845	4.842	4.845	4.845	4.921
3	4.740	4.482	4.582	4.505	4.505	4.505	4.505	4.505	4.505	4.505	4.644
4	3.650	5.476	5.453	5.414	5.414	5.414	5.414	5.414	5.414	5.414	5.619
5	3.292	3.151	3.138	3.244	3.244	3.259	3.244	3.244	3.301	3.244	3.059
6	3.804	3.463	3.543	3.426	3.426	3.431	3.426	3.426	3.443	3.426	3.548
7	3.419	7.198	7.149	7.075	7.075	7.075	7.075	7.075	7.075	7.075	7.011
8	3.405	4.054	3.990	3.932	3.932	3.937	3.932	3.932	3.956	3.932	4.028
9	3.646	6.201	6.032	6.185	6.185	6.185	6.185	6.185	6.187	6.185	5.955
10	3.840	3.800	3.817	3.792	3.783	3.792	3.792	3.775	3.792	3.792	3.907
11	4.530	4.370	4.520	4.598	4.595	4.598	4.598	4.591	4.598	4.598	4.595
12	4.565	4.735	4.633	4.749	4.749	4.749	4.749	4.749	4.749	4.749	4.547

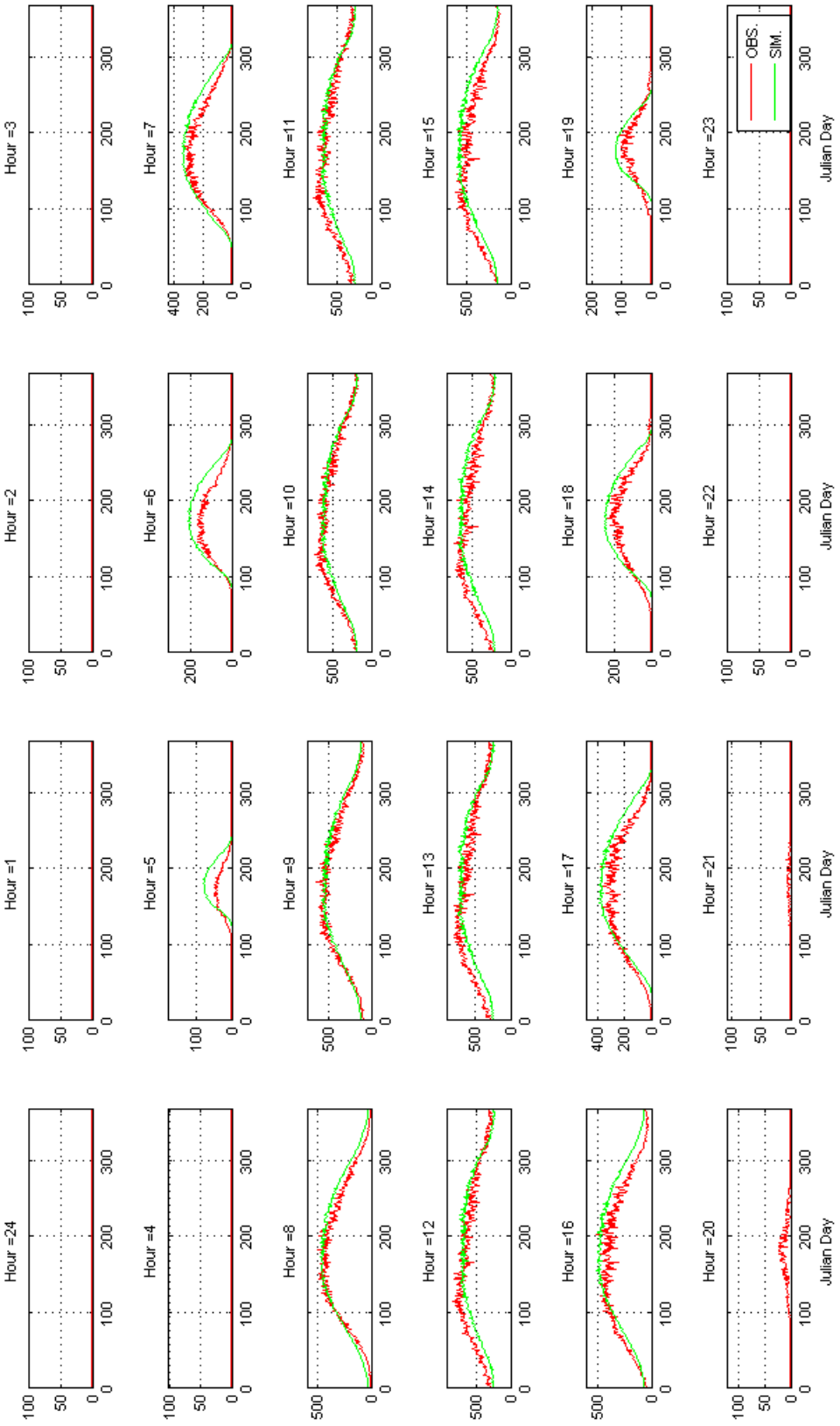

Figure 4.9: Comparison of hourly global solar radiation [W m^{-2}] between observations and REF scenario

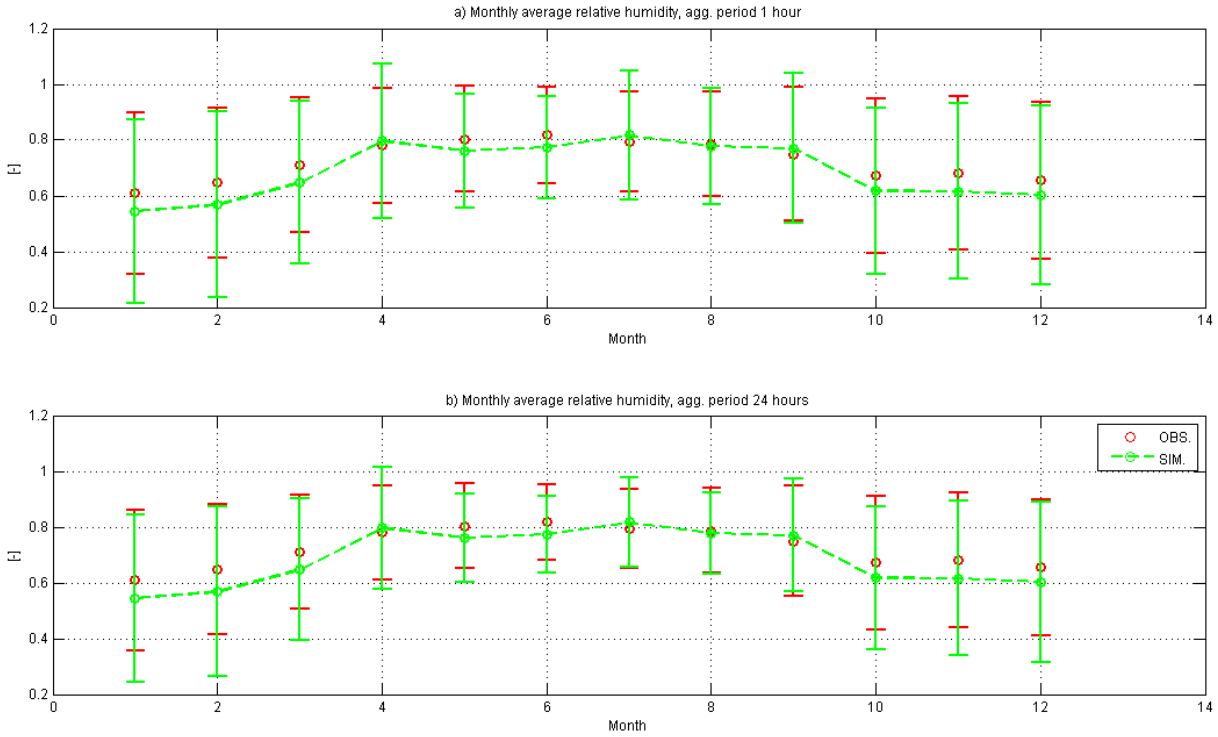

Figure 4.10: A comparison between the observed and generated mean monthly relative humidity for hourly and daily aggregation periods. The bars represent +/− 1 standard deviation.

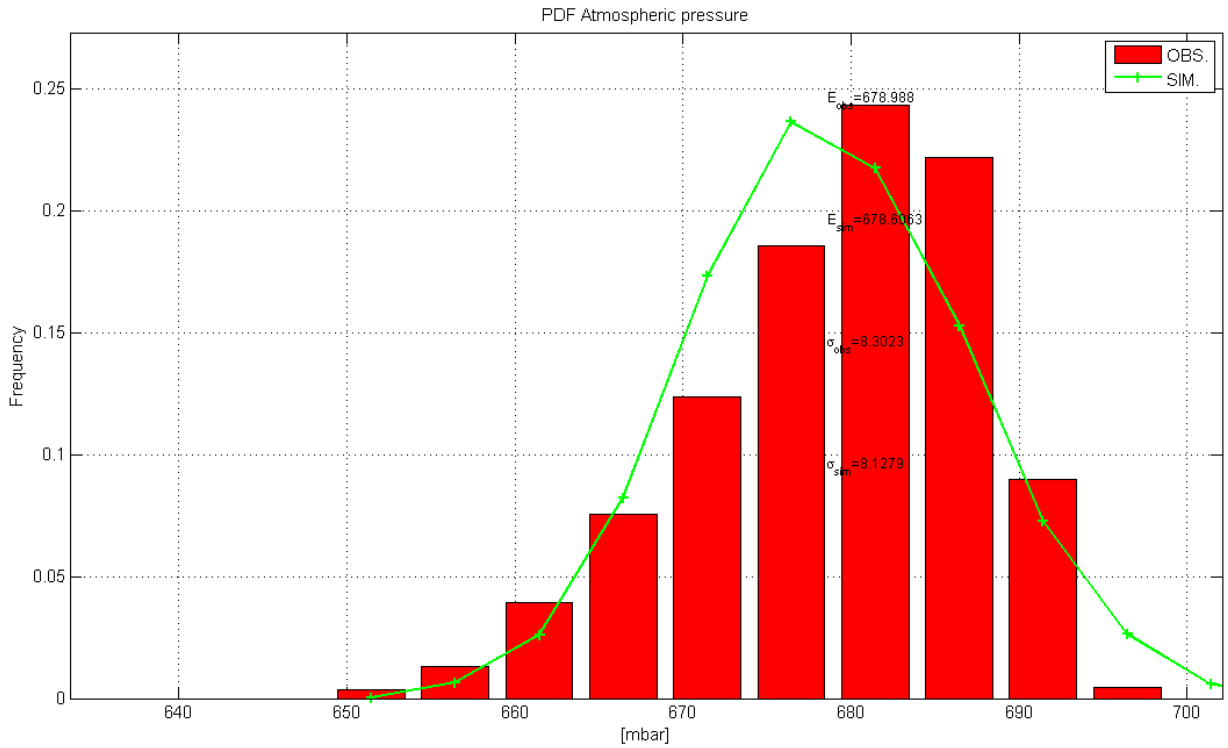

Figure 4.11: A comparison between the observed and generated atmospheric pressure probability density functions. E_{obs} and σ_{obs} are the observed mean and standard deviation and E_{obs} and σ_{obs} are the generated values.

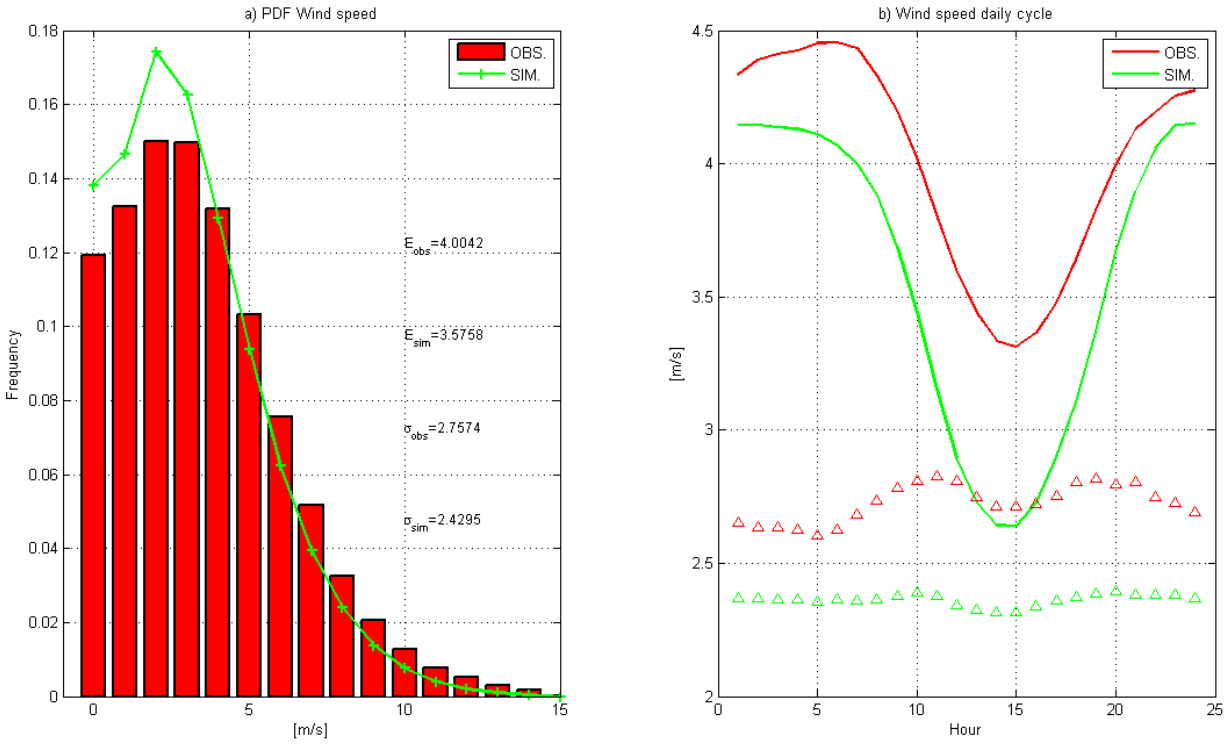

Figure 4.12: A comparison between the observed and generated wind speed probability density functions and daily cycles. E_{obs} and σ_{obs} are the observed mean and standard deviation. and E_{obs} and σ_{obs} are the generated values. In b), the line indicates mean wind speed while the triangles represent the standard deviation thereof.

4.1.3 Climate change scenarios

Other than TA, the daily (or monthly total in the case of Pr) means and standard deviations of the generated weather variables in the climate change scenarios are practically identical to the REF scenario (i.e. equivalent to the first decimal, Appendix A). TA is affected in this regard in very close correspondence with the utilized mean monthly temperature factors of change, with extreme temperatures similarly affected while variability is unaffected (Table 4.2, Table 4.3, Table A.3, Table A.4, Table A.5, Table A.6). Mean annual TA for all of the climate change scenarios are within 0.1°C of the specified factor of change (Table 4.4).

Table 4.4: Mean annual air temperature (MAAT) at PC and for all utilized climate scenarios. ΔMAAT_{PC} and $\Delta\text{MAAT}_{REF1-50}$ refer to the difference between MAAT in each row, and MAAT at Piz Corvatsch and in REF_{1-50} respectively.

	MAAT	ΔMAAT_{PC}	$\Delta\text{MAAT}_{REF1-50}$
Piz Corvatsch	-5.14		+1.82
REF_{1-50}	-6.96	-1.82	
REF_{51-100}	-7.08	-1.94	-0.12
+1All	-6.05	-0.91	+0.91
+1Win	-6.80	-1.66	+0.16
+1Sum	-6.80	-1.66	+0.16
+3All	-4.05	-1.09	+2.91
+3Win	-6.30	-1.16	+0.66
+3Sum	-6.30	-1.16	+0.66
-1All	-8.05	-2.91	-1.09
-3All	-10.06	-4.92	-3.10

4.2 Rock glacier modeling

Five year means of the target variables for each point are assessed prior to and after 50 years of each climate scenario. The time period and scenarios for target variables are specified in the following manner. Years 45–50 are referred to as the 'reference condition' and are shared by all the climate scenarios (Figure 3.1). The target variables after 50 years under the climate change scenarios are indicated by TV_{95-100}, substituting the relevant target variable for TV, along with indicating the climate scenario. Here, the climate scenarios are given descriptive names for readability. 'Moderate warming' or 'severe warming' refer to +1°C or +3°C increases in mean annual air temperature respectively. The seasonal warming scenarios are named 'moderate winter warming' or 'moderate summer warming' for +1°C increases in the corresponding mean monthly air temperature, and 'severe winter warming' or 'severe summer warming' for the +3°C changes to the corresponding mean monthly air temperature. 'Moderate cooling' and 'severe cooling' refer to the -1°C and -3°C scenarios respectively. Changes in target variables from reference conditions to the end of the climate change period are referred to as the 50 year climate sensitivity for a specified target variable and climate change scenario. Following the general overview of the target variables, a detailed examination is made of the modeled permafrost evolution for two notable points.

4.2.1 MAGST

Topographic parameters caused appreciable variation in simulated ground surface temperature while the depth of free lateral drainage and soil type had negligible influences. Simulated temperature under reference conditions, $MAGST_{45-50}$, ranged from -7.39 to 0.84°C (Table C.1). Under reference conditions, simulated mean surface temperatures were warmer by 2.27°C at 2700 m a.s.l. than at 3000 m a.s.l., and 2.30°C at 3000 m a.s.l. than 3300 m a.s.l.. South exposed points at 2700 m a.s.l. were 3.16°C warmer on average than north facing points at the same elevation under reference conditions. This tendency was amplified with elevation; south exposed points at 3300 m were 4.14°C warmer than north facing points at the same elevation. Differences in simulated mean surface temperature among points grouped by soil types and depths of free lateral drainage, FreeLD, were less than 0.01°C.

Changes in mean annual air temperature in the climate change scenarios were amplified in ground surface temperature and winter air temperature increases had a slightly greater

effect on ground surface temperature than summer air temperature increases. After 50 years of adjustment from reference conditions to a moderately warmer climate, simulated surface temperatures ranged from -5.58°C to 2.18°C (Figure 4.13). The air temperature change is amplified in simulated surface temperatures with mean $MAGST_{95-100}$ of all points in the +1All scenario greater by 1.48°C than under reference conditions. After 50 years of adjustment to a severely warmer climate, simulated mean surface temperatures ranged from -3.12°C to 4.22°C. The air temperature change was again amplified in surface temperatures, with mean $MAGST_{95-100}$ of all points in the +3All scenario greater by 3.49°C than under reference conditions. It is noted that the amplification did not increase with increasing air temperature factor of change. Regarding seasonal air temperature changes, simulated surface temperature under moderate and severe winter warming caused increases which were greater by 0.05°C and 0.15°C respectively than the corresponding summer temperature increases.

The effect of air temperature increases on simulated ground surface temperature was related to the topographic circumstances of the rock glacier points. Simulated MAGST was most affected by air temperature changes at high elevation north facing points. The 50 year MAGST sensitivity to severe warming ranged from 3.2°C to 3.4°C for south facing points between 2700 m a.s.l. and 3300 m a.s.l., whereas surface temperature for points with a north exposure increased after severe warming by 3.5°C to 4.2°C at the same elevations. A comparable effect was present in the +1All scenario.

While air temperature increases were amplified in simulated MAGST, decreases were dampened. The mean difference under a moderately cooler climate was -0.85°C from reference conditions, compared to a 1.48°C increase in the adjustment to moderate warming from reference conditions. Similarly, under severe cooling MAGST was cooler by 2.49°C on average than reference conditions. In this case, the amount of dampening had some proportionality with the difference in mean annual air temperature.

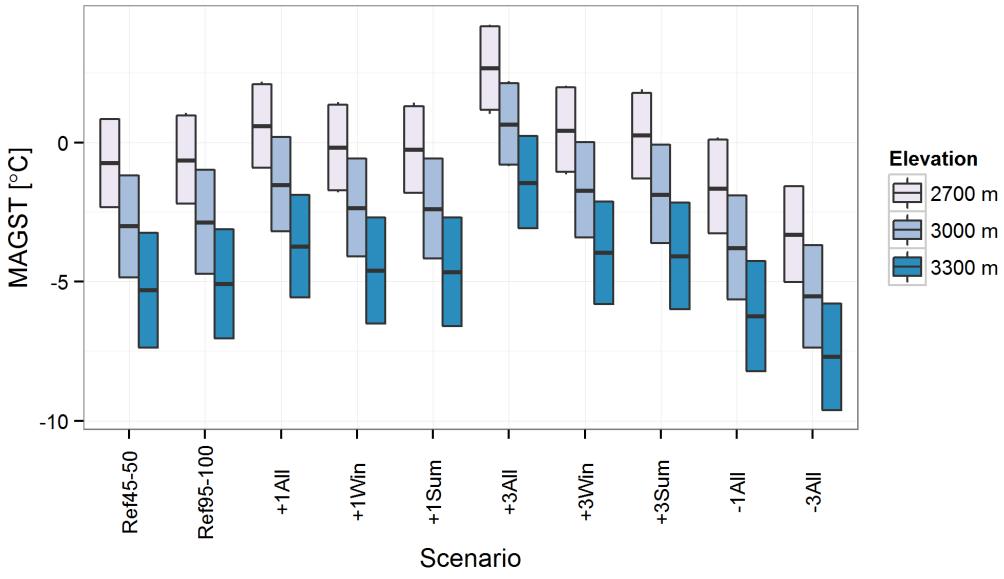

Figure 4.13: Simulated MAGST of all rock glacier points. Values for each point correspond to means of the target variable during years 45 to 50 of the REF scenario (Ref45-50), 95 to 100 of the REF scenario (Ref95-100), or 95 to 100 of the climate change scenarios. Each boxplot contains all the points in Table B.1 with the value of the grouping variable indicated in the legend to the right.

4.2.2 Active layer depth

Simulated active layer depths of low elevation south facing points did not stabilize in the REF scenario. Simulated active layer depths under the reference conditions ranged from 1070 mm to 4188 mm across all the points; minimum D_{AL} remained practically the same by years 95-100 of the reference scenario while the maximum D_{AL} increased to 6830 mm (Table C.2). The increases in D_{AL} between the middle and end of the REF scenario occurred at low elevation south facing points and ranged from 2640 mm to 2855mm, except for points with FreeLD of 15000 mm, for which D_{AL} increased only 459 mm (sand) to 647 mm (gravel). Between sand and gravel soil types there was a 22 mm difference in mean D_{AL} under the reference conditions.

Other than the points with elevation of 2700 m a.s.l. and south aspect, all simulated active layer depths were less than 2000 mm in all scenarios other than the severe warming scenario (Figure 4.14). In the severe warming scenario, points with a south aspect at 2700 m a.s.l. had D_{AL} values of 7712mm to 11771mm while points with the same aspect but elevation of 3000 m a.s.l. had D_{AL} values of 5061 mm to 6775 mm. Points with a north aspect and 2700 m a.s.l. elevation experienced increases in D_{AL} which were smaller than south facing points at the same elevation or 3000 m a.s.l. elevation (Figure 4.15). The apparent damping influence of FreeLD also reversed for points with a north aspect and 2700 m a.s.l. elevation, with points having greater FreeLD undergoing a greater increase in D_{AL}.

4.2.3 Total ice content

The dynamics of simulated total ice content mirror active layer depths (Figure 4.16). Under reference conditions simulated total ice content, IWE_{tot}, ranged from 6580 mm w.e. to 8672 mm w.e. across all points. By the end of the REF scenario minimum IWE_{tot} at lowest elevation south facing points decreased to 5348 mm w.e., regardless of their FreeLD values (Table C.3). There was a 23 mm w.e. difference in mean IWE_{tot} between sand and gravel soil types under reference conditions, and similar or smaller differences existed between the soil types in all scenarios.

Simulated total ice content was hardly affected by increases in mean air temperature, except for those of severe warming conditions. Under moderate and severe warming conditions, median reductions of IWE_{tot} from reference conditions were 55 mm w.e. and 466 mm

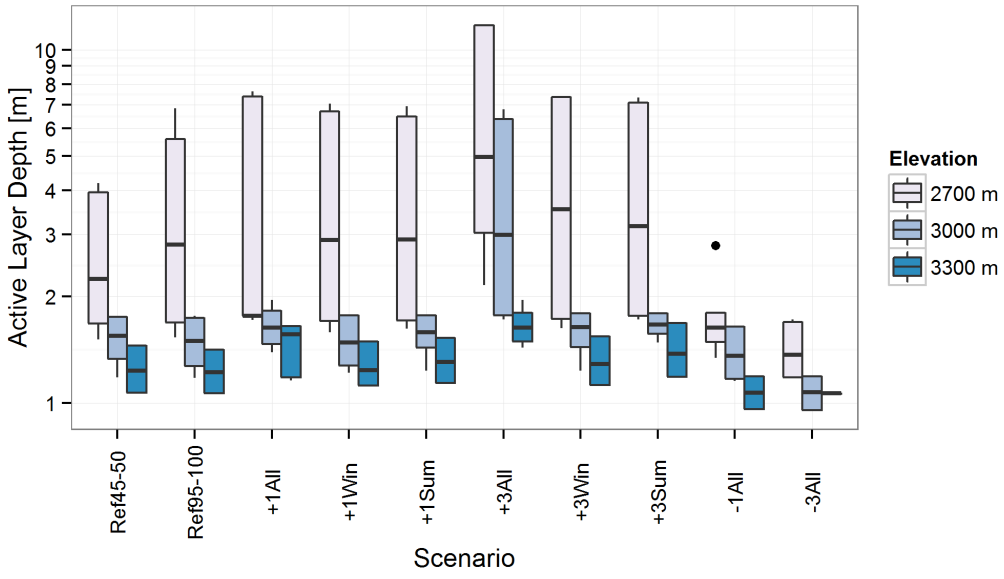

Figure 4.14: Simulated active layer depth of all rock glacier points. Values for each point correspond to means of the target variable during years 45 to 50 of the REF scenario (Ref45-50), 95 to 100 of the REF scenario (Ref95-100), or 95 to 100 of the climate change scenarios. Each boxplot contains all the points in Table B.1 with the value of the grouping variable indicated in the legend to the right.

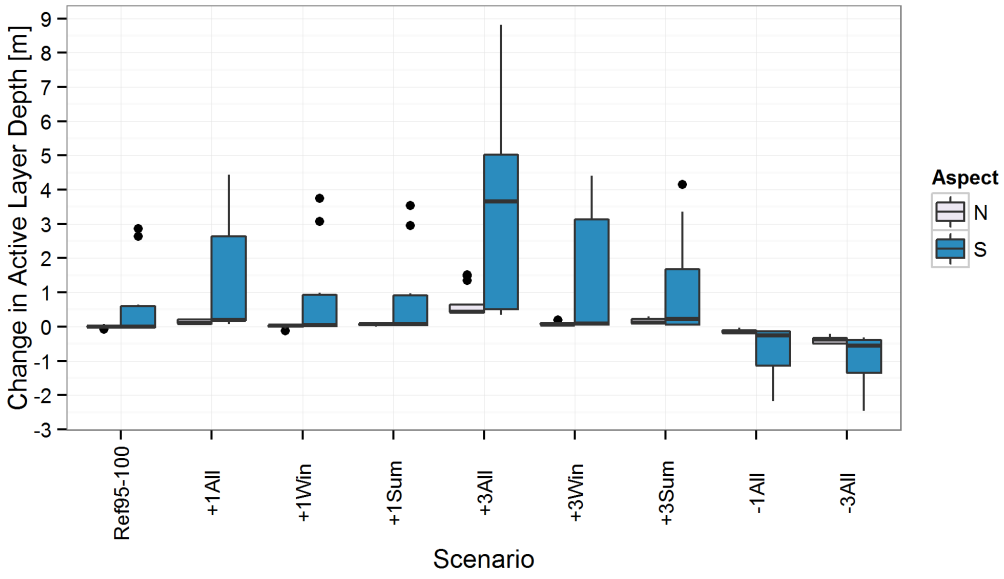

Figure 4.15: Differences in simulated active layer depth of all rock glacier points between the end of the climate change scenarios and reference conditions. Each boxplot contains all the points in Table B.1 with the value of the grouping variable indicated in the legend to the right.

w.e. respectively; the corresponding means are much greater due to the influence of low elevation south-facing points as described above. Changes in IWE_{tot} under severe winter warming conditions are comparable to those described for the moderate annual warming conditions, while little change is apparent under the moderate winter warming, moderate summer warming, and severe summer warming conditions (Figure 4.17).

Under severe warming conditions, FreeLD emerged as a very important parameter. The most climatically sensitive points with FreeLD of 15000 had a reduction in IWE_{tot} which was 1750 mm w.e. less than points with relatively low FreeLD values.

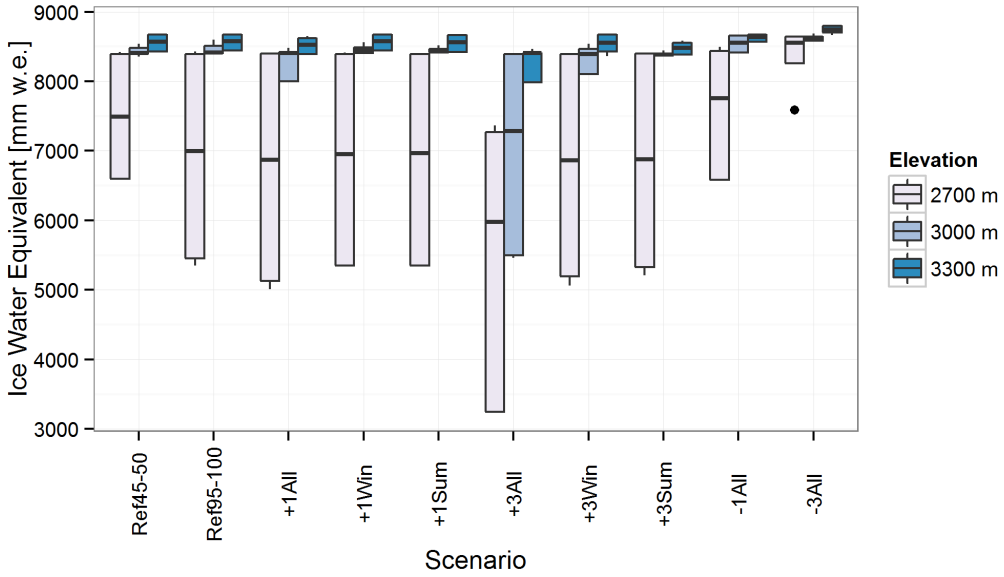

Figure 4.16: Simulated total ice content of all rock glacier points. Values for each point correspond to means of the target variable during years 45 to 50 of the REF scenario (Ref45-50), 95 to 100 of the REF scenario (Ref95-100), or 95 to 100 of the climate change scenarios. Each boxplot contains all the points in Table B.1 with the value of the grouping variable indicated in the legend to the right.

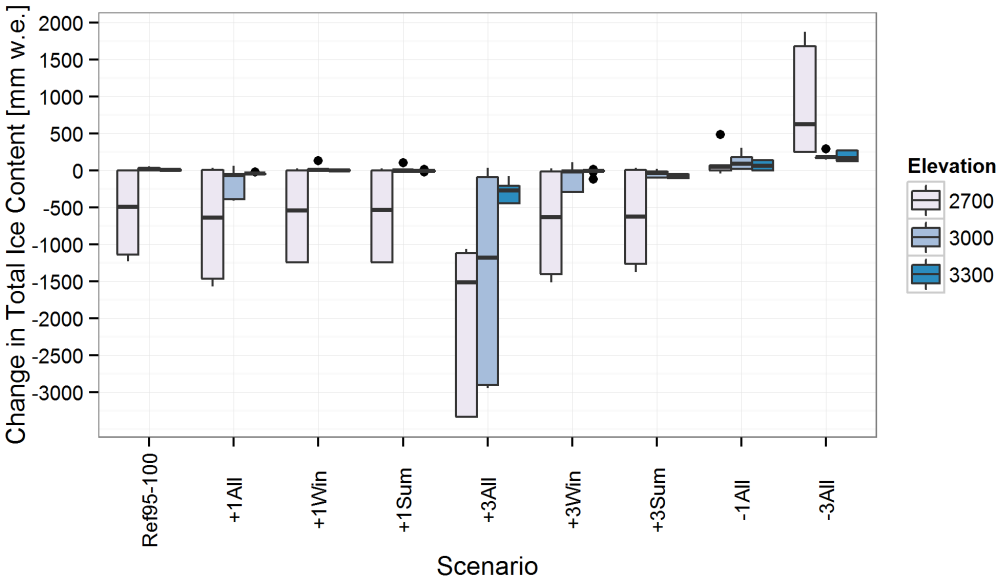

Figure 4.17: Differences in simulated total ice content of all rock glacier points between the end of the climate change scenarios and reference conditions. Each boxplot contains all the points in Table B.1 with the value of the grouping variable indicated in the legend to the right.

4.2.4 Seasonal melt

Simulated $MELT_{sum}$ generally decreased with elevation (Figure 4.18) and was highest for south–exposed slopes (Figure 4.20). Note that the sign of $MELT_{sum}$ in the text reflects the rock glacier soil column water balance so that negative $MELT_{sum}$ values indicate water that is made available to become runoff. Under reference conditions, $MELT_{sum}$ ranged from -22 mm w.e. to -296 mm w.e. (Table C.4). Low elevation points with south aspect and FreeLD of 15000 mm had the smallest $MELT_{sum}$ values under the REF scenario; this was also the case in all of the warming scenarios and in the -1All scenario. Under severe warming conditions, the low elevation south facing points had exceptionally low $MELT_{sum}$ values irrespective of FreeLD values (Table C.4).

Moreso than the other variables investigated, it was difficult to generalize the response of $MELT_{sum}$ to the climate change scenarios. Low elevations had a large range of simulated $MELT_{sum}$ values while medium elevation points were constrained to $MELT_{sum}$ values of -200 mm w.e. to -250 mm w.e. in all scenarios and indicate no systematic response to climate change (Figure 4.18). However, high elevation points show a clear and consistent response of increasingly negative $MELT_{sum}$ values (i.e. greater seasonal thaw) to air temperature increases (Figure 4.19). Under moderate and severe warming conditions mean $MELT_{sum}$ values were -188 mm w.e. and -239 mm w.e. respectively for points at 3300 m a.s.l., equivalent to changes of -75 mm w.e. and -127 mm w.e. from reference conditions. $MELT_{sum}$ also increased substantially in cooling scenarios; all elevations were affected and mean $MELT_{sum}$ for points at 3300 m a.s.l. increased from reference conditions by +61 mm w.e. and +100 w.e. under moderate and severe warming conditions respectively.

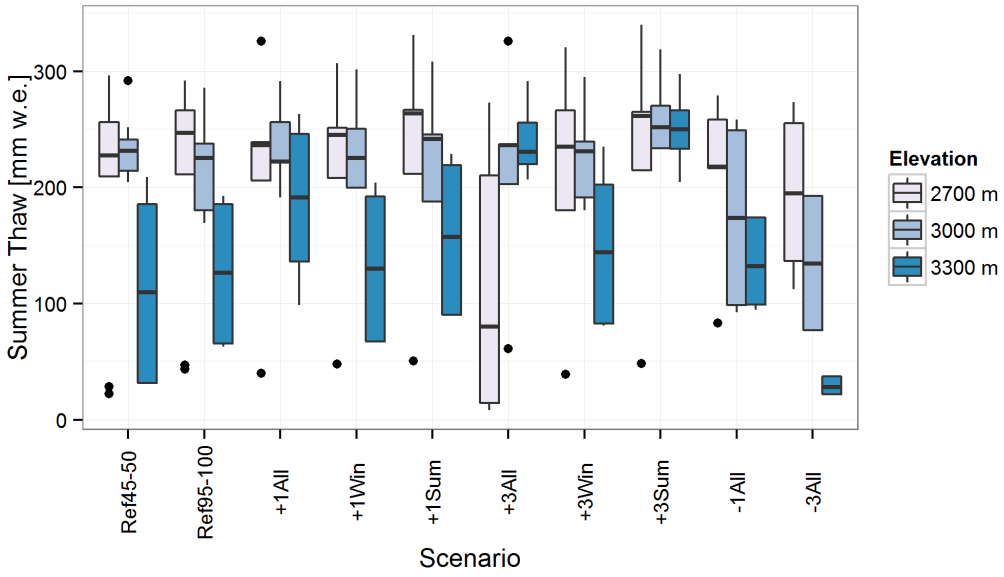

Figure 4.18: Simulated ice melt during summer months of all rock glacier points. Values for each point correspond to means of the target variable during years 45 to 50 of the REF scenario (Ref45-50), 95 to 100 of the REF scenario (Ref95-100), or 95 to 100 of the climate change scenarios. Each boxplot contains all the points in Table B.1 with the value of the grouping variable indicated in the legend to the right. Here, positive values indicate negative ice balance and potential contribution to summer runoff.

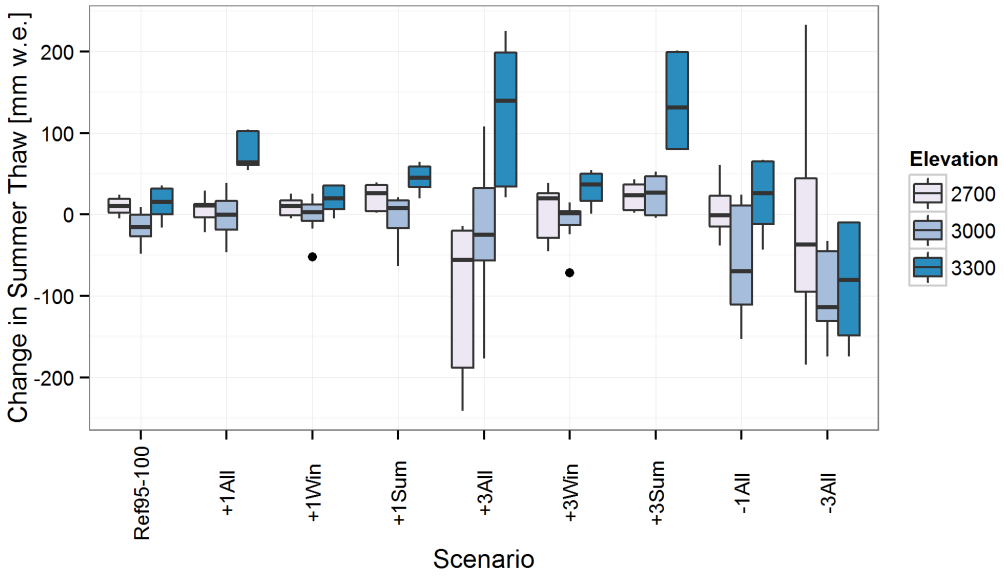

Figure 4.19: Differences in simulated seasonal melt of all rock glacier points between the end of the climate change scenarios and reference conditions. Each boxplot contains all the points in Table B.1 with the value of the grouping variable indicated in the legend to the right. Positive values indicate an increase in the potential contribution to summer runoff.

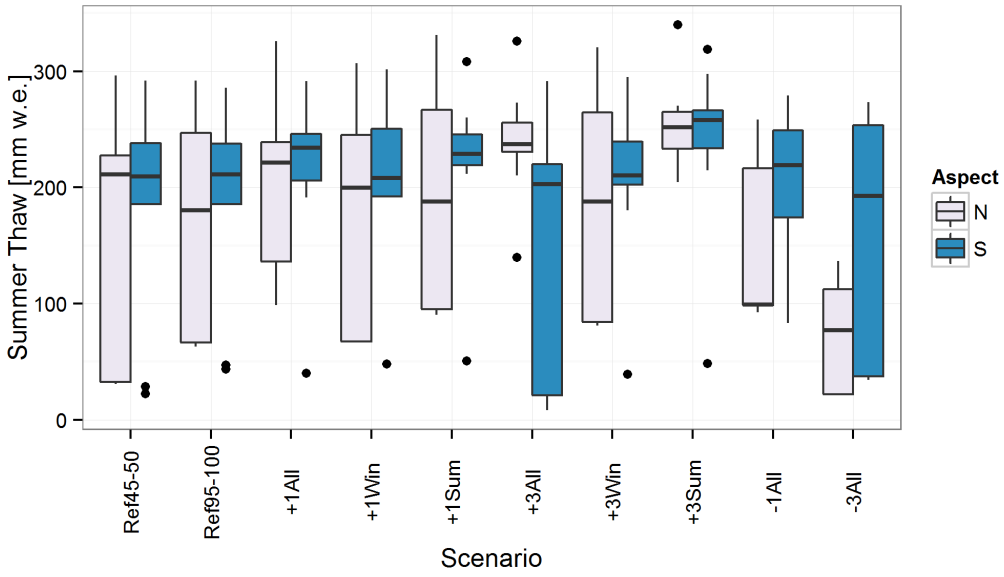

Figure 4.20: Simulated ice melt during summer months of all rock glacier points. Values for each point correspond to means of the target variable during years 45 to 50 of the REF scenario (Ref45-50), 95 to 100 of the REF scenario (Ref95-100), or 95 to 100 of the climate change scenarios. Each boxplot contains all the points in Table B.1 with the value of the grouping variable indicated in the legend to the right. Here, positive values indicate negative ice balance and potential contribution to summer runoff.

4.2.5 Interannual permafrost evolution

Poorly drained (Figure 4.21) and well drained (Figure 4.22) rock glacier points were examined annually on September 1st, a date which approximates the maximum D_{AL} and hence permafrost table. At 3000 m a.s.l. with southern aspect, these points provide the most relevant example of the possible dynamics of real–world rock glaciers under future climate change as they reach an apparent equilibrium under the REF scenario and undergo remarkable permafrost degradation after the onset of the climate change scenario.

In the REF scenario the permafrost quickly approaches the melting point and remains stable thereafter (Figure 4.21, Figure 4.22). D_{AL} stabilizes after 2-3 years at approximately 1.5 m for both points. Interannual fluctuations of the D_{AL} are negligible under the REF scenario. The upper 1.25 m of the soil column is dry, having no ice and only residual water. Ice content increases from 0.05 (ratio of ice to total volume) at ∼0.25 m above the active layer to a maximum of 0.60 at ∼0.25 m beneath D_{AL}. A zone 0.5 m thick with high water content appeared above the active layer after approximately 10 years. The entire permafrost body, which was initially at -2°C, reached 0°C after 10 years.

After the onset of the climate change scenario the permafrost body melts from the top down with response time of just 1 or 2 years (Figure 4.21, Figure 4.22). A step–like thaw front progression is present and presumably relates to increasing lengths of time required to melt larger ice layers defined by the soil discretization; similarly, the gradients in temperature, ice content, and water content decrease with time as the vertical distance they cover increases while their extreme values remain the same. After 50 years under the +3All scenario D_{AL} increased by 2.5 m and 4.5 m for points 17 and 29 (which differ only in FreeLD value) respectively. For point 29, for which lateral drainage is impeded below 2m depth, water gain was commensurate with ice loss (Figure 4.21). After 50 years there is no indication of a new equilibrium between the climatic conditions and permafrost body

The same procedure was applied on March 1st for an assessment of the winter soil thermal and hydrological states (results not shown). Wintertime soil temperatures were consistent through the REF and +3All scenario, although cold temperatures appeared to penetrate less deep into the soil column under the +3All scenario. Ice content remained 0 where permafrost melted from both soils, and the soil with inhibited drainage formed a talik where the water from melted ice was trapped.

These analyses were also performed for other climatic conditions (results not shown). In the +1All scenario, D_{AL} remained the same as during the REF scenario, with intermittent

deviations to greater depths. However, ice content in the upper active layer reduced, indicating a net heating effect in the near–surface soil. In cooling scenarios the permafrost bodies developed a negative thermal gradient rather than warming to the melting point. And in the -3All scenario, D_{AL} decreased to 1m, and near–surface soil ice content increased.

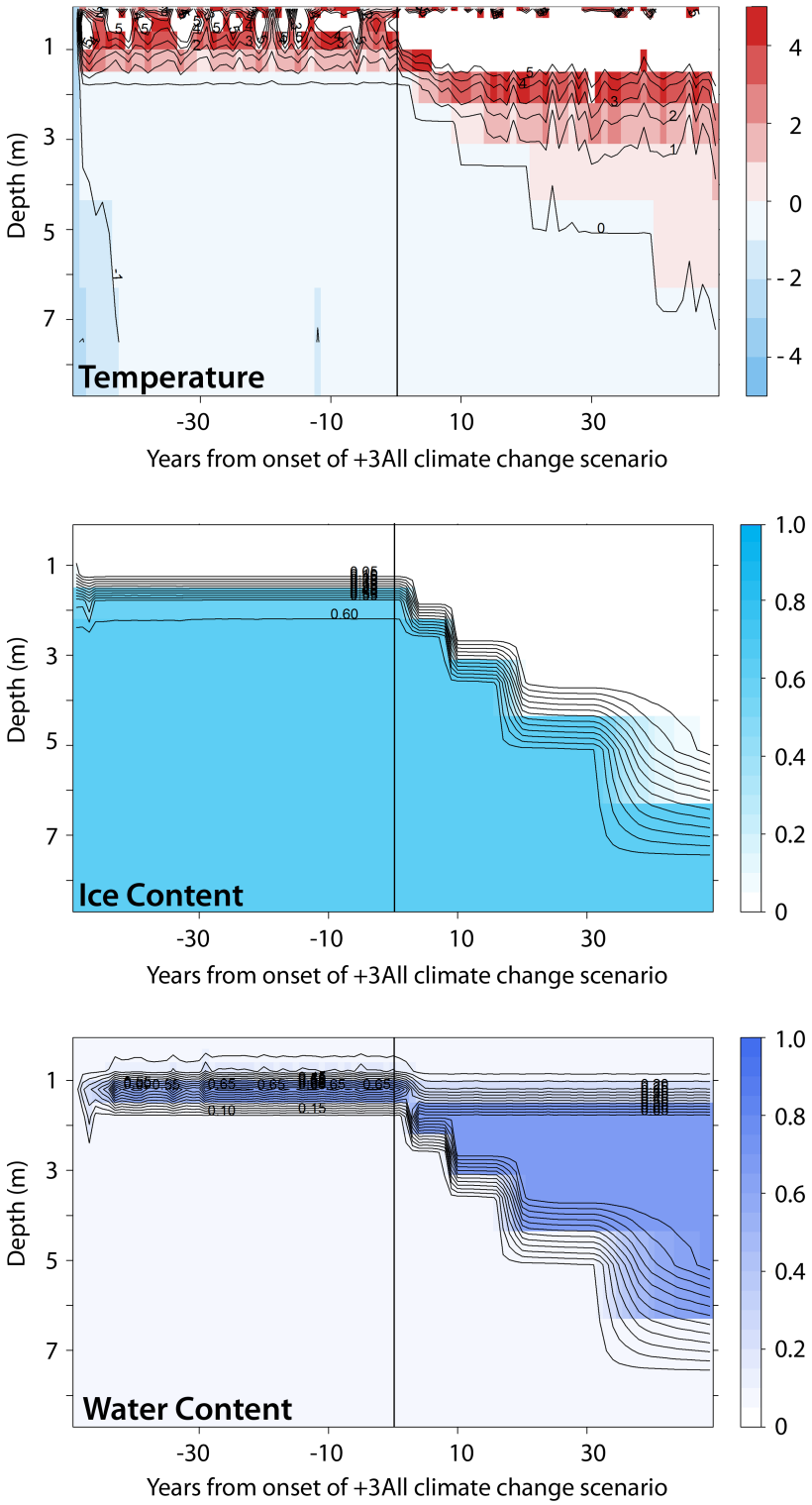

Figure 4.21: Simulated evolution of temperature [°C], ice content [–]. and water content [–] in a rock glacier with elevation of 3000 m a.s.l., south aspect, hydraulic properties of gravel soil, and depth of free lateral drainage limited to 2000 mm. The vertical line at the middle of the x-axis indicates the beginning of the +3All climate scenario.

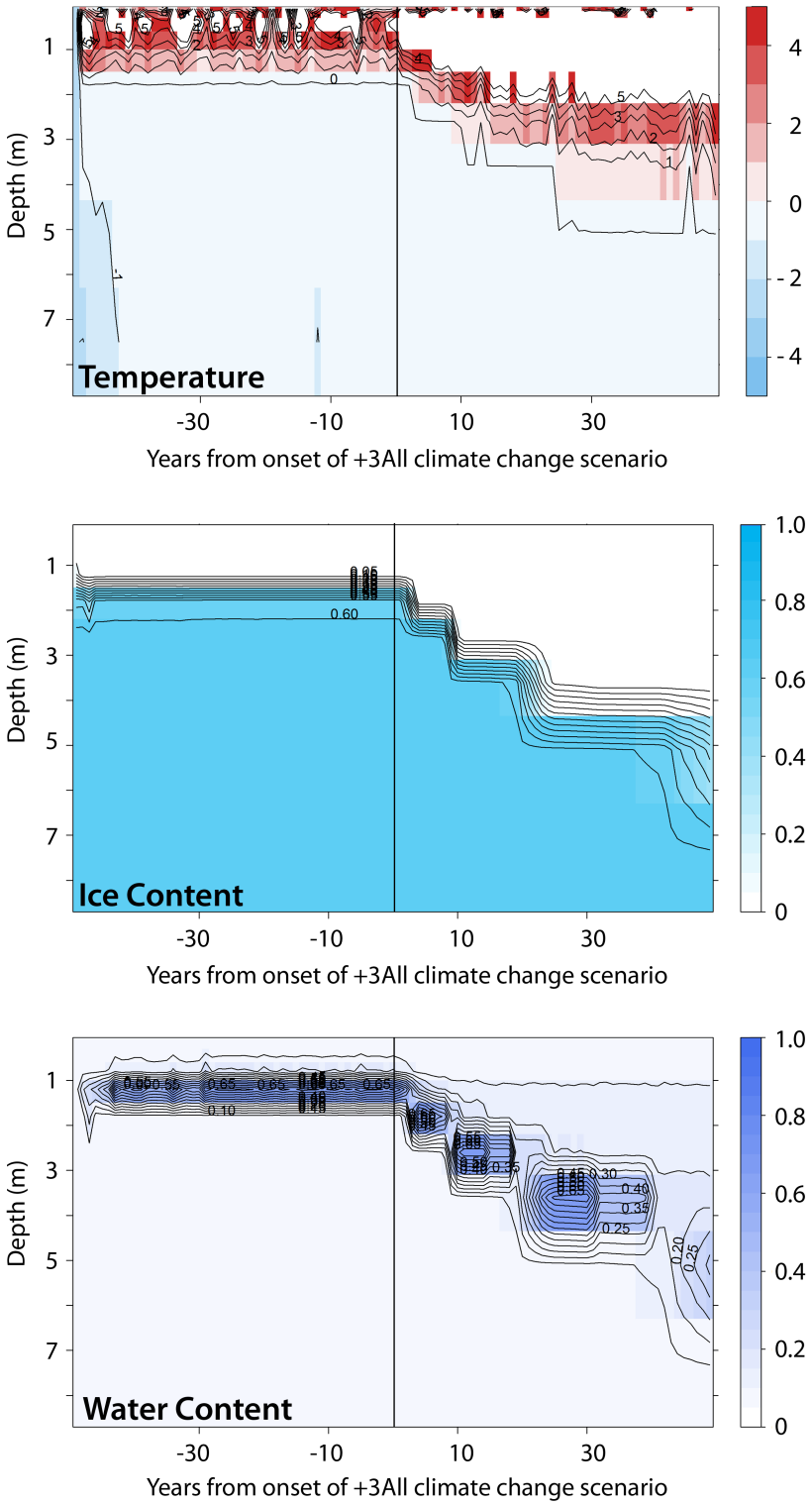

Figure 4.22: Simulated evolution of temperature [°C], ice content [–]. and water content [–] in a rock glacier with elevation of 3000 m a.s.l., south aspect, hydraulic properties of gravel soil, free lateral drainage throughout the entire depth of the soil column. The vertical line at the middle of the x-axis indicates the beginning of the +3All climate scenario.

Chapter 5

Discussion

5.1 Weather generation

Weather generators present an effective tool to asses the variability of hydrological elements (i.e. snow, glaciers, rock glaciers) of the high mountain cryosphere. This work presented one of the first uses of a weather generator in cryospheric studies. Frans et al. (2013) and Uhlmann et al. (2012) used weather generators to investigate glacier dynamics in Southern Switzerland and Bolivia respectively, but did not report on the quality of the generated weather data in detail, so comparisons of weather generator performance between this work and others are precluded.

5.1.1 Quality of generated weather data and effect on rock glacier simulations

There are some shortcomings in the means of application of AWE-GEN herein and in the weather generator itself. The discrepancies between generated and observed TA (Section 4.1.2) have rather complex causes and relate both to the unique climate at Piz Corvatsch and lack of accurate cloud fraction data. Regarding the unique climate at Piz Corvatsch, during January, February, March, May, June, October, November, and December there is no correlation between the TA gradient and the deterministic components of air temperature specified in equation 17 of Fatichi et al. (2011a); consequently, parameters

of the deterministic portion of TA could not be estimated and a fully stochastic representation was applied which failed to capture the diurnal variation of air temperature during these months (Figure 5.1). A solution to this problem was not presently apparent.

Data produced with weather generators should be evaluated in detail. In this work, what appeared to be discrepancies solely in mean TA in a few months in Section 4.1.2 were underlain by more appreciable errors. The concern of those errors to this work is how the permafrost simulations are affected by an approximate substitution of randomly perturbed mean daily temperature for the normal diurnal cycle of hourly temperature. The errors may affect the sensible and long wave heat fluxes in a predictable way with nocturnal (daytime) air temperatures being slightly warmer (cooler) than reality, and the presence of snow cover playing a modulating role. Assuming the errors in nocturnal and daytime air temperatures cancel, the effects may be presumed to be small on the time scales of investigation in this work.

In the other months where application of the fully stochastic TA model was not necessary, a large bias was present in the generated TA data (Figure 5.1). This relates in part to the transformation of transmissivity to cloud fraction based on equation 20 of Gubler et al. (2012) which resulted in left skewed distribution of cloud fraction. Subsequent difficulty in estimation of cloud fraction parameters by AWE-GEN propagated error to the estimation of solar radiation parameters, both of which are components of the physical TA aspect of AWE-GEN and also affect the stochastic component. A simple adjustment of the generated temperature data during such months could be recommended for future works. Otherwise it would be of interest to test the sensitivity of the rock glacier modeling results herein to this shortcoming of the generated weather data. An upstream solution is ideal. Different transformations of transmissivity, or directly measured cloud fraction data, could have provided improved weather generator parameter estimates and performance for Piz Corvatsch. Finally, the issues with TA in the generated weather data are minimized by comparing the climate change scenarios to reference conditions, rather than definitively applying the results of this work to Piz Corvatsch or other real world locations.

The lack of the proper diurnal variation in air temperature may have had an effect on the simulated permafrost thermal regime; since short term near surface temperatures are not considered, it is assumed to not disqualify the results and interpretations herein. If shorter time scale dynamics were to be investigated, a solution to issues with the weather generation is necessary. Other meteorological stations may not suffer the same issues with the weather generation, and should be tested. The quality of the meteorological time series created with AWE-GEN is considered functional but not ideal for the purposes applied in this work. AWE-GEN and and another similar weather generator have been

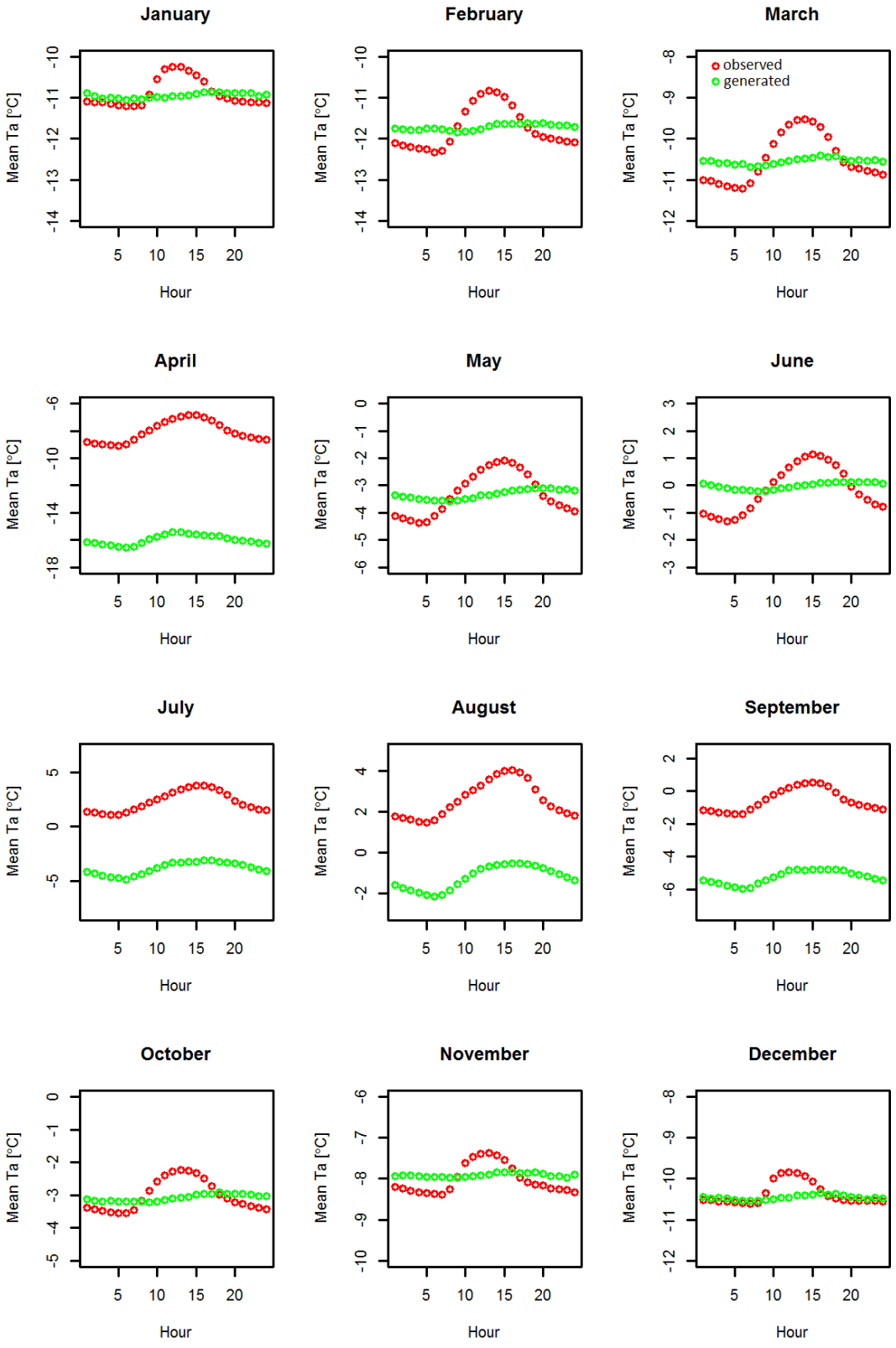

Figure 5.1: Hourly mean air temperature errors present in the data generated with AWE-GEN.

utilized in other studies pertaining to high mountain environments but without extensive quality assessment (Uhlmann et al., 2012; Frans et al., 2013). Additional testing is required before it is possible to consider weather generators as being of general practical use to environmental studies in high mountains. Poor performance in the case of this work was an unfortunate consequence of a particularly challenging case for the weather generator and the necessity of using cloud fraction information which was not directly measured.

The return periods of extreme hot and cold temperature events were much longer in the generated data than for observations at Piz Corvatsch, with heat waves more affected than persistent cold spells. Persistent warm temperatures especially during summer and fall may increase active layer depths which do not recover for several years and this effect is hypothesized as one of the critical means by which permafrost degradation occurs (Marmy et al., 2013). The underrepresentation of extreme temperatures by the weather generator may put estimates of permafrost degradation or aggradation in this work on the conservative side. However, the tendency for underrepresentation of both cold and warm spells may have a canceling effect.

5.1.2 Weather generator extensions and alternatives

There is a case for the conditioning of AWE-GEN parameters on synoptic scale atmospheric states supported by correlations of the climate data from Piz Corvatsch with the NAO index for improved weather generator performance. However, this would require more input data and only seasonal temperature and precipitation means were used in the analysis of climate stationarity at Piz Corvatsch, rather than specific AWE-GEN parameters (Fatichi et al., 2011a). AWE-GEN does not presently support protocols for non-stationary climate datasets, which may present a positive direction for its development.

A considerable limitation of the approach utilized here is that each time series of meteorological data generated with AWE-GEN represents only one possible realization of the fitted weather generator model and considerable uncertainty exists in the distribution of the generated weather data for a given parameter set, which is further incorporated into the rock glacier simulations. A Monte–Carlo approach (e.g. Katz, 2002; Zhang et al., 2004) would be of great benefit to similar studies, as confidence intervals for simulated target variables could be estimated. In this regard it is also important to consider what degree of variability in weather and climate is enough to affect permafrost evolution such that a Monte–Carlo approach is justified.

The climate change functionality of AWE-GEN at the time of this work was limited to changes in air temperature. Factors of change for precipitation would offer substantial benefit to climate change impacts modeling efforts (e.g. Frans et al., 2013). Given the relatively small winter precipitation totals at Piz Corvatsch, increases or decreases thereof might have caused pronounced effects on the rock glacier thermal and hydrological regimes, while changes to summer precipitation amounts may have had little effect (Marmy et al., 2013).

The application of a weather generator for high mountain permafrost modeling represents a novel approach in this work. The primary alternative thereto is the use of climate reanalyses (Marmy et al., 2013; Scherler et al., 2013). The advantages of this approach include historical congruency and excellent spatial coverage. However, their temporal coverage may be limited and there is a significant amount of uncertainty introduced by applying coarse resolution gridded reanalysis data to one dimensional permafrost models in high mountain environments. Future studies similar to the present work in other climatic regions would be a great benefit to this research but few meteorological datasets in rock glacier environments with enough coverage for weather generation exist; climate reanalyses offer a lot of potential in this regard. Regardless of the source of climatological data, high mountains present a special challenge to applications which require high quality weather data and comparisons of weather generation, reanalysis products, and linked methods would make a practical contribution to high mountain climate change impacts modeling.

5.2 Rock glacier modeling

5.2.1 Interpretations of model results

An amplification of the air temperature increase was present in simulated MAGST under the climatic warming scenarios. The amplification can be attributed to changes in snow cover properties, specifically onset and disappearance dates, concurrent with the air temperature increase. The range of MAGST amplifications for north facing points in the severe warming scenario (0.5°C to 1.2°C) correspond to snow cover disappearance dates earlier by 25 days to 60 days than under reference conditions, based on other analyses of the influence of snow cover on ground surface temperatures (Apaloo et al., 2012). The same range in advances of the snow cover disappearance date could be estimated at 10 days to 20 days for south facing points, where amplifications ranged from 0.2°C to 0.4°C.

These estimated changes in snow cover disappearance date based on MAGST amplifications are reasonable based on known sensitivities of snow cover disappearance date to air temperature at lower elevations in the Alps (Hantel & Hirtl-Wielke, 2007; Keller et al., 2005; Hantel et al., 2000), though some works suggest high elevations, such as those in this study, are less affected (Beniston et al., 2003). The greater sensitivity of MAGST to air temperature changes for high elevation north facing points may be attributed to a relatively strong control of air temperature on snow disappearance date, due to low solar radiation inputs. However, relatively late snow cover onset dates that would be expected under the severe warming scenario should have a cooling effect on MAGST, which would need to be exceeded by the warming effect of an early snow disappearance date. Nonlinearities in the effects of changing snow cover dates also present another obstacle to these interpretations (Apaloo et al., 2012; Luetschg et al., 2008). Definitive understanding of the changes in MAGST under climate change scenarios must therefore take into account snow cover properties, which can be extracted from GEOtop results, but were outside the scope of this work.

Similarly, a greater sensitivity to winter TA changes than summer TA increases of the same magnitude may be attributed to earlier snow disappearance dates. The independence of this result from elevation limits interpretation of the differing effects of seasonal warming on MAGST. Elsewhere, spring and autumn seasonal changes have stronger effects on surface temperature than summer or winter changes (Marmy et al., 2013), which may account for the small difference in MAGST changes under the summer and winter warming scenarios in this work.

The lack of appreciable differences between soil types under otherwise equal conditions in the rock glacier simulations was a notable result. Analysis of soil hydrological dynamics on shorter time scales may have revealed appreciable differences in the target variables between the soil types. Overall, few soil configurations were used in this work and further research utilizing more detailed soil columns and incorporations of uncertainty in soil parameters would be a beneficial. The results herein suggest that rock glacier soil type has little influence of the dynamics of permafrost degradation and rock glaciers with different particle size distribution may exhibit the same sensitivity to TA warming.

Where the entire soil column was given free drainage, the lack of consolidation of soil materials to smaller volumes after ice–melt leaves artificially large voids in a rocky layer above remaining ground ice. In this case, the permafrost is insulated from air temperature by this zone of low thermal conductivity to an unrealistically large degree. In cases where lateral drainage was inhibited, the soil column retained the water from melted ice, offering an analogue for the results where consolidation might have been included by preserving

the thermal conductivity of the soil layers above the remaining permafrost. Thus the results may be interpreted with consideration of FreeLD as bounding possible extremes of permafrost degradation in rock glaciers in a real–world environment. However, the upper boundary of rock glacier degradation offered by low FreeLD values is subject to some inaccuracy due to the unique thermal properties of the water retained in the soil column. The model would benefit from inclusion of soil settlement for more accurate simulations of rock glacier dynamics.

Based on these results, it is possible to make general speculation for real world rock glaciers near Piz–Corvatsch. Points 25 and 31 (north aspect, elevation 2700 m a.s.l.) under the +3Sum scenario can be interpreted as the closest to the present day Murtèl Corvatsch rock glacier; in this case the observed active layer depth is nearly reproduced with mean $D_{AL95-100}$ of 1.73 m (Murtèl Corvatsch near 1.75m in 2007, 2008 Arenson et al., 2010). The upper few metres of permafrost in the simulations herein are near 0°C whereas permafrost temperatures are near -2°C at these depths for Murtèl Corvatsch and the model is not calibrated to conditions there, so comparisons are not definitive. Furthermore, Murtèl Corvatsch rock glacier permafrost is approximately 50m deep, with ice content of 80% to 90% in the upper half of the rock glacier (Arenson et al., 2010; Hanson & Hoelzle, 2004), so values pertaining to water balance and storage are conservative. Differences in atmospheric conditions between Piz Corvatsch and the weather data generated with AWE-GEN discussed above also factor into these considerations. As approximated by $MELT_{sum}$, the potential summertime hydrological contribution of rock glacier points 25 and 31 is 266 mm (Table C.4). Additionally, the differences between corresponding points in the +3Sum and REF scenarios is fairly small, so if this analogue is further extended to these points under the REF scenario, the response to climate change can be assessed. Under the +3All scenario, the rock glacier hydrological and thermal properties are appreciably affected after 50 years. D_{AL} increased from 1.68 m to 3.20 m, IWE_{tot} decreased from 8389 mm to 7267 mm, and $MELT_{sum}$ increased from -228 mm to -140 mm, or a decrease in the potential summertime hydrological contribution of 39%. MAGST increased by 3.21°C from -2.19°C to 1.02°C. D_{AL} appeared stable after 50 years under the +3All scenario, but longer simulations would be required for confirmation.

Overall, low elevation south facing points appeared to respond the most dramatically to the climate change scenarios. However, these points also did not reach an apparent equilibrium under reference conditions scenario. The only points which reached an apparent equilibrium under reference conditions and showed a significant degree of response in IWE_{tot} and D_{AL} under other climates had 3000 m a.s.l. elevation and south aspect or, to a lesser degree, 2700 m a.s.l. and north aspect. It is difficult to distinguish if the low elevation

points would have first reached an equilibrium under the reference conditions, though ice aggraded in the cooling scenarios. The result motivates careful investigation of rock glaciers in apparent transitional states with permafrost temperatures near 0°C.

$MELT_{sum}$ was most sensitive to climate change at north facing high elevation points, corroborating with other work (Caine, 2010). Testing of different seasonal melt periods would be beneficial, as Caine (2010) identified an increasing permafrost melt trend in September to October and (Williams et al., 2006) also observed that rock glacier outflow from melted ice was highest in autumn months. Finally, $MELT_{sum}$ was negative for all points under all scenarios, despite summers which were cooler than spring resulting from issues with the data generated with AWE-GEN; this may be indicative of a strong radiative control during the snow-free period. Additional work relating $MELT_{sum}$ to the depth of the 0°C isotherm, i.e. active layer, may offer additional insight as they have been proposed as related (Williams et al., 2006).

Comparing simulated rock glacier IWE_{tot} changes to specific mass balance of glaciers indicates that glaciers contribute more water to runoff, though under certain circumstances glaciers and rock glaciers may be comparable. The estimated annual change in IWE_{tot} under severe warming conditions ranged from -21.2 mm w.e. a^{-1} to -58.9 mm w.e. a^{-1} for points with 3000 m a.s.l. and south aspect or 2700 m a.s.l. and north aspect. Low elevation south facing points were comparable whereas high elevation points were practically unaffected. These values are comparable to some glaciers in the Andes (Gascoin et al., 2011b; Bodin et al., 2010; Vergara et al., 2007). Specific annual mass balances during the period 1970 to 1991 reported for glaciers in watersheds of Bolivian Andes with positive glacial contributions to runoff range from -38 mm w.e. a^{-1} to -541 mm w.e. a^{-1} (Vergara et al., 2007). Five glaciers in the Huasco basin of semi–arid Chile had a mean specific mass balance of -840 mm w.e. during the period 2003 to 2008 (Gascoin et al., 2011b). Also, a glacier in the Punta–Negra sub catchment of the Andes of Santiago had an estimated specific mass balance of -73 mm w.e. a^{-1} during the period 1955 to 1996 (Bodin et al., 2010). The differing regional and temporal climatic regimes limit interpretation, but, in closer proximity to this study, specific mass balances for glaciers in Southwestern Switzerland are estimated at -690 mm w.e. a^{-1} by the year 2050 under moderate warming scenarios (Huss et al., 2008b). Other estimates of present day annual specific mass balance for glaciers in the Swiss and Austrian Alps are an order of magnitude higher (Huss et al., 2008a; Kuhn & Batlogg, 1998).

Regarding seasonal mass balances, mean $MELT_{sum}$ of points with 3000 m a.s.l. elevation was -235 mm w.e. under reference conditions. For comparison, during 2003 to 2009, mean summer mass balance of Guanaco glacier in Pascua–Lama region was -732 mm w.e.

(Rabatel et al., 2011). Definitive comparisons of this kind would require validation for specific rock glaciers, the use of observational weather data or representative weather data generated with a weather generator, and congruent time periods and spatial domains.

The results of this work may transfer to other rock glacierized mid–latitude high mountain areas with continental climates. The Rockies of the Midwest United States present a particularly interesting case. Rock glaciers cover an estimated area of 70.1 km^2 (2.4%) in the San Juan mountains of Colorado, where annual precipitation totals are similar to those at Piz Corvatsch and no glaciers are present (Brenning et al., 2007). This work motivates the inclusion of rock glaciers in the assessment of hydrological resources in Colorado and climatically similar regions.

5.2.2 Uncertainties and limitations

The accuracy of active layer depths is limited by the soil discretization, which increases with depth so that shallow active layers may be better represented than deep ones. Output depths were reduced from all of the soil layers (Figure 3.4) to facilitate processing of the simulation output; values at the output depths are interpolated from the cell above and below, possibly introducing some inaccuracy. Fixed output depths corresponding to the soil column cell centroids are recommended for future work, and should be informed by the objectives of the study. Finally, the exponentially increasing discretization yields a step characteristic to the permafrost degradation as thicker layers require more time to heat and melt - a constant discretization may be better in cases where the permafrost evolution at depth is the primary interest.

Standard sand and gravel hydraulic properties and a uniform soil column were utilized, but rock glacier soils have vertical variability and additional efforts incorporating exact rock glacier soil columns would be advantageous. Information on rock glacier soil hydraulic properties could also benefit similar work, but such studies have yet to be conducted. Knowledge of the specific vertical structures of rock glaciers is readily available for application to similar works (Monnier & Kinnard, 2013; Hausmann et al., 2012; Leopold et al., 2011; Arenson et al., 2002).

A significant limitation of this study was that the rock glacier models were constrained to 70% ice content of the permafrost body while the ice content of rock glaciers is a matter of notable uncertainty. A sensitivity study of ice content would be of interest; presumably rock glaciers with greater ice contents would have a slower response to climatic warming

in terms of the active layer depth, as is generally accepted when comparing ice–rich to ice–poor permafrost (Froese et al., 2008). However, there may be non-linearities in this relationship and a focused analysis of the hydrological response of rock glaciers with ice content in the range of 50% to 90% to climate change is of interest to mountain permafrost research.

Another limitation of this work is the nature of the rock glacier at the lower boundary of the soil column. For simplicity, continuous ice-rich permafrost without a bedrock layer was applied here. Bedrock could be added, and the permafrost at the bedrock initialized in a wet or ice–poor dry state as observed in various rock glaciers (Burger et al., 1999; Zhu et al., 1996). Furthermore, the total soil column depth of 15 m and a fixed zero heat flux at the lower boundary with the time scale utilized in this work may have accelerated the effects of climate change within the permafrost column as the total heat content of the soil may be trapped in less soil than what in reality it could be distributed within. For example, at least 22 m soil depth is recommended based on Equation 2.4 for a 50 year time scale and a thermal diffusivity of 10. MELT_{sum} should be minimally affected by this limitation.

This work was based on one–dimensional heat and mass transfer models and serves as a pilot work for spatial applications. Some of the properties observed herein could be extrapolated over areas absolutely or relative to glaciers or snow. One dimensional simulations are representative of conditions over horizontal distances which depend on heterogeneity of surface and subsurface characteristics, so few to several points may be adequate to simulate conditions of a given rock glacier depending on its size. Furthermore, one-dimensional simulations could be applied in a sub–grid manner over large areas (Fiddes & Gruber, 2012) or the 3D functionality of GEOtop utilized for individual rock glaciers, though many practical limitations to the latter may arise.

As for the climate scenarios, the climate change response in this work is also an idealized and accelerated one, being the result of a discrete transition between two climatic regimes rather than a gradual transition as occurs in the real world. AWE-GEN could be modified to accept trends rather than factors of change to permit more realistic climate change scenarios in the future. Nonetheless, the methodology is elsewhere implemented and serves comparisons of pre and post climate change states (Marmy et al., 2013).

Chapter 6

Summary and Conclusions

The goal of this work was to explore a novel methodology for assessing the thermal and hydrological dynamics of rock glaciers under present day, and possible alternative climatic scenarios. Important thermal and hydrological characteristics of rock glaciers in various topographic situations were quantified under present day climatic conditions and after five decades of response to alternate climatic regimes.

Parameters of the weather generator model were estimated from 27 years of weather observations at Piz Corvatsch near the Murtèl–Corvatsch rock glacier in Southeastern Switzerland, which defined the climatic context of the study. Nonstationarities present in observational data were presumed to have a negative influence on the performance of the weather generator but more sophisticated weather generator models are required to handle such circumstances.

Precipitation statistics between the generated and observed data were in excellent agreement. However, air temperature statistics were not reproduced accurately by the weather generator. In the REF scenario which was based on no change from observed climatic conditions, mean annual air temperature was 1.82°C cooler than observations at Piz Corvatsch. However, the discrepancies limited the opportunity to make comparisons between the simulations in this work and real world rock glaciers with weather conditions similar to Piz Corvatsch. Other locations, or improvements to AWE–GEN, may offer better performance and pursuit of these opportunities is recommended for future studies as weather generators offer unique advantages over observational or reanalysis data.

The thermal and hydrological evolution of rock glacier soils with 70% ice content in the permafrost layer and varying elevation and topographic cases were simulated under the reference and climate change scenarios. The response to climate change was assessed by comparing points from apparent equilibriums after 50 years under the REF scenario to their state 50 years later under the climate change scenarios. Air temperature increases were amplified in mean annual ground surface temperature. The amplifications under warming scenarios were greatest for high elevation north–facing points. Winter air temperature increases had a slightly greater effect on mean annual ground surface temperature than summer air temperature increases.

The simulated dynamics of the active layer depth and total ice content indicated that the ice–rich permafrost in rock glaciers is resistant to degradation from mean annual air temperature increases of of 1°C and summer or winter air temperature increases of up to 3°C. Only in the scenario where mean annual air temperature increased by 3°C was a substantial response observed in the simulations, and even then, only for points with climatically sensitive circumstances, i.e. high radiation conditions with moderate elevation and low radiation conditions with low elevation.

This study also investigated the seasonal ice balance of rock glaciers to estimate their potential contribution to summertime runoff. Under the reference scenario ice melt from stable rock glacier points during summer months ranged from 30 mm w.e. to 296 mm w.e. with more melt occurring at low to moderate elevations or for south facing points. Summer melt increased under all of the warming scenarios for high elevation points but decreased for some low elevation points; the lack of soil settlement in GEOtop limits interpretations of points with severe permafrost degradation. Nonetheless, this work supports real world observations of increased permafrost melt and contribution to runoff under warming climates in high mountains.

The methods applied in this work could feasibly be extended to spatial studies for specific regional assessments of rock glacier hydrological contributions and comparisons with other sources of runoff from the seasonal snow pack and glacier melt. Key recommendations for derivative work include sensitivity analysis of ice content, or the use of local geophysically based estimates of permafrost properties, and deeper soil profiles. Furthermore, this work utilized generic hydraulic properties of soil but ideally properties such as the hydraulic conductivity and parameters of the Van Genuchten model, which define soil water retention and the freezing characteristic curve must be obtained from physical studies of rock glaciers. Such work would be of particular importance in highly rock glacierized areas, such as the Arid Andes and San Juan mountains of Colorado.

References

Aizen, V. B., Aizen, E. M., Melack, J. M., & Dozier, J. (1997). Climatic and hydrologic changes in the Tien Shan, central Asia. *Journal of Climate*, *10*, 1393–1404. doi:10.1175/1520-0442(1997)010<1393:CAHCIT>2.0.CO;2.

Alexeev, V., Nicolsky, D., Romanovsky, V., & Lawrence, D. (2007). An evaluation of deep soil configurations in the CLM3 for improved representation of permafrost. *Geophysical Research Letters*, *34*, L09502. doi:10.1029/2007GL029536.

André, M.-F. (1994). Rock glaciers in Svalbard. Tentative dating and inferred long-term velocities. *Geografiska annaler. Series A. Physical geography*, *76*, 235–245.

Angillieri, E., & Yanina, M. (2009). A preliminary inventory of rock glaciers at 30°S latitude, cordillera frontal of San Juan, Argentina. *Quaternary International*, *195*, 151–157. doi:10.1016/j.quaint.2008.06.001.

Annandale, J., Jovanovic, N., Benade, N., & Tanner, P. (1999). Modelling the long-term effect of irrigation with gypsiferous water on soil and water resources. *Agriculture, ecosystems & environment*, *76*, 109–119. doi:10.1016/S0167-8809(99)00079-1.

Anwar, M., OLeary, G., McNeil, D., Hossain, H., & Nelson, R. (2006). Climate change impact on field crops and adaptation options in Southeastern Australia. In *Turner, NC, Acuna, T. and Johnson, RC (2006). Ground-breaking stuff. Proceedings of the 13th Australian Agronomy Conference* (pp. 10–14).

Aoyama, M. (2005). Rock glaciers in the Northern Japanese Alps: palaeoenvironmental implications since the late glacial. *Journal of Quaternary Science*, *20*, 471–484. doi:10.1002/jqs.935.

Apaloo, J., Brenning, A., & Bodin, X. (2012). Interactions between seasonal snow cover, ground surface temperature and topography (Andes of Santiago, Chile, 33.5 s). *Permafrost and Periglacial Processes*, *23*, 277–291. doi:10.1002/ppp.1753.

Arendt, A. A., Echelmeyer, K. A., Harrison, W. D., Lingle, C. S., & Valentine, V. B. (2002). Rapid wastage of Alaska glaciers and their contribution to rising sea level. *Science*, *297*, 382–386. doi:10.1126/science.1072497.

Arenson, L., Hauck, C., Hilbich, C., Seward, L., Yamamoto, Y., & Springman, S. (2010). Sub-surface heterogeneities in the Murtèl–Corvatsch rock glacier, Switzerland. In *Proceedings of the 6th Canadian Permafrost Conference* (pp. 1494–1500).

Arenson, L., Hoelzle, M., & Springman, S. (2002). Borehole deformation measurements and internal structure of some rock glaciers in Switzerland. *Permafrost and Periglacial Processes*, *13*, 117–135. doi:10.1002/ppp.414.

Avian, M., Kaufmann, V., & Lieb, G. K. (2005). Recent and holocene dynamics of a rock glacier system: The example of Langtalkar (Central Alps, Austria). *Norsk Geografisk Tidsskrift*, *59*, 149–156. doi:10.1080/00291950510020637.

Azócar, G., & Brenning, A. (2010). Hydrological and geomorphological significance of rock glaciers in the dry Andes, Chile (27–33°S). *Permafrost and Periglacial Processes*, *21*, 42–53. doi:10.1002/ppp.669.

Bader, S., & Bantle, H. (2004). *Das Schweizer Klima im Trend Temperatur– und Niederschlagsentwicklung 1864–2001*. Technical Report MeteoSchweiz.

Bardossy, A., & Plate, E. J. (1991). Modeling daily rainfall using a semi-Markov representation of circulation pattern occurrence. *Journal of Hydrology*, *122*, 33–47. doi:10.1016/0022-1694(91)90170-M.

Barnett, T. P., Adam, J. C., & Lettenmaier, D. P. (2005). Potential impacts of a warming climate on water availability in snow-dominated regions. *Nature*, *438*, 303–309. doi:10.1038/nature04141.

Baroni, C., Carton, A., & Seppi, R. (2004). Distribution and behaviour of rock glaciers in the Adamello–Presanella Massif (Italian Alps). *Permafrost and Periglacial Processes*, *15*, 243–259. doi:10.1002/ppp.497.

Barry, R. G. (2008). *Mountain weather and climate*. (3rd ed.). NY, New York: Cambridge University Press.

Barsch, D. (1996). *Rockglaciers*. Berling, Heidelberg: Springer-Verlag.

Barsch, D., & Jakob, M. (1998). Mass transport by active rockglaciers in the Khumbu Himalaya. *Geomorphology*, *26*, 215–222.

Bellone, E., Hughes, J. P., & Guttorp, P. (2000). A hidden Markov model for downscaling synoptic atmospheric patterns to precipitation amounts. *Climate research*, *15*, 1–12. doi:10.3354/cr015001.

Beniston, M. (2006). Mountain weather and climate: a general overview and a focus on climatic change in the Alps. *Hydrobiologia*, *562*, 3–16.

Beniston, M., Diaz, H., & Bradley, R. (1997). Climatic change at high elevation sites: an overview. *Climatic Change*, *36*, 233–251. doi:10.1023/A:1005380714349.

Beniston, M., Keller, F., & Goyette, S. (2003). Snow pack in the swiss alps under changing climatic conditions: an empirical approach for climate impacts studies. *Theoretical and Applied Climatology*, *74*, 19–31. doi:10.1007/s00704-002-0709-1.

Beniston, M., Rebetez, M., Giorgi, F., & Marinucci, M. (1994). An analysis of regional climate change in Switzerland. *Theoretical and applied climatology*, *49*, 135–159. doi:10.1007/BF00865530.

Benjamini, Y., & Hochberg, Y. (1995). Controlling the false discovery rate: a practical and powerful approach to multiple testing. *Journal of the Royal Statistical Society. Series B (Methodological)*, (pp. 289–300).

Bergström, S., & Graham, L. (1998). On the scale problem in hydrological modelling. *Journal of Hydrology*, *211*, 253–265. doi:10.1016/S0022-1694(98)00248-0.

Berthling, I. (2011). Beyond confusion: Rock glaciers as cryo-conditioned landforms. *Geomorphology*, *131*, 98–106. doi:10.1016/j.geomorph.2011.05.002.

Blanchet, J., & Davison, A. (2012). Statistical modelling of ground temperature in mountain permafrost. *Proceedings of the Royal Society A: Mathematical, Physical and Engineering Science*, *468*, 1472–1495. doi:10.1098/rspa.2011.0615.

Blandford, T. R., Humes, K. S., Harshburger, B. J., Moore, B. C., Walden, V. P., & Ye, H. (2008). Seasonal and synoptic variations in near-surface air temperature lapse rates in a mountainous basin. *Journal of Applied Meteorology and Climatology*, *47*, 249–261. doi:10.1175/2007JAMC1565.1.

Bodin, X., Rojas, F., & Brenning, A. (2010). Status and evolution of the cryosphere in the Andes of Santiago (Chile, 33.5°S.). *Geomorphology*, *118*, 453–464. doi:10.1016/j.geomorph.2010.02.016.

Bodin, X., Thibert, E., Fabre, D., Ribolini, A., Schoeneich, P., Francou, B., Reynaud, L., & Fort, M. (2009). Two decades of responses (1986–2006) to climate by the Laurichard rock glacier, French Alps. *Permafrost and Periglacial Processes*, *20*, 331–344. doi:10.1002/ppp.665.

Boeckli, L., Brenning, A., Gruber, S., & Noetzli, J. (2012). A statistical approach to modelling permafrost distribution in the European Alps or similar mountain ranges. *The Cryosphere*, *6*, 125–140. doi:10.5194/tc-6-125-2012.

Bonnaventure, P. P., & Lewkowicz, A. G. (2011). Modelling climate change effects on the spatial distribution of mountain permafrost at three sites in Northwest Canada. *Climatic Change*, *105*, 293–312. doi:10.1007/s10584-010-9818-5.

Brazier, V., Kirkbride, M. P., & Owens, I. F. (1998). The relationship between climate and rock glacier distribution in the Ben Ohau Range, New Zealand. *Geografiska Annaler: Series A, Physical Geography*, *80*, 193–207. doi:10.1111/j.0435-3676.1998.00037.x.

Brenning, A. (2005). Geomorphological, hydrological and climatic significance of rock glaciers in the Andes of Central Chile (33–35 s). *Permafrost and Periglacial Processes*, *16*, 231–240. doi:10.1002/ppp.528.

Brenning, A. (2010). The significance of rock glaciers in the dry Andes–reply to L. Arenson and M. Jakob. *Permafrost and Periglacial Processes*, *21*, 286–288. doi:10.1002/ppp.702.

Brenning, A., Grasser, M., & Friend, D. (2007). Statistical estimation and generalized additive modeling of rock glacier distribution in the san juan mountains, colorado, united states. *Journal of Geophysical Research: Earth Surface (2003–2012)*, *112*. doi:10.1029/2006JF000528.

Brenning, A., Gruber, S., & Hoelzle, M. (2005). Sampling and statistical analyses of BTS measurements. *Permafrost and Periglacial Processes*, *16*, 383–393. doi:10.1002/ppp.541.

Brenning, A., & Trombotto, D. (2006). Logistic regression modeling of rock glacier and glacier distribution: Topographic and climatic controls in the semi-arid Andes. *Geomorphology*, *81*, 141–154. doi:10.1016/j.geomorph.2006.04.003.

Burger, K., Degenhardt, J., & Giardino, J. (1999). Engineering geomorphology of rock glaciers. *Geomorphology*, *31*, 93–132. doi:10.1016/S0169-555X(99)00074-4.

Burton, A., Kilsby, C., Fowler, H., Cowpertwait, P., & O'Connell, P. (2008). Rainsim: A spatial–temporal stochastic rainfall modelling system. *Environmental Modelling & Software*, *23*, 1356–1369. doi:10.1016/j.envsoft.2008.04.003.

Caine, N. (2010). Recent hydrologic change in a Colorado alpine basin: an indicator of permafrost thaw? *Annals of Glaciology*, *51*, 130. doi:10.3189/172756411795932074.

Charles, S. P., Bates, B. C., & Hughes, J. P. (1999). A spatiotemporal model for downscaling precipitation occurrence and amounts. *Journal of Geophysical Research: Atmospheres (1984–2012)*, *104*, 31657–31669. doi:10.1029/1999JD900119.

Chen, J., Brissette, F. P., & Leconte, R. (2010). A daily stochastic weather generator for preserving low-frequency of climate variability. *Journal of hydrology*, *388*, 480–490. doi:10.1016/j.jhydrol.2010.05.032.

Chueca, J., & Julián, A. (2005). Movement of Besiberris rock glacier, central Pyrenees, Spain: data from a 10-year geodetic survey. *Arctic, Antarctic, and Alpine Research*, *37*, 163–170. doi:10.1657/1523-0430(2005)037[0163:MOBRGC]2.0.CO;2.

Clark, D. H., Steig, E. J., Potter Jr, N., & Gillespie, A. R. (1998). Genetic variability of rock glaciers. *Geografiska Annaler: Series A, Physical Geography*, *80*, 175–182. doi:10.1111/j.0435-3676.1998.00035.x.

Corripio, J. G. (2003). Vectorial algebra algorithms for calculating terrain parameters from DEMs and solar radiation modelling in mountainous terrain. *International Journal of Geographical Information Science*, *17*, 1–23. doi:10.1080/713811744.

Croce, F. A., & Milana, J. P. (2002). Internal structure and behaviour of a rock glacier in the arid Andes of Argentina. *Permafrost and Periglacial Processes*, *13*, 289–299. doi:10.1002/ppp.431.

Dadic, R., Mott, R., Lehning, M., & Burlando, P. (2010). Wind influence on snow depth distribution and accumulation over glaciers. *Journal of Geophysical Research*, *115*, F01012. doi:10.1029/2009JF001261.

DallAmico, M., Endrizzi, S., Gruber, S., & Rigon, R. (2011). A robust and energy-conserving model of freezing variably-saturated soil. *The Cryosphere*, *5*, 469–484. doi:10.5194/tc-5-469-2011.

Damm, B., & Langer, M. (2006a). Rockglacier surface kinematics over a 50-years period-examples from the South Tyrolean Alps (Italy). In *Geophysical Research Abstracts* (p. 02585). volume 8.

Damm, B., & Langer, M. (2006b). Rockglacier surface kinematics over a 50-years period-examples from the South Tyrolean Alps (Italy). In *Geophysical Research Abstracts* (p. 02585). European Geosciences Union volume 8.

Degenhardt, J. J. (2009). Development of tongue-shaped and multilobate rock glaciers in alpine environments–interpretations from ground penetrating radar surveys. *Geomorphology*, *109*, 94–107. doi:10.1016/j.geomorph.2009.02.020.

Delaloye, R., Perruchoud, E., Avian, M., Kaufmann, V., Bodin, X., Hausmann, H., Ikeda, A., Kääb, A., Kellerer-Pirklbauer, A., Krainer, K. et al. (2008). Recent interannual variations of rock glacier creep in the European Alps. In *Proceedings of the 9th International Conference on Permafrost, Fairbanks, Alaska*.

Delaloye, R., Reynard, E., Lambiel, C., Marescot, L., & Monnet, R. (2003). Thermal anomaly in a cold scree slope (Creux du Van, Switzerland). In *Proceedings of the 8th International Conference on Permafrost* (pp. 21–25). Balkema: Zurich.

Dubrovskỳ, M., Buchtele, J., & Žalud, Z. (2004). High-frequency and low-frequency variability in stochastic daily weather generator and its effect on agricultural and hydrologic modelling. *Climatic Change*, *63*, 145–179. doi:10.1023/B:CLIM.0000018504.99914.60.

Dyurgerov, M. B., & Meier, M. F. (2000). Twentieth century climate change: Evidence from small glaciers. *Proceedings of the National Academy of Sciences*, *97*, 1406–1411. doi:10.1073/pnas.97.4.1406.

Elconin, R. F., & Lachapelle, E. R. (1997). Flow and internal structure of a rock glacier. *Journal of Glaciology*, *43*, 238–244.

Endrizzi, S. (2007). *Snow cover modelling at a local and distributed scale over complex terrain*. Ph.D. thesis University of Trento.

Endrizzi, S., Dall'Amico, m., Gruber, S., & Rigon, R. (2011a). GEOtop users manual.

Endrizzi, S., & Gruber, S. (forthcoming). GEOtop: Simulating the combined energy and water balance at and below the land surface accounting for soil freezing, snow cover and terrain effects. *Geoscientific Model Development*, .

Endrizzi, S., Quinton, W., & Marsh, P. (2011b). Modelling the spatial pattern of ground thaw in a small basin in the Arctic tundra. *The Cryosphere Discussions*, *5*, 367–400. doi:10.5194/tcd-5-367-2011.

Erickson, T. A., Williams, M. W., & Winstral, A. (2005). Persistence of topographic controls on the spatial distribution of snow in rugged mountain terrain, Colorado, United States. *Water Resources Research*, *41*, W04014. doi:10.1029/2003WR002973.

Etzelmüller, B., Heggem, E. S., Sharkhuu, N., Frauenfelder, R., Kääb, A., & Goulden, C. (2006). Mountain permafrost distribution modelling using a multi-criteria approach in the Hövsgöl area, Northern Mongolia. *Permafrost and Periglacial Processes*, *17*, 91–104. doi:10.1002/ppp.554.

Etzelmüller, B., Hoelzle, M., Flo Heggem, E. S., Isaksen, K., Mittaz, C., Mühll, D. V., ødegård, R. S., Haeberli, W., & Sollid, J. L. (2001a). Mapping and modelling the occurrence and distribution of mountain permafrost. *Norsk Geografisk Tidsskrift*, *55*, 186–194. doi:10.1080/00291950152746513.

Etzelmüller, B., Ødegård, R. S., Berthling, I., & Sollid, J. L. (2001b). Terrain parameters and remote sensing data in the analysis of permafrost distribution and periglacial processes: principles and examples from Southern Norway. *Permafrost and Periglacial Processes*, *12*, 79–92. doi:10.1002/ppp.384.

Evin, M., Fabre, D., & Johnson, P. G. (1997). Electrical resistivity measurements on the rock glaciers of Grizzly Creek, St Elias Mountains, Yukon. *Permafrost and Periglacial Processes*, *8*, 179–189. doi:10.1002/(SICI)1099-1530(199732)8:2<179::AID-PPP247>3.0.CO;2-C.

Farbrot, H., Etzelmuller, B., Guethmundsson, A., Humlum, O., Kellerer-Pirklbauer, A., Eiken, T., & Wangensteen, B. (2007). Rock glaciers and permafrost in Trollaskagi, Northern Iceland. *Zeitschrift für Geomorphologie, Supplementary Issues*, *51*, 1–16. doi:10.1127/0372-8854/2007/0051S2-0001.

Farbrot, H., Isaksen, K., Eiken, T., Kääb, A., & Sollid, J. L. (2005). Composition and internal structures of a rock glacier on the strandflat of Western Spitsbergen, Svalbard. *Norsk Geografisk Tidsskrift*, *59*, 139–148. doi:10.1080/00291950510020619.

Fatichi, S., Ivanov, V., & Caporali, E. (2013). Assessment of a stochastic downscaling methodology in generating an ensemble of hourly future climate time series. *Climate Dynamics*, (pp. 1–21). doi:10.1007/s00382-012-1627-2.

Fatichi, S., Ivanov, V., & E., C. (2011a). AWE-GEN Advanced WEather GENerator technical reference, version 1.0.

Fatichi, S., Ivanov, V., & E., C. (2011b). AWE-GEN Advanced WEather GENerator user manual, version 1.0.

Fatichi, S., Ivanov, V. Y., & Caporali, E. (2011c). Simulation of future climate scenarios with a weather generator. *Advances in Water Resources*, *34*, 448–467. doi:10.1016/j.advwatres.2010.12.013.

Favier, V., Falvey, M., Rabatel, A., Praderio, E., & López, D. (2009). Interpreting discrepancies between discharge and precipitation in high–altitude area of Chile's Norte Chico region (26–32 s). *Water Resources Research*, *45*, W02424. doi:10.1029/2008WR006802.

Fiddes, J., & Gruber, S. (2012). TopoSUB: a tool for efficient large area numerical modelling in complex topography at sub-grid scales. *Geoscientific Model Development*, *5*, 1245–1257. doi:10.5194/gmd-5-1245-2012.

Forster, P., Ramaswamy, V., Artaxo, P., Berntsen, T., Betts, R., Fahey, D. W., Haywood, J., Lean, J., Lowe, D. C., Myhre, G. et al. (2007). Changes in atmospheric constituents and radiative forcing. In S. Solomon, D. Qin, M. Manning, Z. Chen, M. Marquis, K. Averyt, M. Tignor, & H. Miller (Eds.), *Climate Change 2007: The Physical Science Basis. Contribution of Working Group 1 to the Fourth Assessment Report of the Intergovernmental Panel on Climate Change*. Cambridge, United Kingdom and New York, NY, USA: Cambridge University Press.

Frans, C., Istanbulluoglu, E., Naz, B., Lettenmaier, D., & Condom, C. (2013). Dynamic modeling of glaciated watershed processes: Retrospective analysis and future predictions in the headwaters of the Zongo river, Bolivia. Poster presentation at the 2013 International Glaciers Forum, Huaraz, Ancash, Peru. URL: http://students.washington.edu/chrisf2/gf_poster_final.pdf.

Frauenfelder, R., & Kääb, A. (2000). Towards a palaeoclimatic model of rock–glacier formation in the Swiss Alps. *Annals of Glaciology*, *31*, 281–286. doi:10.3189/172756400781820264.

French, H. M. (2007). *The periglacial environment*. (3rd ed.). Chichester, England: Wiley.

Froese, D. G., Westgate, J. A., Reyes, A. V., Enkin, R. J., & Preece, S. J. (2008). Ancient permafrost and a future, warmer Arctic. *Science*, *321*, 1648–1648. doi:10.1126/science.1157525.

Furrer, E. M., & Katz, R. W. (2007). Generalized linear modeling approach to stochastic weather generators. *Climate research*, *34*, 129. doi:10.3354/cr034129.

Gadek, B., & Leszkiewicz, J. (2010). Influence of snow cover on ground surface temperature in the zone of sporadic permafrost, Tatra Mountains, Poland and Slovakia. *Cold Regions Science and Technology*, *60*, 205–211. doi:10.1016/j.coldregions.2009.10.004.

Garambois, P., Roux, H., Larnier, K., Castaings, W., & Dartus, D. (2013). Characterization of process-oriented hydrologic model behavior with temporal sensitivity analysis for flash floods in Mediterranean catchments. *Hydrology and Earth System Sciences*, *17*, 2305–2322. doi:10.5194/hess-17-2305-2013.

Gardaz, J. (1998). Aspects of rock glacier and mountain permafrost hydrology: case studies in the Valais Alps, Swizterland. In *Extended Abstracts of the Seventh International Conference on Permafrost* (pp. 140–141). URL: http://research.iarc.uaf.edu/NICOP/DVD/ICOP%201998%20Permafrost%207th%20conf/CD-ROM/Abstracts/PDFAbs/Abs17.pdf.

Gascoin, S., Kinnard, C., Ponce, R., Lhermitte, S., MacDonell, S., & Rabatel, A. (2011a). Glacier contribution to streamflow in two headwaters of the Huasco River, dry Andes of Chile. *The Cryosphere*, *5*, 1099–1113. URL: http://www.the-cryosphere.net/5/1099/2011/. doi:10.5194/tc-5-1099-2011.

Gascoin, S., Kinnard, C., Ponce, R., Macdonell, S., Lhermitte, S., Rabatel, A. et al. (2011b). Glacier contribution to streamflow in two headwaters of the Huasco River, Dry Andes of Chile. *The Cryosphere*, (pp. 1099–1113). doi:10.5194/tc-5-1099-2011.

Ge, Y., & Gong, G. (2010). Land surface insulation response to snow depth variability. *Journal of Geophysical Research: Atmospheres (1984–2012)*, *115*. doi:10.1029/2009JD012798.

Giardino, J. (1979). *Rock glacier mechanics and chronologies: Mount Mestas, Colorado*. Ph.D. thesis University of Nebraska.

Goodrich, L. (1982). The influence of snow cover on the ground thermal regime. *Canadian Geotechnical Journal*, *19*, 421–432.

Gruber, S., & Hoelzle, M. (2001). Statistical modelling of mountain permafrost distribution: local calibration and incorporation of remotely sensed data. *Permafrost and Periglacial processes*, *12*, 69–77. doi:10.1002/ppp374.

Gruber, S., & Hoelzle, M. (2008). The cooling effect of coarse blocks revisited: a modeling study of a purely conductive mechanism. In *Proceedings of the 9th International Conference on Permafrost, Fairbanks, Alaska*.

Gubler, S., Endrizzi, S., Gruber, S., & Purves, R. (2013). Sensitivities and uncertainties of modeled ground temperatures in mountain environments. *Geoscientific Model Development Discussions*, *6*, 791–840.

Gubler, S., Gruber, S., & Purves, R. (2012). Uncertainties of parameterized surface downward clear–sky shortwave and all–sky longwave radiation. *Atmospheric Chemistry and Physics*, *12*, 5077–5098. doi:10.5194/acp-12-5077-2012.

Guenni, L., Rose, C., Hogarth, W., Braddock, R., & Charles-Edwards, D. (1990). Seasonal changes in interrelationships between climatic variables. *Agricultural and forest meteorology*, *53*, 45–58. doi:10.1016/0168-1923(90)90123-N.

Haeberli, W. (1993). Possible effects of climatic change on the evolution of Alpine permafrost. *Catena Supplement*, *22*, 23–23.

Haeberli, W., Hallet, B., Arenson, L., Elconin, R., Humlum, O., Kääb, A., Kaufmann, V., Ladanyi, B., Matsuoka, N., Springman, S. et al. (2006). Permafrost creep and rock glacier dynamics. *Permafrost and Periglacial Processes*, *17*, 189–214. doi:10.1002/ppp.561.

Haeberli, W., Hoelzle, M., Paul, F., & Zemp, M. (2007). Integrated monitoring of mountain glaciers as key indicators of global climate change: the European Alps. *Annals of Glaciology*, *46*, 150–160.

Haeberli, W., Kääb, A., Wagner, S., Mühll, D., Geissler, P., Haas, J., Glatzel-Mattheier, H., & Wagenbach, D. (1999). Pollen analysis and 14c age of moss remains in a permafrost core recovered from the active rock glacier Murtèl–Corvatsch, Swiss Alps: geomorphological and glaciological implications. *Journal of Glaciology*, *45*, 1–8.

Hanson, S., & Hoelzle, M. (2004). The thermal regime of the active layer at the Murtèl rock glacier based on data from 2002. *Permafrost and Periglacial Processes*, *15*, 273–282. doi:10.1002/ppp.499.

Hantel, M., Ehrendorfer, M., Haslinger, A. et al. (2000). Climate sensitivity of snow cover duration in austria. *International Journal of Climatology*, *20*, 615–640. doi:10.1002/(SICI)1097-0088(200005)20:6<615::AID-JOC489>3.0.CO;2-0.

Hantel, M., & Hirtl-Wielke, L.-M. (2007). Sensitivity of alpine snow cover to european temperature. *International journal of climatology*, *27*, 1265–1275. doi:10.1002/joc.1472.

Harris, C., Arenson, L. U., Christiansen, H. H., Etzelmüller, B., Frauenfelder, R., Gruber, S., Haeberli, W., Hauck, C., Hölzle, M., Humlum, O. et al. (2009). Permafrost and climate in Europe: Monitoring and modelling thermal, geomorphological and geotechnical responses. *Earth-Science Reviews*, *92*, 117–171. doi:10.1016/j.earscirev.2008.12.002.

Harris, S., French, H., Heginbottom, J., GH, J., B, L., Sego, D., & van Everdingen RO (1988). *Glossary of permafrost and related ground–ice terms*. Technical Report Associate Committee on Geotechnical Research, National Research Council of Canada, Ottawa. URL: http://archive.nrc-cnrc.gc.ca/obj/irc/doc/pubs/tm/tm142.pdf.

Harris, S. A., & Pedersen, D. E. (1998). Thermal regimes beneath coarse blocky materials. *Permafrost and Periglacial Processes*, *9*, 107–120. doi:10.1002/(SICI)1099-1530(199804/06)9:2<107::AID-PPP277>3.0.CO;2-G.

Hausmann, H., Krainer, K., Brückl, E., & Ullrich, C. (2012). Internal structure, ice content and dynamics of ölgrube and Kaiserberg rock glaciers (ötztal Alps, Austria) determined from geophysical surveys. *Austrian Journal of Earth Sciences*, *105*, 2.

Henry, K., & Smith, M. (2001). A model-based map of ground temperatures for the permafrost regions of Canada. *Permafrost and Periglacial Processes*, *12*, 389–398. doi:10.1002/ppp.399.

Hewitt, K. (2005). The Karakoram anomaly? Glacier expansion and the 'elevation effect', Karakoram Himalaya. *Mountain Research and Development*, *25*, 332–340.

Hiemstra, C. A., Liston, G. E., & Reiners, W. A. (2006). Observing, modelling, and validating snow redistribution by wind in a Wyoming upper treeline landscape. *Ecological Modelling*, *197*, 35–51. doi:10.1016/j.ecolmodel.2006.03.005.

Hjort, J., & Marmion, M. (2009). Periglacial distribution modelling with a boosting method. *Permafrost and Periglacial Processes*, *20*, 15–25. doi:10.1002/ppp.629.

Hoelzle, M., Chinn, T., Stumm, D., Paul, F., Zemp, M., & Haeberli, W. (2007). The application of glacier inventory data for estimating past climate change effects on mountain glaciers: A comparison between the European Alps and the Southern Alps of New Zealand. *Global and Planetary Change*, *56*, 69–82.

Hoelzle, M., & Gruber, S. (2008). Borehole and ground surface temperatures and their relationship to meteorological conditions in the Swiss Alps. In *Proceedings Ninth International Conference on Permafrost* (pp. 723–728).

Hoelzle, M., Haeberli, W., & Keller, F. (1993). Application of BTS measurements for modelling mountain permafrost distribution. In *Proceedings of the sixth international conference on permafrost, Beijing* (pp. 272–277). volume 1.

Hoelzle, M., Haeberli, W., & Stocker-Mittaz, C. (2003). Miniature ground temperature data logger measurements 2000–2002 in the murtèl–corvatsch area, Eastern Swiss Alps. In *Proceedings of the Eighth International Conference on Permafrost* (p. 25). volume 21.

Hoelzle, M., Wegmann, M., & Krummenacher, B. (1999). Miniature temperature dataloggers for mapping and monitoring of permafrost in high mountain areas: first experience from the Swiss Alps. *Permafrost and Periglacial Processes*, *10*, 113–124.

Hood, J. L., Roy, J. W., & Hayashi, M. (2006). Importance of groundwater in the water balance of an alpine headwater lake. *Geophysical Research Letters*, *33*, L13405. doi:10.1029/2006GL026611,2006.

Humlum, O. (2000). The geomorphic significance of rock glaciers: estimates of rock glacier debris volumes and headwall recession rates in West Greenland. *Geomorphology*, *35*, 41–67. doi:10.1016/S0169-555X(00)00022-2.

Humlum, O., Christiansen, H. H., & Juliussen, H. (2007). Avalanche-derived rock glaciers in Svalbard. *Permafrost and Periglacial Processes*, *18*, 75–88. doi:10.1002/ppp.580.

Huss, M., Bauder, A., Funk, M., & Hock, R. (2008a). Determination of the seasonal mass balance of four Alpine glaciers since 1865. *Journal of Geophysical Research: Earth Surface (2003–2012)*, *113*. doi:10.1029/2007JF000803.

Huss, M., Farinotti, D., Bauder, A., & Funk, M. (2008b). Modelling runoff from highly glacierized alpine drainage basins in a changing climate. *Hydrological Processes*, *22*, 3888–3902. doi:10.1002/hyp.7055.

Ikeda, A. (2006). Combination of conventional geophysical methods for sounding the composition of rock glaciers in the Swiss Alps. *Permafrost and Periglacial Processes*, *17*, 35–48. doi:10.1002/ppp.550.

Ikeda, A., & Matsuoka, N. (2006). Pebbly versus bouldery rock glaciers: Morphology, structure and processes. *Geomorphology*, *73*, 279–296. doi:10.1002/ppp.550.

Ikeda, A., Matsuoka, N., & Kääb, A. (2003). A rapidly moving small rock glacier at the lower limit of the mountain permafrost belt in the Swiss Alps, . *1*, 455–460.

Ikeda, A., Matsuoka, N., & Kääb, A. (2008). Fast deformation of perennially frozen debris in a warm rock glacier in the Swiss Alps: an effect of liquid water. *Journal of Geophysical Research*, *113*, F01021. doi:10.1029/2007JF000859.

IPCC (2013). Fifth assessment report (AR5). URL: http://www.ipcc.ch.

Ishikawa, M., Watanabe, T., & Nakamura, N. (2001). Genetic differences of rock glaciers and the discontinuous mountain permafrost zone in Kanchanjunga Himal, Eastern Nepal. *Permafrost and Periglacial Processes*, *12*, 243–253. doi:10.1002/ppp.394.

Ivanov, V. Y., Bras, R. L., & Curtis, D. C. (2007). A weather generator for hydrological, ecological, and agricultural applications. *Water Resources Research*, *43*. doi:0.1029/2006WR005364.

Janke, J., & Frauenfelder, R. (2008). The relationship between rock glacier and contributing area parameters in the Front Range of Colorado. *Journal of Quaternary Science*, *23*, 153–163.

Jansson, P., Hock, R., & Schneider, T. (2003). The concept of glacier storage: a review. *Journal of Hydrology*, *282*, 116–129. doi:10.1016/S0022-1694(03)00258-0.

Jiang, Y., Zhuang, Q., & O'Donnell, J. A. (2012). Modeling thermal dynamics of active layer soils and near–surface permafrost using a fully coupled water and heat transport model. *Journal of Geophysical Research: Atmospheres (1984–2012)*, *117*. doi:10.1029/2012JD017512.

Johnson, P. (1998). Morphology and surface structures of Maxwell Creek rock glaciers, St Elias mountains, Yukon: rheological implications. *Permafrost and Periglacial Processes*, *9*, 57–70. doi:10.1002/(SICI)1099-1530(199801/03)9:1<57::AID-PPP275>3.0.CO;2-G.

Jones, P., Trenberth, K., Ambenje, P., Bojariu, R., Easterling, D., Klein, T., Parker, D., Renwick, J., Rusticucci, M., Soden, B. et al. (2007). Surface and atmospheric observations. In S. Solomon, D. Qin, M. Manning, Z. Chen, M. Marquis, K. Averyt, M. Tignor, & H. Miller (Eds.), *Climate Change 2007: The Physical Science Basis. Contribution of Working Group 1 to the Fourth Assessment Report of the Intergovernmental Panel on Climate Change*. Cambridge, United Kingdom and New York, NY, USA: Cambridge University Press.

Julián, A., & Chueca, J. (2007). Permafrost distribution from BTS measurements (Sierra de Telera, Central Pyrenees, Spain): assessing the importance of solar radiation in a mid-elevation shaded mountainous area. *Permafrost and Periglacial Processes*, *18*, 137–149. doi:10.1002/ppp.576.

Juliussen, H., & Humlum, O. (2007). Towards a TTOP ground temperature model for mountainous terrain in Central-Eastern Norway. *Permafrost and Periglacial Processes*, *18*, 161–184. doi:10.1002/ppp.586.

Juliussen, H., & Humlum, O. (2008). Thermal regime of openwork block fields on the mountains Elgåhogna and Sølen, Central-Eastern Norway. *Permafrost and Periglacial Processes*, *19*, 1–18. doi:10.1002/ppp.607.

Kääb, A., Frauenfelder, R., & Roer, I. (2007). On the response of rockglacier creep to surface temperature increase. *Global and Planetary Change*, *56*, 172–187. doi:10.1016/j.gloplacha.2006.07.005.

Kääb, A., Haeberli, W., & Gudmundsson, G. H. (1997). Analysing the creep of mountain permafrost using high precision aerial photogrammetry: 25 years of monitoring Gruben rock glacier, Swiss Alps. *Permafrost and Periglacial Processes*, *8*, 409–426. doi:10.1002/(SICI)1099-1530(199710/12)8:4<409::AID-PPP267>3.0.CO;2-C.

Kane, D. L., Hinkel, K. M., Goering, D. J., Hinzman, L. D., & Outcalt, S. I. (2001). Non-conductive heat transfer associated with frozen soils. *Global and Planetary Change*, *29*, 275–292. doi:10.1016/S0921-8181(01)00095-9.

Kasurak, A., Kelly, R., & Brenning, A. (2011). Linear mixed modelling of snow distribution in the central Yukon. *Hydrological Processes*, *25*, 3332–3346. doi:10.1002/hyp.8168.

Katz, R. W. (1996). Use of conditional stochastic models to generate climate change scenarios. *Climatic Change*, *32*, 237–255. doi:10.1007/BF00142464.

Katz, R. W. (2002). Techniques for estimating uncertainty in climate change scenarios and impact studies. *Climate Research*, *20*, 167–185.

Katz, R. W., & Parlange, M. B. (1998). Overdispersion phenomenon in stochastic modeling of precipitation. *Journal of Climate*, *11*, 591–601. doi:10.1175/1520-0442(1998)011<0591:OPISMO>2.0.CO;2.

Kaufmann, V., & Ladstädter, R. (2009). Documentation and visualization of the morphodynamics of Hinteres Langtalkar rock glacier (Hohe Tauern Range, Austrian Alps)

based on aerial photographs (1954–2006) and geodetic measurements (1999–2007). In *Proceedings of the 10th International Symposium on High Mountain Remote Sensing Cartography, Kathmandu, Nepal* (pp. 103–116).

Keller, F., Goyette, S., & Beniston, M. (2005). Sensitivity analysis of snow cover to climate change scenarios and their impact on plant habitats in alpine terrain. *Climatic Change*, *72*, 299–319. doi:10.1007/s10584-005-5360-2.

Keller, F., & Tamás, M. (2003). Enhanced ground cooling in periods with thin snow cover in the Swiss National Park. In *Proceedings of the Eighth International Conference on Permafrost, Zurich, Switzerland* (pp. 531–536). volume 1.

Kellerer-Pirklbauer, A., Wangensteen, B., Farbrot, H., & Etzelmüller, B. (2008). Relative surface age–dating of rock glacier systems near Hólar in Hjaltadalur, Northern Iceland. *Journal of Quaternary Science*, *23*, 137–151. doi:10.1002/jqs.1117.

Klok, E., Jasper, K., Roelofsma, K., Gurtz, J., & Badoux, A. (2001). Distributed hydrological modelling of a heavily glaciated Alpine river basin. *Hydrological Sciences Journal*, *46*, 553–570. doi:10.1080/02626660109492850.

Koboltschnig, G., & Schöner, W. (2010). The relevance of glacier melt in the water cycle of the Alps: an example from Austria. *Hydrol. Earth Syst. Sci. Discuss*, *7*, 2897–2913. doi:10.5194/hess-15-2039-2011.

Koning, D. M., & Smith, D. J. (1999). Movement of King's Throne rock glacier, Mount Rae area, Canadian Rocky Mountains. *Permafrost and Periglacial Processes*, *10*, 151–162. doi:10.1002/(SICI)1099-1530(199904/06)10:2<151::AID-PPP312>3.0.CO;2-R.

Krainer, K., & Mostler, W. (2002). Hydrology of active rock glaciers: Examples from the Austrian Alps. *Arctic, Antarctic, and Alpine Research*, (pp. 142–149).

Krysiecki, J.-M., Bodin, X., Schoeneich, P. et al. (2008). Collapse of the Bérard rock glacier (Southern French Alps). In *Proceedings 9th International Conference on Permafrost, Fairbanks, Alaska* (pp. 153–154).

Kuhn, M., & Batlogg, N. (1998). Glacier runoff in Alpine headwaters in a changing climate. In *Proceedings of the HeadWater conference, Merano* 248 (pp. 77–88). International Association of Hydrological Sciences.

Kumar, L., Skidmore, A. K., & Knowles, E. (1997). Modelling topographic variation in solar radiation in a GIS environment. *International Journal of Geographical Information Science*, *11*, 475–497. doi:10.1080/136588197242266.

Lambiel, C., & Delaloye, R. (2004). Contribution of real-time kinematic GPS in the study of creeping mountain permafrost: Examples from the Western Swiss Alps. *Permafrost and periglacial processes*, *15*, 229–241. doi:10.1002/ppp.496.

Langston, G., Bentley, L. R., Hayashi, M., McClymont, A., & Pidlisecky, A. (2011). Internal structure and hydrological functions of an alpine proglacial moraine. *Hydrological Processes*, *25*, 2967–2982. doi:10.1002/hyp.8144.

Lapp, S., Byrne, J., Townshend, I., & Kienzle, S. (2005). Climate warming impacts on snowpack accumulation in an Alpine watershed. *International Journal of Climatology*, *25*, 521–536. doi:10.1002/joc.1140.

Lawrence, D. M., Slater, A. G., Romanovsky, V. E., & Nicolsky, D. J. (2008). Sensitivity of a model projection of near-surface permafrost degradation to soil column depth and representation of soil organic matter. *Journal of Geophysical Research*, *113*, F02011. doi:10.1029/2007JF000883.

Lehning, M., Löwe, H., Ryser, M., & Raderschall, N. (2008). Inhomogeneous precipitation distribution and snow transport in steep terrain. *Water Resources Research*, *44*. doi:10.1029/2007WR006545.

Leopold, M., Williams, M., Caine, N., Völkel, J., & Dethier, D. (2011). Internal structure of the Green Lake 5 rock glacier, Colorado Front Range, USA. *Permafrost and Periglacial Processes*, *22*, 107–119. doi:10.1002/ppp.706.

Leverington, D. W., & Duguay, C. R. (1997). A neural network method to determine the presence or absence of permafrost near Mayo, Yukon Territory, Canada. *Permafrost and Periglacial Processes*, *8*, 205–215. doi:10.1002/(SICI)1099-1530(199732)8:2<205::AID-PPP252>3.0.CO;2-5.

Lewkowicz, A. G., & Ednie, M. (2004). Probability mapping of mountain permafrost using the BTS method, Wolf Creek, Yukon Territory, Canada. *Permafrost and Periglacial Processes*, *15*, 67–80. doi:10.1002/ppp.480.

Li, J., Sheng, Y., Wu, J., Chen, J., & Zhang, X. (2009). Probability distribution of permafrost along a transportation corridor in the northeastern Qinghai province of China. *Cold Regions Science and Technology*, *59*, 12–18. doi:10.1016/j.coldregions.2009.05.012.

Ling, F., & Zhang, T. (2004). A numerical model for surface energy balance and thermal regime of the active layer and permafrost containing unfrozen water. *Cold Regions Science and Technology*, *38*, 1–15. doi:10.1016/S0165-232X(03)00057-0.

Luetschg, M., Lehning, M., & Haeberli, W. (2008). A sensitivity study of factors influencing warm/thin permafrost in the swiss alps. *Journal of Glaciology*, *54*, 696–704. doi:10.3189/002214308786570881.

Marchenko, S., Romanovsky, V., & Tipenko, G. (2008). Numerical modeling of spatial permafrost dynamics in Alaska. In *Proceedings of the ninth international conference on permafrost* (pp. 1125–1130). Institute of Northern Engineering, University of Alaska Fairbanks volume 29.

Marmy, A., Salzmann, N., Scherler, M., & Hauck, C. (2013). Permafrost model sensitivity to seasonal climatic changes and extreme events in mountainous regions. *Environmental Research Letters*, *8*, 035048. doi:doi:10.1088/1748-9326/8/3/035048.

Marshall, J., & Plumb, R. (2008). *Atmosphere, Ocean, and Climate Dynamics: An Introductory Text*. NY, New York: Cambridge University Press.

Martin, H. E., & Whalley, W. B. (1987). Rock glaciers part 1: rock glacier morphology: classification and distribution. *Progress in Physical Geography*, *11*, 260–282. doi:10.1177/030913338701100205.

Maurer, H., & Hauck, C. (2007). Geophysical imaging of alpine rock glaciers. *Journal of Glaciology*, *53*, 110–120. doi:10.3189/172756507781833893.

McClymont, A., Hayashi, M., Bentley, L., & Liard, J. (2012). Locating and characterising groundwater storage areas within an alpine watershed using time-lapse gravity, gpr and seismic refraction methods. *Hydrological Processes*, . doi:10.1002/hyp.9316.

McClymont, A., Hayashi, M., Bentley, L., Muir, D., & Ernst, E. (2010). Groundwater flow and storage within an alpine meadow-talus complex. *Hydrology and Earth System Sciences*, *14*, 859–872. doi:10.5194/hess-14-859-2010.

McKague, K., Rudra, R., Ogilvie, J., Ahmed, I., & Gharabaghi, B. (2005). Evaluation of weather generator ClimGen for Southern Ontario. *Canadian Water Resources Journal*, *30*, 315–330. doi:10.4296/cwrj3004315.

Meehl, G. A., Stocker, T. F., Collins, W. D., Friedlingstein, P., Gaye, A. T., Gregory, J. M., Kitoh, A., Knutti, R., Murphy, J. M., Noda, A. et al. (2007). Global climate projections.

In S. Solomon, D. Qin, M. Manning, Z. Chen, M. Marquis, K. Averyt, M. Tignor, & H. Miller (Eds.), *Climate Change 2007: The Physical Science Basis. Contribution of Working Group 1 to the Fourth Assessment Report of the Intergovernmental Panel on Climate Change*. Cambridge, United Kingdom and New York, NY, USA: Cambridge University Press.

Messerli, B., Viviroli, D., & Weingartner, R. (2004). Mountains of the world: vulnerable water towers for the 21st century. *Ambio*, (pp. 29–34).

MeteoSwiss (2010). *SwissMetNet: an Observation Network for the Future*. Technical Report MeteoSwiss.

MeteoSwiss (2012). Valeurs mesures produits individuels. URL: `https://shop.meteoswiss.ch/productView.html?type=psc&id=17&n=0&request_locale=fr`.

MeteoSwiss (2013). Tendencies in Switzerland. URL: `http://www.meteoswiss.admin.ch/web/fr/climat/climat_aujourdhui/tendances_en_suisse.html`.

Minder, J. R., Mote, P. W., & Lundquist, J. D. (2010). Surface temperature lapse rates over complex terrain: Lessons from the Cascade Mountains. *Journal of Geophysical Research*, *115*, D14122. doi:`10.1029/2009JD013493`.

Monnier, S., & Kinnard, C. (2013). Internal structure and composition of a rock glacier in the Andes (upper Choapa valley, Chile) using borehole information and ground-penetrating radar. *Annals of Glaciology*, *54*, 61. doi:`0.3189/2013AoG64A107`.

Morin, S., Domine, F., Arnaud, L., & Picard, G. (2010). ¡ i¿ in–situ¡/i¿ monitoring of the time evolution of the effective thermal conductivity of snow. *Cold Regions Science and Technology*, *64*, 73–80. doi:`10.1016/j.coldregions.2010.02.008`.

Mott, R., Schirmer, M., Bavay, M., Grünewald, T., & Lehning, M. (2010). Understanding snow-transport processes shaping the mountain snow-cover. *The Cryosphere*, *4*, 545–559. doi:`10.5194/tc-4-545-2010`.

Mühll, D. V., Arenson, L., & Springman, S. (2003). Temperature conditions in two Alpine rock glaciers. In *8th International Conference on Permafrost, Zürich, Swets & Zeitlinger, Lisse* (pp. 1195–1200).

Muneer, T. (2004). *Solar Radiation and Daylight Models*. (2nd ed.). Burlington, Massachusetts: Elsevier.

Musa, M., Grüter, E., Abbt, M., Häberli, C., Häller, E., Küng, U., Konzelmann, T., & Dössegger, R. (2003). Quality control tools for meteorological data in the meteoSwiss data warehouse system. In *Proceedings of the International Conference on Alpine Meteorology and Mesoscale Alpine Programme (ICAMMAP). Brig, Switzerland* (pp. 19–23). MeteoSwiss.

Nelson, R. (2002). ClimGen–climatic data generator, users manual. *Washington State University*, . URL: `http://www.sipeaa.it/bellocchi/publications/CAP-STRAT/ClimGen/ClimGen_manual.pdf`.

NOAA (2013). North Atlantic Oscillation. URL: `http://www.cpc.ncep.noaa.gov/products/precip/CWlink/pna/nao.shtml`.

Noetzli, J., & Gruber, S. (2009). Transient thermal effects in Alpine permafrost. *The Cryosphere*, *3*, 85–99.

O'Connor, T. (1994). Emergent properties. *American Philosophical Quarterly*, *31*, 91–104.

Oerlemans, J. (2005). Extracting a climate signal from 169 glacier records. *Science*, *308*, 675–677.

Oke, T. R. (1987). *Boundary Layer Climates*. (2nd ed.). NY, New York: Methuen.

Otto, J.-C., Schrott, L., Jaboyedoff, M., & Dikau, R. (2009). Quantifying sediment storage in a high Alpine valley (Turtmanntal, Switzerland). *Earth Surface Processes and Landforms*, *34*, 1726–1742. doi:`10.1002/esp.1856`.

Palmentola, G., Baboci, K., Gruda, G., & Zito, G. (1995). A note on rock glaciers in the Albanian Alps. *Permafrost and Periglacial Processes*, *6*, 251–257. doi:`10.1002/ppp.3430060306`.

Payne, D. (1998). Climatic implications of rock glaciers in the arid western cordillera of the central Andes. *Glacial Geology and Geomorphology*, . URL: `http://ggg.qub.ac.uk/ggg/papers/full/1998/rp031998/rp03.htm`.

Perl, M., Häberli, C., Grüter, E., Musa, M., Küng, U., & M., A. (2010). *Werkzeuge für die Qualitätskontrolle und die Bearbeitung von Meteorologischen Daten*. Technical Report MeteoSwiss.

Pigeon, K. E., & Jiskoot, H. (2008). Meteorological controls on snowpack formation and dynamics in the southern Canadian Rocky Mountains. *Arctic, Antarctic, and Alpine Research*, *40*, 716–730. doi:`10.1657/1523-0430(07-054)[PIGEON]2.0.CO;2`.

Putnam, A. E., & Putnam, D. E. (2009). Inactive and relict rock glaciers of the Deboullie Lakes Ecological Reserve, Northern Maine, USA. *Journal of Quaternary Science*, *24*, 773–784. doi:10.1002/jqs.1252.

Rabatel, A., Castebrunet, H., Favier, V., Nicholson, L., & Kinnard, C. (2011). Glacier changes in the Pascua-Lama region, Chilean Andes (29 s): Recent mass balance and 50 yr surface area variations. *The Cryosphere*, *5*, 1029–1041. doi:10.5194/tc-5-1029-2011.

Randall, D. A., Wood, R. A., Bony, S., Colman, R., Fichefet, T., Fyfe, J., Kattsov, V., Pitman, A., Shukla, J., Srinivasan, J. et al. (2007). Climate models and their evaluation. In S. Solomon, D. Qin, M. Manning, Z. Chen, M. Marquis, K. Averyt, M. Tignor, & H. Miller (Eds.), *Climate Change 2007: The Physical Science Basis. Contribution of Working Group 1 to the Fourth Assessment Report of the Intergovernmental Panel on Climate Change*. Cambridge, United Kingdom and New York, NY, USA: Cambridge University Press.

Ribolini, A., Guglielmin, M., Fabre, D., Bodin, X., Marchisio, M., Sartini, S., Spagnolo, M., & Schoeneich, P. (2010). The internal structure of rock glaciers and recently deglaciated slopes as revealed by geoelectrical tomography: insights on permafrost and recent glacial evolution in the central and Western Alps (Italy–France). *Quaternary Science Reviews*, *29*, 507–521. doi:10.1016/j.quascirev.2009.10.008.

Richardson, C. W. (1981). Stochastic simulation of daily precipitation, temperature, and solar radiation. *Water Resources Research*, *17*, 182–190. doi:10.1029/WR017i001p00182.

Richardson, C. W., & Wright, D. A. (1984). WGEN: A model for generating daily weather variables.

Rignot, E., Rivera, A., & Casassa, G. (2003). Contribution of the Patagonia icefields of South America to sea level rise. *Science*, *302*, 434–437. doi:10.1126/science.1087393.

Rigon, R., Bertoldi, G., & Over, T. (2006). GEOtop: A distributed hydrological model with coupled water and energy budgets. *Journal of Hydrometeorology*, *7*, 371–388. doi:10.1175/JHM497.1.

Riseborough, D., Shiklomanov, N., Etzelmüller, B., Gruber, S., & Marchenko, S. (2008). Recent advances in permafrost modelling. *Permafrost and Periglacial Processes*, *19*, 137–156. doi:10.1002/ppp.615.

Rixen, C., Haeberli, W., & Stoeckli, V. (2004). Ground temperatures under ski pistes with artificial and natural snow. *Arctic, Antarctic, and Alpine Research*, *36*, 419–427. doi:10.1657/1523-0430(2004)036[0419:GTUSPW]2.0.CO;2.

Roer, I., Haeberli, W., Avian, M., Kaufmann, V., Delaloye, R., Lambiel, C., & Kääb, A. (2008). Observations and considerations on destabilizing active rock glaciers in the European Alps. In *Ninth International Conference on Permafrost* (pp. 1505–1510). volume 2.

Rolland, C. (2003). Spatial and seasonal variations of air temperature lapse rates in alpine regions. *Journal of Climate*, *16*, 1032–1046. doi:10.1175/1520-0442(2003)016<1032:SASVOA>2.0.CO;2.

Romanovsky, V., Osterkamp, T., & Duxbury, N. (1997). An evaluation of three numerical models used in simulations of the active layer and permafrost temperature regimes. *Cold Regions Science and Technology*, *26*, 195–203. doi:10.1016/S0165-232X(97)00016-5.

Safeeq, M., & Fares, A. (2011). Accuracy evaluation of ClimGen weather generator and daily to hourly disaggregation methods in tropical conditions. *Theoretical and applied climatology*, *106*, 321–341. doi:10.1007/s00704-011-0438-4.

Salzmann, N., Frei, C., Vidale, P.-L., & Hoelzle, M. (2007). The application of regional climate model output for the simulation of high mountain permafrost scenarios. *Global and Planetary Change*, *56*, 188–202. doi:10.1016/j.gloplacha.2006.07.006.

Santer, B. D., Wigley, T., Mears, C., Wentz, F., Klein, S., Seidel, D., Taylor, K., Thorne, P., Wehner, M., Gleckler, P. et al. (2005). Amplification of surface temperature trends and variability in the tropical atmosphere. *Science*, *309*, 1551–1556. doi:10.1126/science.1114867.

Scherler, D., Bookhagen, B., & Strecker, M. R. (2011). Spatially variable response of Himalayan glaciers to climate change affected by debris cover. *Nature geoscience*, *4*, 156–159. doi:10.1038/ngeo1068.

Scherler, M., Hauck, C., Hoelzle, M., & Salzmann, N. (2013). Modeled sensitivity of two Alpine permafrost sites to RCM–based climate scenarios. *Journal of Geophysical Research: Earth Surface*, . doi:10.1002/jgrf.20069.

Scherler, M., Hauck, C., Hoelzle, M., Stähli, M., & Völksch, I. (2010). Meltwater infiltration into the frozen active layer at an Alpine permafrost site. *Permafrost and Periglacial Processes*, *21*, 325–334. doi:10.1002/ppp.694.

Schrott, L. (1996). Some geomorphological-hydrological aspects of rock glaciers in the Andes (San Juan, Argentina). *ZEITSCHRIFT FUR GEOMORPHOLOGIE SUPPLEMENTBAND*, (pp. 161–173).

Semenov, M. A., & Barrow, E. M. (1997). Use of a stochastic weather generator in the development of climate change scenarios. *Climatic change*, *35*, 397–414.

Semenov, M. A., Barrow, E. M., & LARS-WG, A. (2002). A stochastic weather generator for use in climate impact studies. URL: `http://www.rothamsted.ac.uk/mas-models/download/LARS-WG-Manual.pdf`.

Serrano, E., San José, J., & Agudo, C. (2006). Rock glacier dynamics in a marginal periglacial high mountain environment: Flow, movement (1991–2000) and structure of the Argualas rock glacier, the Pyrenees. *Geomorphology*, *74*, 285–296. doi:`10.1016/j.geomorph.2005.08.014`.

Serrano, E., de Sanjosé, J. J., & González-Trueba, J. J. (2010). Rock glacier dynamics in marginal periglacial environments. *Earth Surface Processes and Landforms*, *35*, 1302–1314. doi:`10.1002/esp.1972`.

Smith, M., & Riseborough, D. (1996). Permafrost monitoring and detection of climate change. *Permafrost and Periglacial Processes*, *7*, 301–309. doi:`10.1002/(SICI)1099-1530(199610)7:4<301::AID-PPP231>3.0.CO;2-R`.

Smith, M., & Riseborough, D. (2002). Climate and the limits of permafrost: a zonal analysis. *Permafrost and Periglacial Processes*, *13*, 1–15. doi:`10.1002/ppp.410`.

Srikanthan, R., & McMahon, T. (2001). Stochastic generation of annual, monthly and daily climate data: A review. *Hydrology and Earth System Sciences Discussions*, *5*, 653–670.

Stewart, I. T. (2009). Changes in snowpack and snowmelt runoff for key mountain regions. *Hydrological Processes*, *23*, 78–94. doi:`10.1002/hyp.7128`.

Sturman, A., & Wanner, H. (2001). A comparative review of the weather and climate of the southern alps of new zealand and the european alps. *Mountain Research and Development*, *21*, 359–369. doi:`10.1659/0276-4741(2001)021[0359:ACROTW]2.0.CO;2`.

Suter, S., Konzelmann, T., Mühlhäuser, C., Begert, M., & Heimo, A. (2006). SwissMetNet–the new automatic meteorological network of Switzerland: transition from old to new

network, data management and first results. In *Proceedings of the 4th International Conference on Experiences with Automatic Weather Stations (4th ICEAWS). Altis Park Hotel, Lisbon, Portugal*. volume 24.

Trombotto, D., Arena, L., & Caranti, G. (2008). Glacial ice as cryogenic factor in the periglaciation zone of the composed rockglacier Morenas Coloradas, central Andes of Mendoza, Argentina. In *Ninth International Conference on Permafrost, Fairbanks, Alaska, Proceedings* (pp. 1781–1786). volume 2.

Trombotto, D., & Borzotta, E. (2009). Indicators of present global warming through changes in active layer-thickness, estimation of thermal diffusivity and geomorphological observations in the Morenas Coloradas rockglacier, Central Andes of Mendoza, Argentina. *Cold Regions Science and Technology*, *55*, 321–330. doi:10.1016/j.coldregions.2008.08.009.

Uhlmann, B., Jordan, F., & Beniston, M. (2012). Modelling runoff in a Swiss glacierized catchment–part ii: daily discharge and glacier evolution in the Findelen basin in a progressively warmer climate. *International Journal of Climatology*, .

USDA (2012). Rosetta class average hydraulic parameters. URL: http://ars.usda.gov/Services/docs.htm?docid=8955.

Van Genuchten, M. T. (1980). A closed–form equation for predicting the hydraulic conductivity of unsaturated soils. *Soil Science Society of America Journal*, *44*, 892–898.

Verbunt, M., Gurtz, J., Jasper, K., Lang, H., Warmerdam, P., & Zappa, M. (2003). The hydrological role of snow and glaciers in alpine river basins and their distributed modeling. *Journal of hydrology*, *282*, 36–55. doi:10.1016/S0022-1694(03)00251-8.

Vergara, W., Deeb, A., Valencia, A., Bradley, R., Francou, B., Zarzar, A., Grünwaldt, A., & Haeussling, S. (2007). Economic impacts of rapid glacier retreat in the Andes. *Eos, Transactions American Geophysical Union*, *88*, 261–264. doi:10.1029/2007EO250001.

Viviroli, D., & Weingartner, R. (2004). The hydrological significance of mountains: from regional to global scale. *Hydrology and Earth System Sciences Discussions*, *8*, 1017–1030.

Viviroli, D., Weingartner, R., & Messerli, B. (2003). Assessing the hydrological significance of the world's mountains. *Mountain research and Development*, *23*, 32–40.

Vonder Mühll, D., & Klingelé, E. (1994). Gravimetrical investigation of ice-rich permafrost within the rock glacier Murtèl-Corvatsch (upper Engadin, Swiss Alps). *Permafrost and Periglacial Processes*, *5*, 13–24. doi:10.1002/ppp.3430050103.

Vonder Muhll, D. S., Hauck, C., & Lehmann, F. (2000). Verification of geophysical models in Alpine permafrost using borehole information. *Annals of Glaciology*, *31*, 300–306. doi:10.3189/172756400781820057.

Vuille, M., Francou, B., Wagnon, P., Juen, I., Kaser, G., Mark, B. G., & Bradley, R. S. (2008). Climate change and tropical Andean glaciers: Past, present and future. *Earth-Science Reviews*, *89*, 79–96. doi:10.1016/j.earscirev.2008.04.002.

Wagner, S. (1992). Creep of Alpine permafrost, investigated on the Murtèl rock glacier. *Permafrost and Periglacial Processes*, *3*, 157–162. doi:10.1002/ppp.3430030214.

Wahrhaftig, C., & Cox, A. (1959). Rock glaciers in the Alaska Range. *Geological Society of America Bulletin*, *70*, 383–436. doi:10.1130/0016-7606(1959)70[383:RGITAR]2.0.CO;2.

Whalley, W. B., & Palmer, C. F. (1998). A glacial interpretation for the origin and formation of the Marinet rock glacier, Alpes Maritimes, France. *Geografiska Annaler: Series A, Physical Geography*, *80*, 221–236. doi:10.1111/j.0435-3676.1998.00039.x.

Wilks, D. S. (1992). Adapting stochastic weather generation algorithms for climate change studies. *Climatic Change*, *22*, 67–84.

Wilks, D. S., & Wilby, R. L. (1999). The weather generation game: a review of stochastic weather models. *Progress in Physical Geography*, *23*, 329–357. doi:10.1177/030913339902300302.

Williams, M., Knauf, M., Caine, N., Liu, F., & Verplanck, P. (2006). Geochemistry and source waters of rock glacier outflow, Colorado Front Range. *Permafrost and Periglacial Processes*, *17*, 13–33. doi:10.1002/ppp.535.

Wright, J., Duchesne, C., & Côté, M. (2003). Regional–scale permafrost mapping using the TTOP ground temperature model. In *Proceedings 8th International Conference on Permafrost. Swets and Zeitlinger, Lisse* (pp. 1241–1246).

Zhang, M., Zhang, J., & Lai, Y. (2005). Numerical analysis for critical height of railway embankment in permafrost regions of Qinghai–Tibetan plateau. *Cold Regions Science and Technology*, *41*, 111–120.

Zhang, X., Zwiers, F. W., & Li, G. (2004). Monte Carlo experiments on the detection of trends in extreme values. *Journal of Climate*, *17*, 1945–1952. doi:10.1175/1520-0442(2004)017<1945:MCEOTD>2.0.CO;2.

Zhang, Y., Carey, S. K., & Quinton, W. L. (2008). Evaluation of the algorithms and parameterizations for ground thawing and freezing simulation in permafrost regions. *Journal of Geophysical Research: Atmospheres (1984–2012)*, *113*. doi:10.1029/2007JD009343.

Zhu, C., Zhang, J., & Cheng, P. (1996). Rock glaciers in the central Tianshan Mountains, China. *Permafrost and Periglacial Processes*, *7*, 69–78. doi:10.1002/(SICI)1099-1530(199601)7:1<69::AID-PPP210>3.0.CO;2-B.

APPENDICES

Appendix A

AWE-GEN Climate Scenarios

Table A.1: Mean total monthly Pr at Piz Corvatsch and for all generated climate scenarios. $1-50$ and $51-100$ indicate the years of the REF scenario used for the statistics, and are separated since each climate change scenario begins with REF_{1-50}.

month	Piz Corvatsch	REF_{1-50}	REF_{51-100}	+1All	+1Win	+1Sum	+3All	+3Win	+3Sum	-1All	-3All
1	43	50	40	47	47	47	47	47	47	47	46
2	44	42	44	43	43	43	43	43	43	43	44
3	48	55	47	55	55	55	55	55	55	55	47
4	69	66	66	68	68	68	68	68	68	68	73
5	86	77	96	78	78	78	78	78	78	78	86
6	109	105	114	112	112	112	112	112	112	112	110
7	109	113	107	106	106	106	106	106	106	106	108
8	106	98	107	103	103	103	103	103	103	103	113
9	79	80	74	79	79	79	79	79	79	79	81
10	77	86	75	77	77	77	77	77	77	77	74
11	76	85	72	82	82	82	82	82	82	82	70
12	57	49	61	55	55	55	55	55	55	55	57

Table A.2: Standard deviation of total monthly Pr at Piz Corvatsch and for all generated climate scenarios.$1-50$ and $51-100$ indicate the years of the REF scenario used for the statistics, and are separated since each climate change scenario begins with REF_{1-50}.

month	Piz Corvatsch	REF_{1-50}	REF_{51-100}	+1All	+1Win	+1Sum	+3All	+3Win	+3Sum	-1All	-3All
1	32.914	24.131	18.431	27.105	27.105	27.105	27.105	27.105	27.105	27.105	26.818
2	28.754	20.052	24.895	24.048	24.048	24.048	24.048	24.048	24.048	24.048	19.323
3	24.653	28.466	26.264	33.678	33.678	33.678	33.678	33.678	33.678	33.678	25.000
4	38.124	26.362	27.193	30.616	30.616	30.616	30.616	30.616	30.616	30.616	25.410
5	41.675	33.363	45.924	36.365	36.365	36.365	36.365	36.365	36.365	36.365	42.006
6	41.383	33.643	32.078	37.082	37.082	37.082	37.082	37.082	37.082	37.082	34.490
7	32.493	37.991	36.097	43.589	43.589	43.589	43.589	43.589	43.589	43.589	33.814
8	40.295	33.301	40.287	33.621	33.621	33.621	33.621	33.621	33.621	33.621	36.956
9	45.258	38.044	33.154	41.422	41.422	41.422	41.422	41.422	41.422	41.422	47.577
10	49.772	46.809	37.604	32.930	32.930	32.930	32.930	32.930	32.930	32.930	39.148
11	67.587	51.800	41.016	51.777	51.777	51.777	51.777	51.777	51.777	51.777	45.343
12	41.373	28.888	34.151	35.688	35.688	35.688	35.688	35.688	35.688	35.688	33.909

Table A.3: Mean daily TA at Piz Corvatsch and for all generated climate scenarios. $1-50$ and $51-100$ indicate the years of the REF scenario used for the statistics, and are separated since each climate change scenario begins with REF_{1-50}.

month	Piz Corvatsch	REF_{1-50}	REF_{51-100}	+1All	+1Win	+1Sum	+3All	+3Win	+3Sum	-1All	-3All
1	-10.882	-10.964	-10.920	-10.044	-10.057	-11.044	-8.044	-8.083	-11.044	-12.044	-13.986
2	-11.737	-11.680	-11.747	-10.942	-11.939	-11.942	-8.942	-11.933	-11.942	-12.942	-14.838
3	-10.488	-10.305	-10.789	-9.504	-10.504	-10.504	-7.504	-10.504	-10.504	-11.504	-13.321
4	-8.051	-15.809	-16.165	-14.830	-15.830	-15.830	-12.830	-15.830	-15.830	-16.830	-19.031
5	-3.291	-3.189	-3.470	-2.284	-3.284	-3.271	-0.284	-3.284	-3.245	-4.284	-6.259
6	-0.144	-0.009	-0.006	1.062	0.062	1.059	3.062	0.062	3.054	-0.938	-3.343
7	2.302	-3.591	-4.034	-2.783	-3.783	-2.783	-0.783	-3.783	-0.783	-4.783	-6.800
8	2.592	-1.234	-1.200	-0.240	-1.240	-0.252	1.760	-1.240	1.722	-2.240	-4.489
9	-0.541	-5.290	-5.224	-4.229	-5.229	-5.226	-2.229	-5.229	-5.221	-6.229	-8.353
10	-3.014	-3.024	-3.139	-2.336	-3.323	-3.336	-0.336	-3.297	-3.336	-4.336	-6.133
11	-8.015	-8.138	-7.687	-7.010	-7.013	-8.010	-5.010	-5.018	-8.010	-9.010	-10.898
12	-10.367	-10.318	-10.597	-9.419	-9.419	-10.419	-7.419	-7.419	-10.419	-11.419	-13.228

Table A.4: Standard deviation of daily TA at Piz Corvatsch and for all generated climate scenarios. $1-50$ and $51-100$ indicate the years of the REF scenario used for the statistics, and are separated since each climate change scenario begins with REF_{1-50}.

month	Piz Corvatsch	REF_{1-50}	REF_{51-100}	+1All	+1Win	+1Sum	+3All	+3Win	+3Sum	-1All	-3All
1	4.609	4.056	4.187	4.251	4.254	4.251	4.251	4.269	4.251	4.251	3.930
2	5.253	4.443	4.739	4.645	4.644	4.645	4.645	4.643	4.645	4.645	4.796
3	4.889	4.346	4.449	4.360	4.360	4.360	4.360	4.360	4.360	4.360	4.440
4	3.783	5.194	5.220	5.265	5.265	5.265	5.265	5.265	5.265	5.265	5.357
5	3.336	3.062	3.022	3.165	3.165	3.178	3.165	3.165	3.217	3.165	2.891
6	3.699	3.321	3.369	3.294	3.294	3.298	3.294	3.294	3.310	3.294	3.342
7	3.216	6.708	6.740	6.641	6.641	6.641	6.641	6.641	6.641	6.641	6.608
8	3.178	3.841	3.762	3.692	3.692	3.704	3.692	3.692	3.740	3.692	3.750
9	3.610	5.874	5.768	5.897	5.897	5.899	5.897	5.897	5.904	5.897	5.695
10	4.032	3.660	3.678	3.697	3.688	3.697	3.697	3.678	3.697	3.697	3.804
11	4.865	4.229	4.344	4.418	4.415	4.418	4.418	4.411	4.418	4.418	4.396
12	4.829	4.464	4.463	4.563	4.563	4.563	4.563	4.563	4.563	4.563	4.328

Table A.5: Mean daily minimum TA at Piz Corvatsch and for all generated climate scenarios. $1-50$ and $51-100$ indicate the years of the REF scenario used for the statistics, and are separated since each climate change scenario begins with REF_{1-50}.

month	Piz Corvatsch	REF_{1-50}	REF_{51-100}	+1All	+1Win	+1Sum	+3All	+3Win	+3Sum	-1All	-3All
1	-13.096	-15.131	-15.059	-14.261	-14.274	-15.260	-12.262	-12.301	-15.260	-16.260	-18.110
2	-14.043	-16.408	-16.479	-15.615	-16.612	-16.615	-13.615	-16.607	-16.615	-17.615	-19.501
3	-12.744	-14.609	-15.080	-13.915	-14.915	-14.915	-11.915	-14.915	-14.915	-15.915	-17.708
4	-10.152	-21.145	-21.488	-20.128	-21.128	-21.128	-18.128	-21.128	-21.128	-22.128	-24.392
5	-5.275	-6.218	-6.528	-5.310	-6.310	-6.297	-3.310	-6.310	-6.272	-7.310	-9.264
6	-2.172	-3.321	-3.295	-2.216	-3.216	-2.219	-0.216	-3.216	-0.224	-4.216	-6.664
7	0.096	-12.094	-12.461	-11.217	-12.217	-11.217	-9.217	-12.217	-9.217	-13.217	-15.362
8	0.546	-5.365	-5.297	-4.407	-5.407	-4.420	-2.407	-5.407	-2.445	-6.407	-8.653
9	-2.370	-11.827	-11.698	-10.767	-11.767	-11.765	-8.767	-11.767	-11.759	-12.767	-14.821
10	-4.960	-6.650	-6.792	-5.862	-6.849	-6.862	-3.862	-6.823	-6.862	-7.862	-9.787
11	-10.092	-12.502	-12.025	-11.401	-11.404	-12.401	-9.401	-9.409	-12.401	-13.401	-15.228
12	-12.568	-14.673	-14.986	-13.776	-13.776	-14.776	-11.776	-11.776	-14.776	-15.776	-17.530

Table A.6: Standard deviation of daily minimum TA at Piz Corvatsch and for all generated climate scenarios. $1-50$ and $51-100$ indicate the years of the REF scenario used for the statistics, and are separated since each climate change scenario begins with REF_{1-50}.

month	Piz Corvatsch	REF_{1-50}	REF_{51-100}	+1All	+1Win	+1Sum	+3All	+3Win	+3Sum	-1All	-3All
1	4.874	4.243	4.378	4.444	4.448	4.445	4.443	4.462	4.445	4.445	4.119
2	5.558	4.682	4.886	4.814	4.813	4.814	4.814	4.813	4.814	4.814	5.034
3	5.146	4.537	4.544	4.576	4.576	4.576	4.576	4.576	4.576	4.576	4.643
4	4.035	5.416	5.400	5.531	5.531	5.531	5.531	5.531	5.531	5.531	5.553
5	3.598	3.194	3.173	3.347	3.347	3.359	3.347	3.347	3.394	3.347	3.042
6	3.830	3.475	3.508	3.500	3.500	3.504	3.500	3.500	3.514	3.500	3.540
7	3.315	7.142	7.112	7.112	7.112	7.112	7.112	7.112	7.112	7.112	7.289
8	3.285	3.981	3.954	3.914	3.914	3.932	3.914	3.914	3.978	3.914	3.945
9	3.740	6.133	6.025	6.212	6.212	6.215	6.212	6.212	6.223	6.212	5.991
10	4.411	3.795	3.858	3.894	3.883	3.894	3.894	3.871	3.894	3.894	3.989
11	5.202	4.493	4.514	4.485	4.482	4.485	4.485	4.476	4.485	4.485	4.505
12	5.203	4.682	4.648	4.682	4.682	4.682	4.682	4.682	4.682	4.682	4.473

Table A.7: Mean daily SWR at Piz Corvatsch and for all generated climate scenarios. $1-50$ and $51-100$ indicate the years of the REF scenario used for the statistics, and are separated since each climate change scenario begins with REF_{1-50}.

month	Piz Corvatsch	REF_{1-50}	REF_{51-100}	+1All	+1Win	+1Sum	+3All	+3Win	+3Sum	-1All	-3All
1	85.084	75.234	75.399	75.237	75.241	75.541	74.558	74.574	75.541	75.817	76.417
2	130.598	123.991	122.924	124.103	124.557	124.558	123.101	124.556	124.558	124.979	125.166
3	194.704	180.437	179.284	178.667	179.299	179.299	177.316	179.299	179.299	179.903	182.066
4	247.493	241.741	240.428	240.761	241.206	241.206	239.729	241.206	241.206	241.613	240.621
5	270.756	281.302	278.510	279.644	280.613	280.601	277.678	280.613	280.578	281.566	284.220
6	259.828	282.385	279.169	279.810	280.667	279.812	278.133	280.667	278.140	281.518	285.901
7	248.647	273.298	270.973	270.943	271.192	270.943	270.685	271.192	270.685	271.515	271.463
8	213.003	243.884	243.258	242.881	243.452	242.887	241.872	243.452	241.891	244.018	242.877
9	177.644	197.696	200.512	197.301	197.719	197.717	196.427	197.719	197.714	198.116	199.656
10	134.816	141.825	141.782	141.249	141.924	141.930	139.822	141.912	141.930	142.580	143.587
11	88.221	81.569	81.702	81.830	81.831	82.206	81.031	81.035	82.206	82.568	82.983
12	68.775	62.079	61.818	61.505	61.505	61.781	60.896	60.896	61.781	62.038	63.053

Table A.8: Standard deviation of daily SWR at Piz Corvatsch and for all generated climate scenarios. $1-50$ and $51-100$ indicate the years of the REF scenario used for the statistics, and are separated since each climate change scenario begins with REF_{1-50}.

month	Piz Corvatsch	REF_{1-50}	REF_{51-100}	+1All	+1Win	+1Sum	+3All	+3Win	+3Sum	-1All	-3All
1	24.461	15.080	14.967	15.170	15.178	15.227	15.022	15.055	15.227	15.271	15.447
2	34.064	25.298	25.068	25.202	25.297	25.295	24.986	25.299	25.295	25.390	24.995
3	45.213	39.253	38.667	39.228	39.355	39.355	38.905	39.355	39.355	39.476	39.126
4	55.796	50.777	51.669	51.042	51.153	51.153	50.783	51.153	51.153	51.251	50.096
5	69.321	58.048	56.277	56.920	57.140	57.139	56.470	57.140	57.136	57.368	57.721
6	81.070	63.387	63.980	64.416	64.626	64.416	63.987	64.626	63.987	64.827	65.772
7	84.813	66.442	65.830	66.275	66.273	66.275	66.359	66.273	66.359	66.308	66.330
8	80.858	56.092	54.734	55.350	55.490	55.348	55.212	55.490	55.207	55.648	56.634
9	65.666	43.930	44.064	43.650	43.720	43.720	43.522	43.720	43.720	43.787	44.033
10	46.169	28.370	28.108	28.591	28.742	28.733	28.273	28.760	28.733	28.875	29.139
11	29.351	16.709	16.264	16.757	16.761	16.838	16.576	16.586	16.838	16.914	17.297
12	20.572	12.591	12.455	12.250	12.250	12.300	12.115	12.115	12.300	12.341	12.618

Table A.9: Mean daily RH at Piz Corvatsch and for all generated climate scenarios. $1-50$ and $51-100$ indicate the years of the REF scenario used for the statistics, and are separated since each climate change scenario begins with REF_{1-50}.

month	Piz Corvatsch	REF_{1-50}	REF_{51-100}	+1All	+1Win	+1Sum	+3All	+3Win	+3Sum	-1All	-3All
1	0.609	0.543	0.546	0.587	0.587	0.580	0.608	0.608	0.580	0.577	0.546
2	0.647	0.559	0.578	0.585	0.578	0.578	0.606	0.578	0.578	0.575	0.603
3	0.710	0.641	0.652	0.657	0.648	0.648	0.681	0.648	0.648	0.641	0.649
4	0.779	0.795	0.798	0.770	0.782	0.782	0.752	0.782	0.782	0.797	0.839
5	0.804	0.764	0.758	0.774	0.763	0.763	0.797	0.763	0.764	0.755	0.743
6	0.818	0.774	0.772	0.780	0.776	0.780	0.785	0.776	0.785	0.772	0.777
7	0.794	0.814	0.820	0.798	0.817	0.798	0.757	0.817	0.757	0.835	0.859
8	0.786	0.776	0.779	0.768	0.778	0.769	0.749	0.778	0.749	0.788	0.823
9	0.750	0.772	0.769	0.756	0.770	0.770	0.733	0.770	0.770	0.784	0.821
10	0.672	0.623	0.611	0.630	0.616	0.616	0.662	0.617	0.616	0.605	0.591
11	0.682	0.605	0.628	0.603	0.603	0.592	0.632	0.632	0.592	0.583	0.623
12	0.655	0.588	0.617	0.592	0.592	0.582	0.617	0.617	0.582	0.576	0.584

Table A.10: Standard deviation of daily RH at Piz Corvatsch and for all generated climate scenarios. $1-50$ and $51-100$ indicate the years of the REF scenario used for the statistics, and are separated since each climate change scenario begins with REF_{1-50}.

month	Piz Corvatsch	REF_{1-50}	REF_{51-100}	+1All	+1Win	+1Sum	+3All	+3Win	+3Sum	-1All	-3All
1	0.254	0.299	0.298	0.292	0.292	0.301	0.273	0.273	0.301	0.310	0.309
2	0.233	0.303	0.302	0.303	0.311	0.311	0.284	0.311	0.311	0.318	0.311
3	0.204	0.260	0.249	0.246	0.255	0.255	0.227	0.255	0.255	0.263	0.264
4	0.169	0.220	0.220	0.226	0.225	0.225	0.223	0.225	0.225	0.223	0.206
5	0.151	0.155	0.162	0.153	0.161	0.161	0.136	0.161	0.161	0.169	0.177
6	0.135	0.132	0.140	0.128	0.134	0.128	0.117	0.134	0.117	0.139	0.156
7	0.142	0.160	0.161	0.165	0.158	0.165	0.182	0.158	0.182	0.151	0.142
8	0.152	0.148	0.143	0.141	0.144	0.141	0.139	0.144	0.139	0.147	0.150
9	0.199	0.202	0.201	0.207	0.207	0.207	0.203	0.207	0.207	0.207	0.193
10	0.240	0.254	0.261	0.258	0.266	0.266	0.239	0.266	0.266	0.274	0.283
11	0.242	0.281	0.274	0.284	0.284	0.293	0.265	0.265	0.293	0.301	0.301
12	0.245	0.292	0.282	0.280	0.280	0.289	0.262	0.262	0.289	0.296	0.293

Table A.11: Mean daily WS at Piz Corvatsch and for all generated climate scenarios. $1-50$ and $51-100$ indicate the years of the REF scenario used for the statistics, and are separated since each climate change scenario begins with REF_{1-50}.

month	Piz Corvatsch	REF_{1-50}	REF_{51-100}	+1All	+1Win	+1Sum	+3All	+3Win	+3Sum	-1All	-3All
1	5.300	3.848	3.896	3.803	3.803	3.802	3.805	3.805	3.802	3.801	3.867
2	5.011	3.711	3.711	3.683	3.682	3.682	3.686	3.682	3.682	3.680	3.839
3	4.675	3.579	3.576	3.695	3.693	3.693	3.699	3.693	3.693	3.692	3.579
4	3.917	3.345	3.448	3.474	3.473	3.473	3.477	3.473	3.473	3.472	3.409
5	3.310	3.326	3.364	3.265	3.263	3.263	3.271	3.263	3.263	3.260	3.248
6	2.936	3.263	3.270	3.249	3.247	3.249	3.254	3.247	3.254	3.245	3.276
7	2.618	3.316	3.395	3.300	3.300	3.300	3.301	3.300	3.301	3.299	3.380
8	2.622	3.441	3.366	3.346	3.344	3.346	3.348	3.344	3.348	3.342	3.407
9	3.189	3.586	3.500	3.601	3.600	3.600	3.604	3.600	3.600	3.599	3.588
10	4.040	3.731	3.607	3.663	3.661	3.661	3.668	3.661	3.661	3.659	3.664
11	5.030	3.828	3.796	3.940	3.940	3.939	3.942	3.942	3.939	3.938	3.741
12	5.350	4.032	3.887	3.944	3.944	3.943	3.946	3.946	3.943	3.942	3.923

Table A.12: Standard deviation of daily WS at Piz Corvatsch and for all generated climate scenarios. $1-50$ and $51-100$ indicate the years of the REF scenario used for the statistics, and are separated since each climate change scenario begins with REF_{1-50}.

month	Piz Corvatsch	REF_{1-50}	REF_{51-100}	+1All	+1Win	+1Sum	+3All	+3Win	+3Sum	-1All	-3All
1	2.201	1.613	1.694	1.591	1.591	1.591	1.591	1.591	1.591	1.591	1.657
2	2.202	1.689	1.629	1.646	1.646	1.646	1.646	1.646	1.646	1.646	1.695
3	2.017	1.586	1.656	1.698	1.698	1.698	1.699	1.698	1.698	1.698	1.660
4	1.841	1.547	1.587	1.604	1.603	1.603	1.604	1.603	1.603	1.603	1.611
5	1.702	1.627	1.672	1.590	1.589	1.589	1.591	1.589	1.589	1.589	1.604
6	1.431	1.629	1.596	1.621	1.620	1.621	1.621	1.620	1.621	1.620	1.669
7	1.333	1.598	1.634	1.629	1.629	1.629	1.629	1.629	1.629	1.629	1.581
8	1.353	1.616	1.592	1.644	1.643	1.644	1.644	1.643	1.644	1.643	1.667
9	1.714	1.661	1.685	1.656	1.656	1.656	1.656	1.656	1.656	1.655	1.663
10	2.158	1.694	1.616	1.644	1.644	1.644	1.644	1.644	1.644	1.644	1.637
11	2.301	1.660	1.652	1.657	1.657	1.657	1.657	1.657	1.657	1.657	1.659
12	2.323	1.636	1.567	1.709	1.709	1.709	1.709	1.709	1.709	1.709	1.744

Appendix B

GEOtop Rock Glacier Point Topographic and Model Parameters

Table B.1: Key parameters of points used in rock glacier modeling

pointid	Elevation [m a.s.l.]	Aspect [°]	Soil	FreeLD [mm]
1	2700	0	1	0
2	3000	0	1	0
3	3300	0	1	0
4	2700	180	1	0
5	3000	180	1	0
6	3300	180	1	0
7	2700	0	2	0
8	3000	0	2	0
9	3300	0	2	0
10	2700	180	2	0
11	3000	180	2	0
12	3300	180	2	0
13	2700	0	1	2000
14	3000	0	1	2000
15	3300	0	1	2000
16	2700	180	1	2000
17	3000	180	1	2000
18	3300	180	1	2000
19	2700	0	2	2000
20	3000	0	2	2000
21	3300	0	2	2000
22	2700	180	2	2000
23	3000	180	2	2000
24	3300	180	2	2000
25	2700	0	1	15000
26	3000	0	1	15000
27	3300	0	1	15000
28	2700	180	1	15000
29	3000	180	1	15000
30	3300	180	1	15000
31	2700	0	2	15000
32	3000	0	2	15000
33	3300	0	2	15000
34	2700	180	2	15000
35	3000	180	2	15000
36	3300	180	2	15000

Appendix C

Rock Glacier Modeling Results

Table C.1: Mean MAGST [°C] of rock glacier simulations during years 45–50 of the reference scenario (which precedes all scenarios as an equilibrium period), and years 96–100 (not indicated for climate change scenarios) of the reference and climate change scenarios. P_{id} indicates the point identification number.

P_{id}	REF_{45-50}	REF_{95-100}	+1All	+1Sum	+1Win	+3All	+3Sum	+3Win	-1All	-3All
1	-2.32	-2.23	-0.93	-1.80	-1.81	1.18	-1.14	-1.29	-3.31	-5.02
2	-4.85	-4.76	-3.23	-4.13	-4.20	-0.85	-3.46	-3.65	-5.65	-7.36
3	-7.39	-7.03	-5.58	-6.51	-6.60	-3.12	-5.80	-5.99	-8.23	-9.62
4	0.84	0.96	2.06	1.34	1.29	4.04	1.90	1.78	0.10	-1.62
5	-1.19	-1.03	0.11	-0.63	-0.65	2.09	-0.08	-0.16	-1.94	-3.70
6	-3.25	-3.14	-1.91	-2.72	-2.73	0.15	-2.15	-2.20	-4.27	-5.79
7	-2.32	-2.23	-0.93	-1.80	-1.81	1.18	-1.14	-1.29	-3.31	-5.02
8	-4.85	-4.76	-3.23	-4.13	-4.20	-0.85	-3.46	-3.65	-5.65	-7.36
9	-7.39	-7.03	-5.58	-6.51	-6.60	-3.12	-5.80	-5.99	-8.23	-9.62
10	0.84	0.96	2.06	1.34	1.29	4.04	1.90	1.78	0.10	-1.62
11	-1.19	-1.03	0.11	-0.63	-0.65	2.09	-0.08	-0.16	-1.94	-3.70
12	-3.25	-3.14	-1.91	-2.72	-2.73	0.15	-2.15	-2.20	-4.27	-5.79
13	-2.32	-2.19	-0.90	-1.72	-1.82	1.30	-1.06	-1.29	-3.27	-5.01
14	-4.85	-4.72	-3.19	-4.10	-4.17	-0.80	-3.41	-3.61	-5.64	-7.37
15	-7.38	-7.04	-5.57	-6.51	-6.59	-3.09	-5.80	-5.98	-8.22	-9.62
16	0.83	1.05	2.18	1.45	1.42	4.22	2.04	1.90	0.17	-1.57
17	-1.18	-0.99	0.21	-0.57	-0.58	2.20	0.00	-0.09	-1.91	-3.70
18	-3.25	-3.12	-1.88	-2.69	-2.70	0.24	-2.12	-2.16	-4.26	-5.79
19	-2.32	-2.19	-0.90	-1.72	-1.82	1.30	-1.06	-1.29	-3.27	-5.01
20	-4.85	-4.72	-3.19	-4.10	-4.17	-0.80	-3.41	-3.61	-5.64	-7.37
21	-7.38	-7.04	-5.57	-6.51	-6.59	-3.09	-5.80	-5.98	-8.22	-9.62
22	0.83	1.05	2.18	1.45	1.42	4.22	2.04	1.90	0.17	-1.57
23	-1.18	-0.99	0.21	-0.57	-0.58	2.20	0.00	-0.09	-1.91	-3.70
24	-3.25	-3.12	-1.88	-2.69	-2.70	0.24	-2.12	-2.16	-4.26	-5.79
25	-2.32	-2.19	-0.90	-1.72	-1.82	1.02	-1.06	-1.29	-3.27	-5.01
26	-4.85	-4.72	-3.19	-4.10	-4.17	-0.80	-3.41	-3.61	-5.64	-7.37
27	-7.38	-7.04	-5.57	-6.51	-6.59	-3.09	-5.80	-5.98	-8.22	-9.62
28	0.83	0.89	2.10	1.36	1.30	4.17	1.99	1.78	-0.05	-1.57
29	-1.18	-0.99	0.20	-0.57	-0.58	2.12	0.00	-0.09	-1.91	-3.70
30	-3.25	-3.12	-1.88	-2.69	-2.70	0.24	-2.12	-2.16	-4.26	-5.79
31	-2.32	-2.19	-0.90	-1.72	-1.82	1.02	-1.06	-1.29	-3.27	-5.01
32	-4.84	-4.71	-3.19	-4.10	-4.17	-0.80	-3.41	-3.61	-5.64	-7.37
33	-7.38	-7.04	-5.57	-6.51	-6.59	-3.09	-5.80	-5.98	-8.22	-9.62
34	0.84	0.89	2.10	1.36	1.30	4.17	1.99	1.78	-0.05	-1.57
35	-1.18	-0.99	0.20	-0.57	-0.58	2.12	0.00	-0.09	-1.91	-3.70
36	-3.25	-3.12	-1.88	-2.69	-2.70	0.24	-2.12	-2.16	-4.26	-5.79

Table C.2: Mean D_{AL} [mm] of rock glacier simulations during years 45–50 of the reference scenario (which precedes all scenarios as an equilibrium period), and years 96–100 (not indicated for climate change scenarios) of the reference and climate change scenarios. * indicates cases where D_{AL} could not be estimated, presumably due to discrepancies in the format of GEOtop output tables; the values indicated are those of identical points with the alternate soil type, a substitution which should not affect the outcomes based on the equivalence of D_{AL} between soil types in all other cases. P_{id} indicates the point identification number.

P_{id}	REF_{45-50}	REF_{95-100}	+1All	+1Sum	+1Win	+3All	+3Sum	+3Win	-1All	-3All
1	1515	1533	1719	1587	1624	2156	1629	1726	1340	1177
2	1183	1176	1393	1217	1234	1724	1235	1482	1153	966
3	1070	1065	1159	1119	1137	1436	1124	1185	964	0
4	2940	5582	7369	6693	6478	11752	7353	7087	1794	1582
5	1714	1702	1782	1724	1750	6366	1772	1774	1572	1187
6	1380	1361	1566	1368	1497	1784	1455	1598	1188	1060
7	1515	1533	1719	1587	1624	2156	1629	1726	1340	1177
8	1183	1176	1393	1217	1234	1724	1235	1482	1153	966
9	1070	1065	1159	1119	1137	1436	1124	1185	964	0
10	2940	5582	7369	6693	6478	11752	7353	7087	1794	1582
11	1714	1702	1782	1724	1750	6366	1780	1774	1572	1187
12	1380	1361	1566	1368	1497	1784	1519	1598	1188	1060
13	1676	1687	1765	1704	1712	3029	1749	1764	1489	1181
14	1334	1273	1493	1274	1433	1768	1521	1569	1171	953
15	1070	1066	1183	1119	1137	1494	1144	1186	961	0
16	3975	6830	7626	7046	6927	11771	7410	7331	1799	1697
17	1751	1743	1956	1771	1773	6775	1796	1793	1645	1187
18	1453	1417	1651	1493	1528	1799	1542	1682	1189	1066
19	1676	1687	1765	1704	1712	3029	1730	1764	1489	1181
20	1334	1273	1493*	1274	1433	1768	1437	1569	1171	953
21	1070	1066	1183*	1119	1137	1494	1124	1186	961	0
22	3975	6830	7626*	7046	6927	11771	7410	7331	1799	1697
23	1751	1743	1956*	1771	1773	6775	1796	1793	1645	1187
24	1453	1417	1651*	1493	1528	1799	1542	1682	1189	1066
25	1676	1687	1765*	1704	1712	3195	1730	1764	1489	1181
26	1334	1273	1493*	1274	1433	1768	1437	1569	1171	953
27	1070	1066	1183*	1119	1137	1494	1124	1186	961	0
28	3931	4577	6822*	4922	4905	7712	7128	5676	2792	1721
29	1751	1743	1956*	1771	1773	5061	1796	1793	1645	1187
30	1453	1417	1651	1493	1528	1955	1542	1682	1189	1066
31	1709	1717	1765	1704	1712	3195	1730	1764	1489	1181
32	1398	1315	1493	1274	1433	1768	1437	1569	1171	953
33	1099	1097	1183	1119	1137	1494	1124	1186	961	0
34	4188	4648	6822	4922	4905	7712	7128	5676	2792	1721
35	1764	1761	1956	1771	1773	5061	1796	1793	1645	1187
36	1453	1417	1651	1493	1528	1955	1542	1682	1189	1066

Table C.3: Mean IWE_{tot} [mm w.e.] of rock glacier simulations during years 45–50 of the reference scenario (which precedes all scenarios as an equilibrium period), and years 96–100 (not indicated for climate change scenarios) of the reference and climate change scenarios. P_{id} indicates the point identification number.

P_{id}	REF_{45-50}	REF_{95-100}	+1All	+1Sum	+1Win	+3All	+3Sum	+3Win	-1All	-3All
1	8423	8429	8387	8415	8396	7362	8400	8388	8493	8658
2	8542	8596	8478	8564	8519	8378	8536	8445	8670	8685
3	8672	8670	8651	8670	8667	8467	8670	8581	8673	8794
4	6597	5487	5131	5348	5353	3244	5194	5328	7083	8472
5	8400	8411	8398	8402	8399	5498	8399	8400	8450	8581
6	8478	8504	8427	8478	8454	8402	8456	8404	8591	8667
7	8423	8429	8387	8415	8396	7362	8400	8388	8493	8658
8	8542	8596	8478	8564	8519	8378	8536	8445	8670	8685
9	8672	8670	8651	8670	8667	8467	8670	8581	8673	8794
10	6597	5487	5131	5348	5353	3244	5194	5328	7083	8472
11	8400	8411	8398	8402	8399	5498	8380	8400	8450	8581
12	8478	8504	8427	8478	8454	8402	8359	8404	8591	8667
13	8389	8389	8395	8390	8392	6958	8368	8398	8437	8642
14	8481	8512	8419	8490	8463	8393	8353	8381	8661	8646
15	8672	8669	8618	8670	8667	8403	8654	8555	8675	8797
16	6580	5348	5011	5335	5338	3244	5062	5207	6579	8262
17	8404	8407	7991	8405	8414	5459	8101	8367	8414	8587
18	8432	8444	8389	8442	8424	7987	8426	8381	8569	8700
19	8389	8389	8395	8390	8392	6958	8392	8398	8437	8642
20	8481	8512	8419	8490	8463	8393	8468	8381	8661	8646
21	8672	8669	8618	8670	8667	8403	8670	8555	8675	8797
22	6580	5348	5011	5335	5338	3244	5062	5207	6579	8262
23	8404	8407	7991	8405	8414	5459	8101	8367	8414	8587
24	8432	8444	8389	8442	8424	7987	8426	8381	8569	8700
25	8389	8389	8395	8390	8392	7267	8392	8398	8437	8642
26	8481	8512	8419	8490	8463	8393	8468	8381	8661	8646
27	8672	8669	8618	8670	8667	8403	8670	8555	8675	8797
28	6616	5636	5350	5515	5546	4993	5353	5372	6575	7584
29	8404	8407	8002	8405	8414	6189	8102	8367	8414	8587
30	8432	8444	8389	8442	8424	7978	8426	8381	8569	8700
31	8363	8363	8395	8390	8392	7267	8392	8398	8437	8642
32	8357	8396	8419	8490	8463	8393	8468	8381	8661	8646
33	8656	8653	8618	8670	8667	8403	8670	8555	8675	8797
34	6589	5362	5350	5515	5546	4993	5353	5372	6575	7584
35	8387	8388	8002	8405	8414	6189	8102	8367	8414	8587
36	8432	8444	8389	8442	8424	7978	8426	8381	8569	8700

Table C.4: Mean $MELT_{sum}$ [mm w.e.] of rock glacier simulations during years 45–50 of the reference scenario (which precedes all scenarios as an equilibrium period), and years 96–100 (not indicated for climate change scenarios) of the reference and climate change scenarios. P_{id} indicates the point identification number.

P_{id}	REF_{45-50}	REF_{95-100}	+1All	+1Sum	+1Win	+3All	+3Sum	+3Win	-1All	-3All
1	-296	-292	-326	-307	-331	-273	-321	-340	-258	-112
2	-218	-169	-256	-200	-238	-326	-223	-270	-92	-76
3	-31	-66	-98	-67	-95	-256	-84	-204	-94	-21
4	-256	-266	-234	-251	-260	-15	-211	-258	-279	-274
5	-292	-286	-291	-302	-308	-235	-295	-319	-258	-192
6	-209	-193	-263	-204	-229	-292	-210	-298	-166	-34
7	-296	-292	-326	-307	-331	-273	-321	-340	-258	-112
8	-218	-169	-256	-200	-238	-326	-223	-270	-92	-76
9	-31	-66	-98	-67	-95	-256	-84	-204	-94	-21
10	-256	-266	-234	-251	-260	-15	-211	-258	-279	-274
11	-292	-286	-291	-302	-308	-235	-288	-319	-258	-192
12	-209	-193	-263	-204	-229	-292	-235	-298	-166	-34
13	-228	-247	-239	-245	-267	-210	-259	-265	-216	-136
14	-205	-180	-221	-200	-188	-237	-195	-252	-99	-77
15	-32	-63	-136	-67	-90	-230	-86	-233	-99	-22
16	-209	-211	-206	-208	-212	-21	-180	-215	-219	-254
17	-238	-238	-223	-250	-246	-203	-240	-234	-249	-193
18	-186	-186	-246	-192	-219	-220	-202	-266	-174	-37
19	-228	-247	-239	-245	-267	-210	-266	-265	-216	-136
20	-205	-180	-221	-200	-188	-237	-180	-252	-99	-77
21	-32	-63	-136	-67	-90	-230	-81	-233	-99	-22
22	-209	-211	-206	-208	-212	-21	-180	-215	-219	-254
23	-238	-238	-223	-250	-246	-203	-240	-234	-249	-193
24	-186	-186	-246	-192	-219	-220	-202	-266	-174	-37
25	-228	-247	-239	-245	-267	-140	-266	-265	-216	-136
26	-205	-180	-221	-200	-188	-237	-180	-252	-99	-77
27	-32	-63	-136	-67	-90	-230	-81	-233	-99	-22
28	-22	-47	-40	-48	-51	-8	-39	-48	-83	-255
29	-238	-238	-191	-250	-246	-61	-240	-234	-249	-193
30	-186	-186	-246	-192	-219	-207	-202	-266	-174	-37
31	-243	-250	-239	-245	-267	-140	-266	-265	-216	-136
32	-252	-217	-221	-200	-188	-237	-180	-252	-99	-77
33	-34	-67	-136	-67	-90	-230	-81	-233	-99	-22
34	-28	-43	-40	-48	-51	-8	-39	-48	-83	-255
35	-225	-234	-191	-250	-246	-61	-240	-234	-249	-193
36	-186	-186	-246	-192	-219	-207	-202	-266	-174	-37